

# FU JEN STUDIES

## NATURAL SCIENCES

NO. 23

1989

### 目次 CONTENTS

|  | Page |
|--|------|
| The Spectral Analysis of Amplitude Scintillation at Fu Jen .....   |      |
| .....by John R. Koster and Elin-Peng Wang...   | 1    |
| 閃爍現象之振幅頻譜分析.....高士達 王 芃  |      |
| 石油產物燃燒前後及空氣中懸浮粒子多苯環碳氫化合物之分析.....   |      |
| .....葉裕釗 蕭國峰 李偉平...  | 13   |
| Analysis of Polynuclear Aromatic Hydrocarbons (PAHs) in<br>Petroleum Products and Air Particulates ..... |      |
| .....by Yue-Jau Yeh, Kwo-Fen Hsiao and Wai-Ping Lee  |      |
| 自動化多功能實驗卡.....汪彥緯 陳壽椿...   | 41   |
| A Multifunction Lab Card for Automation .....  |      |
| ..... by Yen-Wei Wang and Show-Chuen Chen  |      |
| 聚吡咯及其衍生物之電化學合成及金屬離子吸附現象之研究.....  |      |
| .....饒忠儒 劉保華 陳壽椿...  | 49   |
| Study of the Electrosynthesis and Metal Ion Adsorption of<br>Polypyrroles .....                          |      |
| ..... by Jong-Ru Rau, Bao-Hwa Liou and Show-Chuen Chen   |      |

續 (Continued)

60th Anniversary of the Founding  
of Fu Jen Catholic University,  
Commemorative Issue

## 目次(續) CONTENTS (Continued)

|   | Page |
|---|------|
| NMR Investigation of the Interaction between ATP and<br>Macrocyclic Polyamines .....by <i>Elizabeth H. Mei</i> ...  | 67   |
| 核磁共振光譜研究腺苷三磷酸與大環多胺化合物之作用力.....梅宏綺   |      |
| Abstracts of Papers by Faculty Members of the College of<br>Science and Engineering that Appeard in Other Journals<br>During the 1988 Academic Year ..... | 77   |

# THE SPECTRAL ANALYSIS OF AMPLITUDE SCINTILLATION AT FU JEN

JOHN R. KOSTER AND ELIN PENG WANG

Department of Physics

## ABSTRACT

It is shown that, in spite of the presence of a large doppler-induced component in the radio signal radiated by earth satellite ETS-2, it is possible to produce useful spectra of the amplitude variations of the received radio waves. The power spectrum of data taken during periods of strong scintillation gives convincing evidence of severe multiple scattering of the wave, and points to the equatorial bubble formation mechanism as the physical cause of the ionospheric irregularities responsible for the scintillations. Some very mild scintillations have also been observed. The typical "summer time" scintillations previously observed during June and July at Fu Jen were nearly entirely absent during the summer of 1989, and the problem of their physical cause is still to be solved.

## 1. INTRODUCTION

Satellite ETS-2 is in an equatorial earth-synchronous orbit at longitude  $130^{\circ}\text{E.}$  and at a nominal height of 35,800 km. As an aid to ionospheric studies its design included provision for the production and radiation of a constant amplitude, plane polarized wave at a frequency of 136.112 MHz (wavelength=2.2 meters). From a study of the variation in amplitude, phase and polarization angle of the received signal, an observer on the ground is able to deduce some useful information about the state of the ionosphere through which the wave has passed on its journey from satellite to receiving aerial. In this study we shall ignore phase as well as polarization angle variations and consider only the variations of the signal amplitude as a function of time. Such amplitude variations in a radio wave are usually referred to as scintillations, since they are analogous to the variations in apparent brightness or twinkling of visible stars,

## 2. WEAK SCINTILLATIONS

A radio wave, in passing from satellite borne transmitter to earth-bound receiver, must pass through the ionosphere. Often, especially at middle latitudes, it is appropriate to think of this as a thin slab of partially ionized gas, containing relatively small electron density irregularities which have a small scattering effect on radio waves. An incident plane wave emerges from the slab with constant amplitude, but with small variations in phase across the wave front. As the wave proceeds from slab to ground, these phase variations develop into a corresponding pattern of amplitude variations. In our case the satellite is fixed in position relative to the observer, but the ionospheric irregularities themselves have a drift motion, normally eastward at night. And so the amplitude pattern drifts over an observing site, leading to an observed variation in the wave amplitude as a function of time—amplitude scintillations.

The mathematical description of this single scattering or thin screen type of scintillations is difficult, but manageable (see, e.g., Crane<sup>(1)</sup>, Lovelace<sup>(2)</sup>, Rino<sup>(3)</sup>, Rufenach<sup>(4)</sup>, Singleton<sup>(5)</sup>, Tatarski<sup>(6)</sup>). It predicts, among other things, that if one determines the power spectrum of the amplitude variations observed on the ground, the falloff portion of the spectrum will, at least in the ideal case, have a slope of  $-2$ .

## 3. STRONG SCINTILLATIONS

When the restrictions of a thin, single-scattering layer are relaxed, the mathematics of the problem become exceedingly involved (see, e.g., Marians<sup>(7)</sup>, Yeh<sup>(8)</sup>). The wave is now scattered not only once, but repeatedly; and not only through a very small angle, but through relatively large angles. However, one relatively simple prediction of theory still survives. Even under conditions of strong scintillation, the power spectrum should roll off with a constant slope. Values of this slope will no longer be  $-2$ , however, but it will normally become much steeper. Slopes of  $-5$  or  $-6$  are common during times of severe scintillation.



#### 4. THE NEED FOR SPECTRA

Ionospheric disturbances, as we have mentioned above, can and do manifest themselves by producing variations in the signal amplitude. It is possible to record these radio wave amplitude variations on a moving paper chart, or store them as digitized values in the storage medium of a computer, and this is routinely done. In the analysis of these data, however, it is frequently more useful to express the amplitude variations as a function of frequency rather than as a function of time.

This is conceptually simple—one merely takes a finite length of record of amplitude versus time and transforms it, via the well known Fourier Transform technique, to a function of amplitude versus frequency. Given the prevalence of digital computers and their ability to implement the Fast Fourier Transform (FFT) algorithm, the actual task is equally simple to implement.

If the amplitude of the received signal were truly constant, one would expect its spectrum to show low-level variations of amplitude with frequency (electrical noise) but no spectral peaks.

Figure 1 shows part of the spectrum of a daytime record taken at the ionospheric physics lab at Fu Jen, using our best receiver and the maximum attainable signal to noise ratio. Since there is little scintillation during the day at our station, one would expect to see little more than the inevitable background noise. The spectrum does indeed show the background noise, with noise power decreasing slowly with increasing frequency, as would be normal. But another feature is much more striking—a huge spectral peak at 6.24 Hertz, 50 db (i. e., a factor of 100,000) above the noise level. This component is real, not just a random noise "spike", or artifact of a particular record. The present spectrum was produced by averaging 48 individual spectra, each determined from an analysis of 1,024 readings. The observant reader will notice that there are several other much weaker spectral components present also. These will be mentioned later,

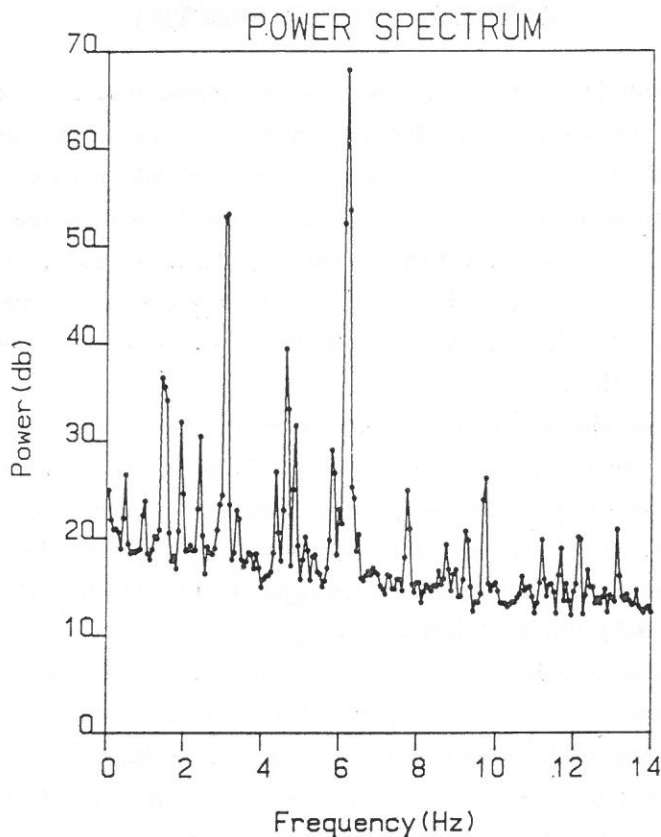


Fig. 1. The lower frequencies of the spectrum of ETS-2 when there is no scintillation. Noise and the doppler component of the signal appear.

## 5. ORIGIN OF THE SPECTRAL PEAK

The origin of the 6.24 Hz spectral peak is easily explained. The satellite uses a so-called "turnstile" aerial, consisting of two dipoles at 90 degrees to one another, and fed 90 degrees out of phase. The elements of the dipoles are fastened symmetrically around one end of the cylindrical spacecraft. When in orbit, the satellite is caused to spin around its axis of symmetry to give it positional stability, similar to that of a spinning top or gyroscope. The axis of symmetry points permanently towards the celestial north pole.

It will be recalled that the satellite is in a nearly equatorial orbit. For an observer on the ground, each of the spinning elements will have a component of velocity along his line of sight, and thus the received wave will suffer a small doppler shift. The doppler frequencies will be of the order of:

$$1 + \frac{v}{c} \text{ or } 1 - \frac{v}{c} \text{ times the normal frequency,}$$

where  $v$  is the component of velocity along the line of sight, and  $c$  is the velocity of light.

It should be noted that  $v/c$  is exceedingly small—about 3 parts in 136 million—so that the doppler shifted components of the signal will differ from the main frequency by +3.12 and -3.12 Hertz respectively.

Corroboration of the truth of this explanation of the origin of the spectral line is easily obtained. Since the orbit of the satellite has deteriorated somewhat since its 1977 launch and there is little or no fuel left for station keeping, the plane of the satellite orbit is now inclined to the equator by several degrees, and the apparent position of the satellite from the ground is not stationary in time, but describes a daily "figure 8" path. Hence the angle between the observers line of sight and the satellite spin axis has a daily variation also. The velocity component along the line of sight is proportional to the sine of this angle—and hence the doppler frequency should show a daily variation, with two peaks corresponding to the times when the angle is equal to 90 degrees, and its sine is equal to one.

Figure 2, shows the measured percent variation of the period of the doppler component over a continuous 32 hours time interval. The two peaks occur as expected. The minima are unequal in amplitude, due to our position being 25 degrees north of the equator, and hence not symmetrically located with respect to the satellites movement across the equator.

## 6. THE EFFECTS OF SCINTILLATION ON OUR SPECTRA

The spectrum shown in Fig. 1 requires a little further explanation,

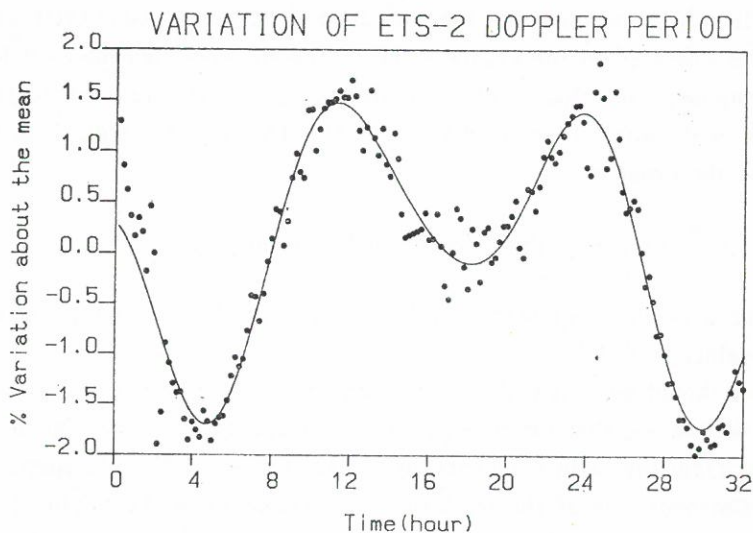


Fig. 2. Percent variation of the observed period of the doppler component of ETS-2 over a 32-hour period.

It should be remembered that these so-called power spectra show energy per unit bandwidth as a function of frequency. Our analysis yields values for each of 512 equally spaced frequencies, ranging from 0.0625 Hz to 32 Hz inclusive. Our Fig. 1 shows only the spectral components up to 14 Hz, with frequency drawn on a linear scale.

Firstly, it will be noted that there is no "zero frequency" component on the plot. It is usual to remove this constant or d.c. term before performing the Fourier Transform since it is often very much larger than the a.c. components, and interferes with the accuracy of the analysis. Hence, in considering Fig. 1, one should remember that there is also a d.c. term, and that the energy it represents is 25 times larger than the total energy contained in all the a.c. terms combined.

The second thing to note is that the 6.24 Hz doppler peak is really large. It contains 94% of the total energy found in the a.c. terms. This becomes evident when one realizes that the vertical scale is logarithmic and the height of the peak is about 50 db (a factor of 100,000) above the surrounding noise.

We must now consider the effect of amplitude variations, or scintillations, on such a spectrum. Amplitude variations lead to a "smearing" of energy from the d.c. term into the low frequency components of our spectrum. If the amplitude of these spectral components due to noise is greater than, or at least comparable to that of the Doppler component, we may be able to ignore the contributions of the latter; otherwise, we must take the doppler line into account. It will be appreciated, too, that scintillation will also smear energy from this doppler line into adjacent frequencies, so that it may now be impossible to completely remove its effect from the spectrum.

As a demonstration of the above effects we now turn to Fig. 3.

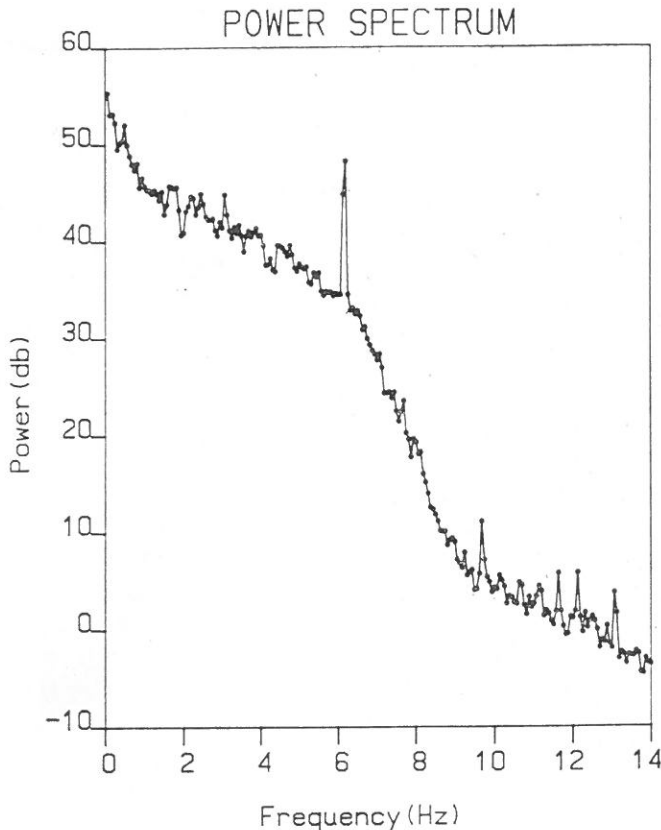


Fig. 3. The spectrum of the amplitude variations of ETS-2 during a time of severe scintillation,

This figure was produced by precisely the same technique as that used for Fig. 1, but the data were taken over a 768 second period when severe night time scintillations were being experienced. It will be noted that in this spectrum a relatively large amount of energy is present for all frequency components up to about 10 hertz. The 6.24 Hz doppler peak is still present, but both its absolute level, and its level relative to neighboring frequencies is now much smaller. It represents a mere 3.18% of the total energy. In this case it seems safe to assume that the spectral line can have little effect on the general shape of the spectrum, and to ignore it in many applications.

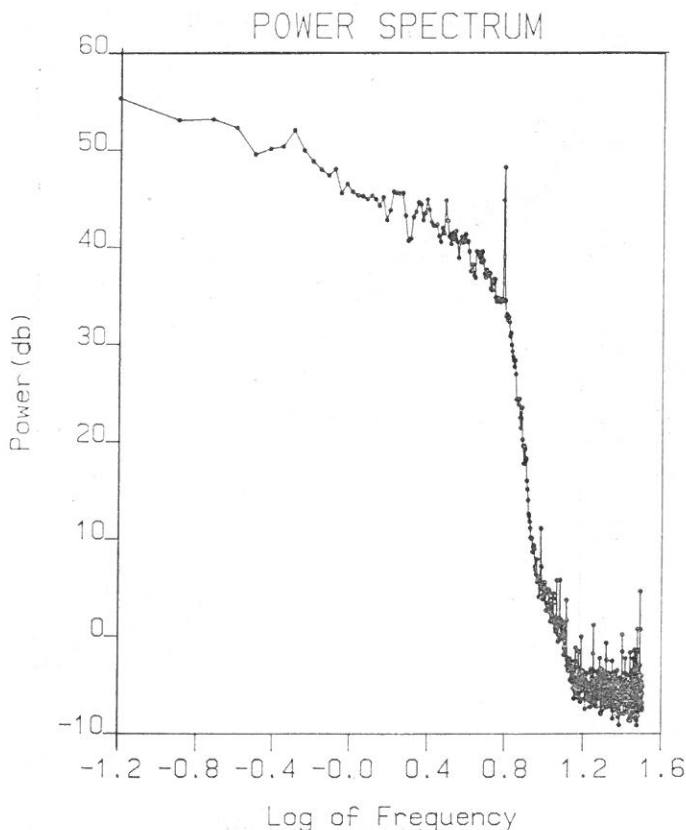


Fig. 4. The log-log plot of the data of Fig. 3. The maximum slope of falling part of the spectrum is  $-17$ .



## 7. A USEFUL PROPERTY OF THE SPECTRUM— LOG-LOG PLOTS

In Fig. 4 we present the same data as that of Fig. 3, but in this case we plot frequency on a logarithmic rather than on a linear scale. We also include all 512 frequency componency arising from the analysis. The doppler line has not been removed.

Theory predicts that such log-log spectral plots should be relatively flat at low frequencies, then fall off rather sharply as the frequency increases. The ideal spectrum can be approximated by a horizontal straight line for the low frequencies and an inclined straight line at the high end of the spectrum. Theory also tells us, as mentioned above, that the slope of the inclined straight line contains important information about the ionospheric irregularities giving rise to the scintillations. A straight line with slope  $-2.0$  arises when the electron density irregularities in the ionosphere can be likened to a thin, phase changing screen. If, however, multiple scattering of the waves occurs, the slope of the line will become increasingly steep—typically to a value of  $-5.0$  or greater when the scintillation is severe. Figure 4 has a slope of  $-17$ .

## 8. "BUBBLE TYPE" SCINTILLATION AT FU JEN

Figure 4 is typical of the type of spectrum we get during cases of severe night-time scintillations at or near the equator. We refer to this as "bubble type" scintillation, since its occurrence correlates very highly with the signature of ionospheric bubbles in the TEC records taken at an equatorial station—in this case, Manila. The slope of the straight line portion of Fig. 4 is indicative of very severe multiple scattering.

## 9. "SUMMER TYPE" SCINTILLATIONS

In contrast to the violent scintillation described above, there is a much milder type that occurs mainly in the summer month of June and July. This type of scintillation does not seem to be associated

with equatorial bubble formation; it often occurs at times when Manila TEC records show no evidence of the occurrence of the bubble formation mechanism. This "summer-time" scintillation does correlate quite highly with corresponding scintillations at Tokyo—a mid-latitude station. Figure 5 is an example of the spectrum of a very "shallow" type of scintillation recorded on the night of 1st September, 1989.

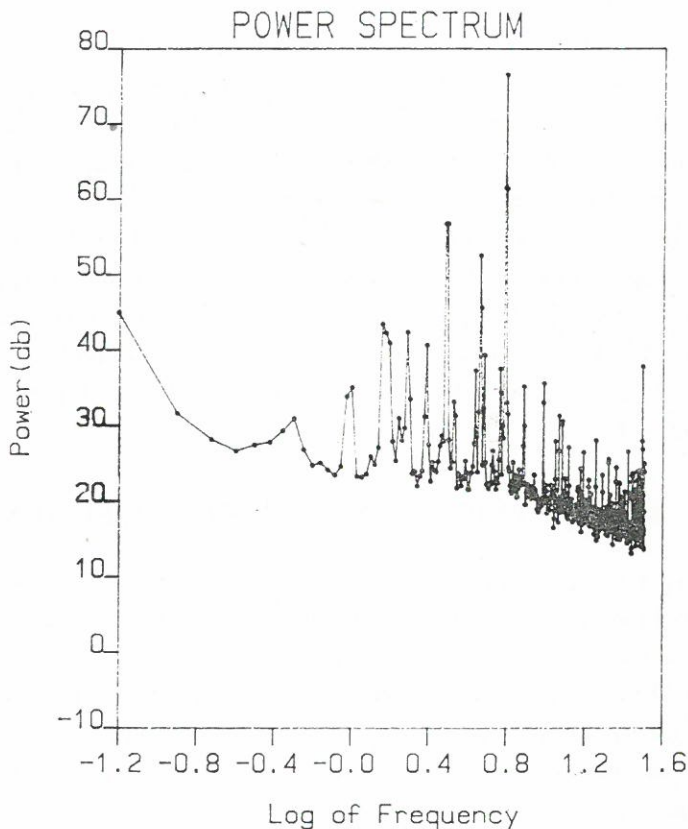


Fig. 5. A spectrum obtained during a period of very small scintillations on the night of 1st September, 1989.

The figure is not a very impressive specimen. What it does show are the following things:

- (a) The dominance of the 6.24 Hz doppler line. This is 100 times larger than anything else in the spectrum.
- (b) The presence of some smaller peaks, with energies less than 1% of that of the peak. These seem to be related to the doppler frequency in a harmonic way—but their origin is not yet known.
- (c) The maximum slope of the log-log plot is of the order of  $-2$ .

It must be noted that Fig. 5 shows the log-log plot of some small September scintillation. This does seem to be a case of very mild scintillation which could be adequately explained by a thin diffracting screen mechanism. Whether this case is exceptional, or whether it is typical of the usual summer time scintillation is presently unclear.

## 10. CONCLUSIONS

As a result of the spectral analysis of scintillation records done to date, we can list the following conclusions:

- (a) In spite of the presence of a large doppler induced line it is possible to get good spectra of amplitude scintillations of ETS-2 at The Fu Jen ionospheric laboratory.
- (b) Numerous spectra of intense scintillations have been made, and their large slope indicates that the mechanism leading to their production involves severe multiple scattering of the radio waves. The evidence is overwhelmingly in favor of identifying this scintillation with the equatorial bubble formation mechanism.
- (c) A few cases of the "thin screen" type of scintillation have been observed at Fu Jen.
- (d) The origin of the "summer type" of scintillation observed during past years at Fu Jen is still unknown. Very little of it occurred during the summer of 1989. Only the analysis of future June-July scintillation records will clarify the issue.

## REFERENCES

- (1) R.K. Crane, *J. Geophys. Res.*, **81**, 2041 (1976).

- (2) R.V.E. Lovelace, E.E. Saltpeter and L.E. Sharp, *Astrophys. J.*, **159**, 1047 (1970).
- (3) C.L. Rino, *Radio Sci.*, **14**, 1135 (1979).
- (4) C.L. Rufenach, *J. Geophys. Res.*, **77**, 4761 (1972).
- (5) D.G. Singleton, *J. Atmos. Terr. Phys.*, **36**, 113 (1974).
- (6) V.I. Tatarski, The Effects of the Turbulent Atmosphere on Wave Propagation, *U. S. Dept. of Commerce, National Technical information service, Springfield, Va.* (1971).
- (7) M. Marians, *Radio Sci.*, **10**, 115 (1975).
- (8) K.C. Yeh, C.H. Liu and M.Y. Youakim, *Radio Sci.*, **10**, 97 (1975).

## 閃爍現象之振幅頻譜分析

高 士 達      王      梵

輔 仁 大 學 物 理 系

### 摘      要

雖然由地球衛星 ETS-2 所發出之無線電訊號中有極強的杜普勒效應分量，我們仍可由所得之無線電波製出有效的振幅變化頻譜。閃爍現象強烈時期所得數據的功率頻譜，確實證明了電波的嚴重多次散射及赤道氣泡形成機制乃造成電離層不規則性的物理原因，而此種不規則性以閃爍現象呈現。一些平緩的閃爍現象亦曾觀測到。但是以往於輔仁大學觀測到的典型夏季閃爍現象，在今年（1989）幾乎絕跡，而其物理原因仍待了解。

# 石油產物燃燒前後及空氣中 懸浮粒子多苯環碳氫化合物之分析

葉裕釗 蕭國峰 李偉平

輔仁大學化學系

## 摘要

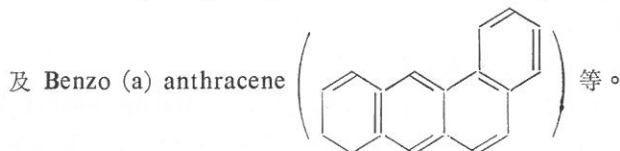
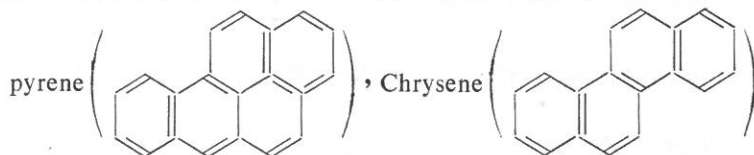
多苯環芳香族化合物在自然環境中所送成的污染與日俱增，不容忽視。我們把市面上所購得之柴油及汽油放在模擬燃燒內，觀察它們在燃燒前、後之變化。在實地採樣方面，我們是使用一個經過改良的大型氣體採樣器，內置玻璃纖維濾紙及 PU 泡棉，前者可收集空氣中的懸浮粒子，而後者則可採集揮發性較高的物質。我們是利用傅利葉轉換紅外光譜儀，氣層分析儀及氣層分析儀／質譜儀為主要的分析、鑑定儀器。

**關鍵詞：**多苯環芳香族化合物 (Polycyclic Aromatic Hydrocarbons, PAHs)，懸浮粒子 (Total Suspended Particles, TSP)，PU 泡棉 (Polyurethane Foam, PUF)，小型空氣採樣器 (Handy sampler)，大型空氣採樣器 (Hi-volume sampler)，玻璃纖維濾紙 (Glass Fiber Filter, GFF)。

## 一、結 論

隨着工、商業的發達，人類生存的環境被污染的程度與日俱增，本研究小組主要的研究方向為探討、分析在自然環境中的多苯環芳香族化合物 (Polycyclic Aromatic Hydrocarbons, PAHs)。本篇報告主要是以空氣為研究對象，我們選擇 PAHs 為研究對象的原因如下：

- (1) 在臨床上，越來越多證明有好幾種的 PAHs 為致癌物及引起腫瘤的物質，美國環保單位 (EPA) 已證實的 PAHs 致癌物為：Benzo (a)



- (2) 原油及石油產物內蘊含豐富的 PAHs，以目前國內工業發達，交通頻繁的情形，自然環境中受 PAHs 之污染已不容坐視。
- (3) PAHs 在自然界中有持續存在的頑固性 (Persistence)，可作為自然環境中受到油污染的指標。

收集空氣中污染物的方式有如幾種，主要是利用 Hi-volume sampler (大型空氣採樣器)，內裝有 Glass Fiber Filter (玻璃纖維濾紙, GFF) 或某些吸附劑，如 Amberlite XAD-2, Chromosorb-102, Tenax-GC 及 Openpore polyurethane foam 等。

採樣後之萃取方法計有：Ultrasonic extraction, Vibration, Stirring 及 Soxhlet extraction 等。所用溶劑則視所要分析物種之不同而各異。

在本篇內，我們將報告石油產物模擬燃燒之結果，此外，亦會對小型空氣採樣器及大型空氣採樣器作一比較。我們主要是以傅利葉轉換紅外光譜儀 (Fourier Transform Infrared Spectrometer, FTIR) 對苯物中之官能基作一初步之鑑定；繼之以 GC 及 GC/MS 進行分析及鑑定的工作。

大氣中 PAHs 的主要來源為燃燒不完全所致，隨着飛灰 (Flyash) 及煙霧 (Soot) 散佈於大氣中，由呼吸器官進入人體，為害人類健康；在引起各種的病例中，以肺癌病例為最多。此外，苯亦為引起白血病之物質之一，在本篇報告中，原以偵測大氣中的 PAHs 為主，但在樣品分析的過程中，發現了其它的物種，如鄰苯二甲酸酯類的化合物 (Phthalate esters) 及長鏈形之飽和碳氫化合物 (Aliphatics)，前者為塑膠工業上所用之可塑劑 (Plasticizers)；而後者則由石油產物而來。

## 二、實 驗

由於所使用的空氣採樣器各有不同，所以分成下述甲、乙兩部份敘述之：

### 1. 小型空氣採樣器 (Handy sampler, 圖 1)

把適當的溶劑置於圖中所示之集氣瓶④，把整個採樣器置於適當之地點，馬達開動後，便可採集空氣樣品。

#### (1) 燃燒石油產物的模擬實驗：

裝置如圖 2 所示，把 50 ml 之環己烷置於 Handy sampler 之集氣瓶內；將柴油、汽油及正己烷分別盛入酒精燈中，再放入高溫爐內；點燃



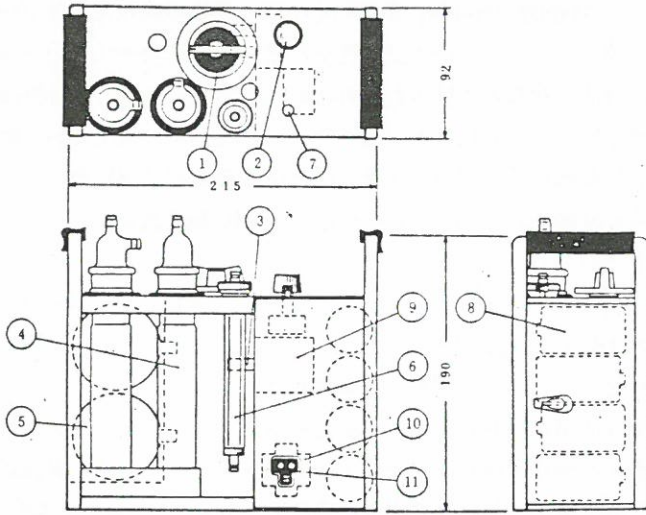


圖 1 小型空氣採樣器。

- |        |        |
|--------|--------|
| ①計時器   | ⑦流速控制鈕 |
| ②馬達控制鈕 | ⑧電池櫃   |
| ③排氣口   | ⑨抽氣機   |
| ④集氣瓶   | ⑩充電器   |
| ⑤氣槽    | ⑪插頭    |
| ⑥流速計   |        |

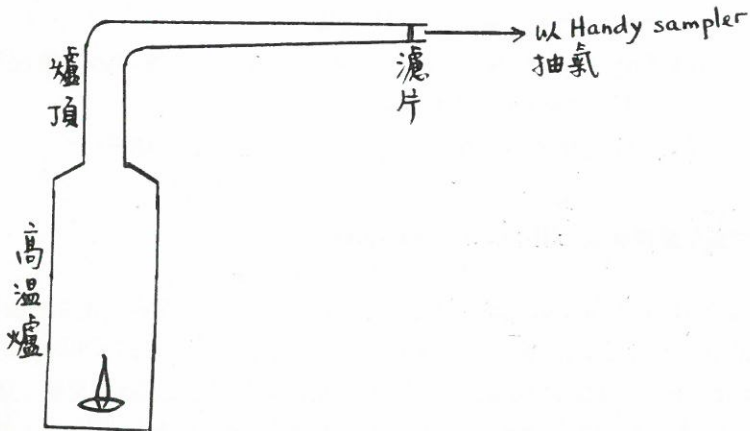


圖 2 石油產物燃燒之模擬裝置。

後以 Handy sampler 採集約兩小時之後收集爐頂及濾片 ( $0.45\ \mu\text{m}$ ) 上的煤灰樣品，分別以正己烷為萃取液，混合萃取物以離心機分離之，取出澄清之萃取液，Handy sampler 中之集氣瓶內的混合溶液亦以離心機分離出其中的粒子，取出澄清之萃取液，將上述三者的萃取液分別以真空旋轉濃縮器 (Rotary evaporator) 濃縮至 1 ml 左右，所得之溶液可直接注入 GC 內分析，並以 FTIR 輔助鑑定。

(2) 未燃燒前石油產物之分析：

分別取柴油及汽油各 0.5 ml，將之溶於 5 ml 的環己烷內，以 GC 及 FTIR 分析鑑定之。

(3) 採集二行程機車在開動時所排放的廢氣：

把 Handy sampler 分別直接置於兩部二行程之機車排氣管口，開動機車，收集其所排放出的氣體，每部機車開動約一小時，混合萃取液以離心機分離出顆粒後，將澄清液濃縮至 1 ml，再分別注入 GC 及 FTIR 內分析。

(4) 實地採樣：

曾把 Handy sampler 分別置於臺北辛亥路及新生南路口與辛亥路地鐵施工處收集空氣樣品，但效果不彰，故以 High-volume sampler 取代之。

(5) GC 之分析條件：

- (a) Injector 之溫度為  $200^{\circ}\text{C}$ ，而 Detector (FID) 的溫度為  $300^{\circ}\text{C}$ 。
- (b) 起始溫度為  $70^{\circ}\text{C}$ ，停留 2 分鐘後，以  $5^{\circ}\text{C}/\text{min}$  之速度上升至  $300^{\circ}\text{C}$  為止，繼續停留 15 分鐘。
- (c) Carrier gas ( $\text{N}_2$ ) 之流速為 30 cc/min；空氣流速為 300 cc/min； $\text{H}_2$  之流速為 30 cc/min。
- (d) GC 之機型為 VA 3700 型，所使用之管柱為 DB-5。

## 2. 大型空氣採樣品 (Hi-volume sampler)

由於 Handy sampler 抽氣馬達力量不足，且採樣時間有限，故在實地採樣之效果不彰，我們改用 Hi-vol sampler 來採集空氣樣品，我們所用的 Hi-vol sampler 乃一經過改良之裝置 (圖 3)，是把傳統所用之玻璃纖維濾紙 (Glass Fiber Filter, GFF) 與價廉，易得之 PU 泡棉 (Polyurethane Foam, PUF) 呈前後串聯方式一起使用。茲將整個實驗過程以一流程圖表示如下：

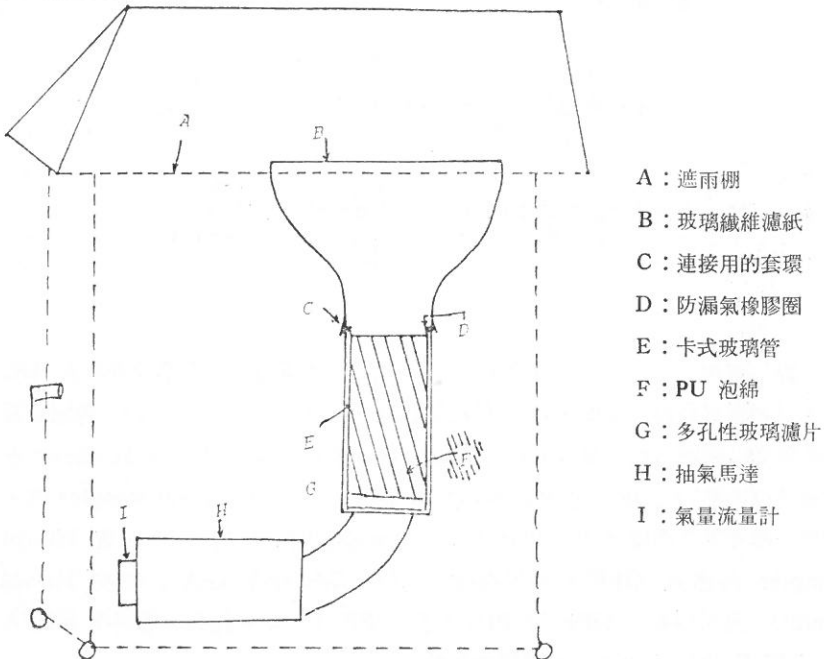
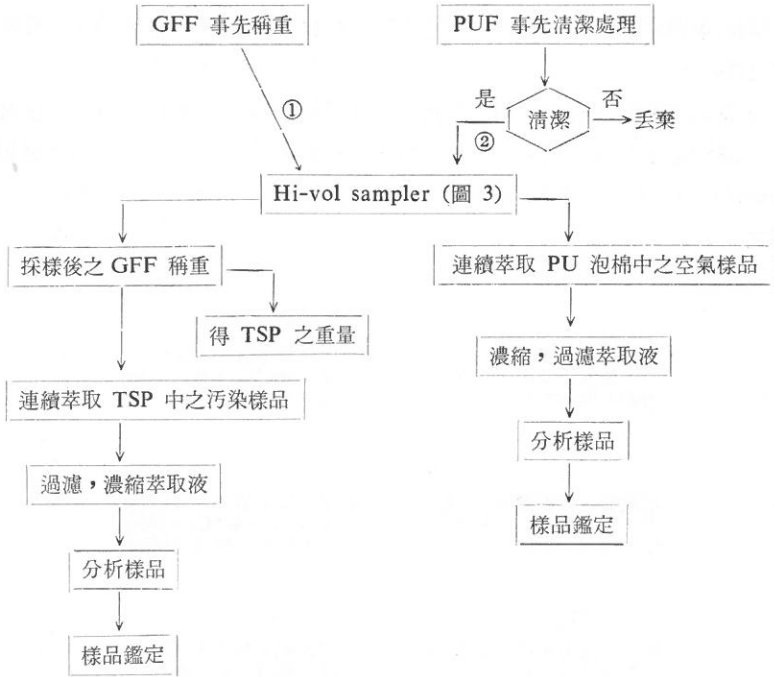
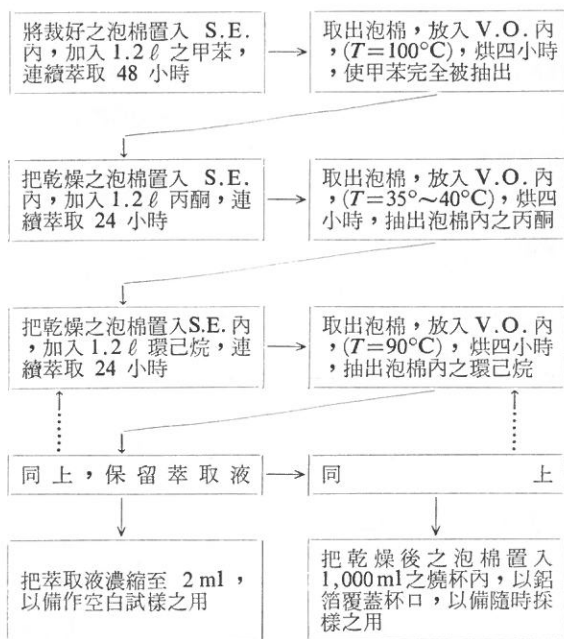


圖 3 大型空氣採樣器裝置。

採樣過程以①及①+②各乙次之方式為完整之週期，而後重複採樣分析做此研究之探討。

在採樣方面所要用到的 PU 泡棉，由於組成複雜，故在使用前需要經過一連串的清潔過程，現亦將其清潔過程以一流程圖表示之，其中大型的 Soxhlet Extractor (圖 4) 以 S.E. 簡稱之；而真空烘箱 (Vacuum Oven) 則以 V.O. 表示之。



PU 泡棉在經過上法處理之後，可把第二次之環己烷萃取濃縮液注入 GC 內，以判斷其是否已清潔，此 GC 圖譜可作為空白試樣之結果，PU 泡棉是否已乾淨是以圖譜出現之波峯數目為準繩，(波峯數目在 40 內者，認為已乾淨，否則則予以丟棄)，已乾淨之 PU 泡棉可與 GFF 一起放入 Hi-vol sampler 內，置於一樓樓頂之高度，以 56 ft<sup>3</sup>/min 之流速連續採樣 24 小時，若 Hi-vol sampler 內僅置 GFF，則所採得之空氣樣品編號為 NFA；若在 Hi-vol sampler 內同時置入 GFF 及 PUF，則 GFF 上之空氣樣品、編號為 WPFA，而 PUF 的則為 P<sub>n</sub>A (n 為阿拉伯數字)。

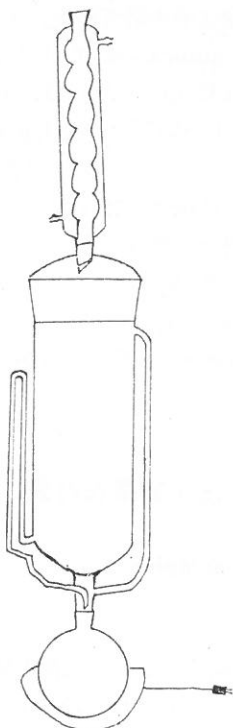


圖 4 大型 Soxhlet Extractor。

GFF 之萃取過程如 (2) 所述，採樣後之 PUF 可置入大型 S.E. 中，以 1.2  $\ell$  環己烷萃取 24 小時，所有萃取液均分別以真空旋轉濃縮器濃縮至 2 ml 為止。所有樣品均置入咖啡色之樣品瓶內，所有的瓶口皆以 Teflon tape 加封之，欲作 GC/MS 分析之樣品，需再以純  $N_2$  濃縮至 0.3 ml 為止。

採樣前之 GFF 及 Cellulase thimble filter 均事先做空白試驗。

在本研究中所用之 GC 為 VA 3700 機型；所用之管柱為 SE-54，30 m  $\times$  0.32 mm i. d.；0.25  $\mu$ m Film thickness 之 Fused silica capillary column；Carrier gas： $N_2$  (10 psi)；Make-up gas： $N_2$  (30 ml/min)；Air rate: 300 ml/min； $H_2$  rate: 30 ml/min；FID；各項溫度為：Injection port：230°C；Detector port：300°C；Column port：80°C (1 min)，以 4°C/min 之階進溫度提高速度至 300°C，停留 15 分鐘；注射量為 0.3  $\mu$ l；Splitless mode；所用之積分儀為 SP-4290 機型。

作 GC/MS 分析之樣品送往中央研究院生醫所，其所用 MS 為 HP 5988A MS 機型，Electron-impact, ionization 70 eV; Carrier gas: He (10 psi); 所用管柱為 Ultra-1, 25 m×0.32 mm i.d.; 0.52  $\mu$ m Film thickness 之 Fused silica capillary column。各項溫度為: Injection port: 250°C; Column port: 50°C (1 min), 以 4°C/min 之階進溫度提高速度至 300°C 為止; 注射量為 1.5  $\mu$ l; 採 Split mode; Scan time: 0.25 sec; 其 NBS mass spectral library search system 為 43,000 參考化合物。

有關樣品之鑑定，我們採用三種方法進行：

- (1) Internal standard method。
- (2) Retention indices method (滯留指數法)。
- (3) GC/MS 分析鑑定。

### 三、結果與討論

#### 1. 小型空氣採樣器 (Handy sampler)

##### (1) 燃燒石油產物之模擬實驗：

- (a) 柴油：柴油在模擬燃燒爐中燃燒後，產生大量氣體及半徑大小不一之顆粒，圖 5(A) 及圖 5(B) 分別為柴油之 GC 及 FTIR 圖譜，由 GC 圖譜上可看出柴油內之成份繁多，包含許多低沸點及高沸點的物質，而其 IR 圖中則顯示柴油中除含有大量之飽和碳氫化合物 ( $1,380\text{ cm}^{-1}\sim 1,480\text{ cm}^{-1}$ ) 外，亦含有相當豐富之芳香族化合物 ( $620\text{ cm}^{-1}\sim 820\text{ cm}^{-1}$  為  $-\text{CH}$  之 Out-of-plane bending mode)，圖 6(A)，圖 6(B) 及圖 6(C) 為在模擬燃燒爐中三個不同位置（爐頂，濾片及集氣瓶）所得到之萃取物的 GC 圖譜，可以很清楚的看出它們之間的不同。在爐頂及濾片上所得到的均是黑色顆粒，分別刮下來之後以環己烷萃取，若比較它們的 GC 圖譜，可以知道在爐頂上所收集到的是沸點較高，分子量較大的化合物（圖 6(A)）；而在濾片上所得到的物質，不論在沸點或分子量均次於爐頂上所得到的物質（圖 6(B)），在集氣瓶上所得到的則為低沸點及低分子量之物質（圖 6(C)），由此圖中，我們亦可看出使用 Rotary evaporator，並不會使低沸點或揮發性高的物質損失，若把圖 6(C) 與圖 5(A) 相比較，我們亦可看出柴油在燃燒後會產生較多低沸點的物質，至於高沸點之物質（在爐頂及濾片上所收集的物質），由於它們出現的波峰析離程度比未燃燒前的高，這可能與柴油中各組成份在燃燒時的反應機構有關，由 FTIR 圖上可以很明顯的看出燃燒



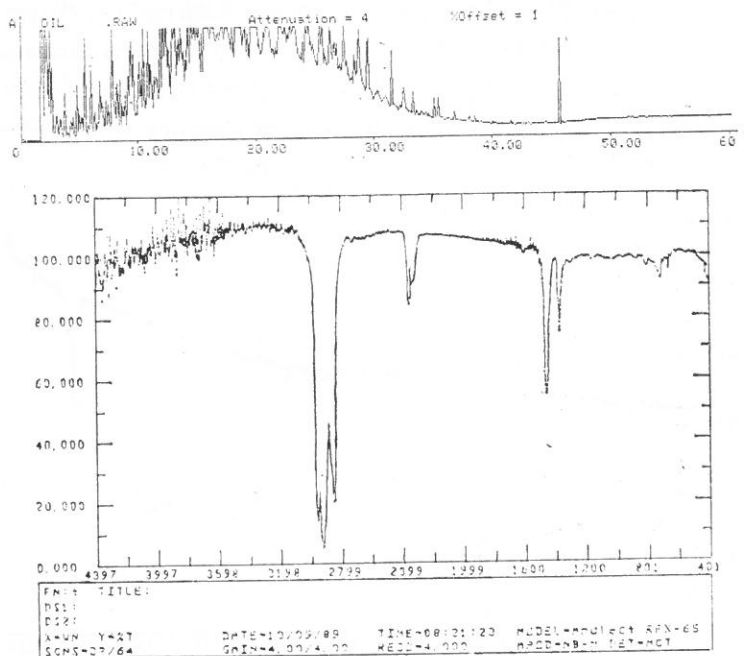


圖 5 (A) 柴油之 GC 圖譜。  
(B) 柴油之 FTIR 圖譜。

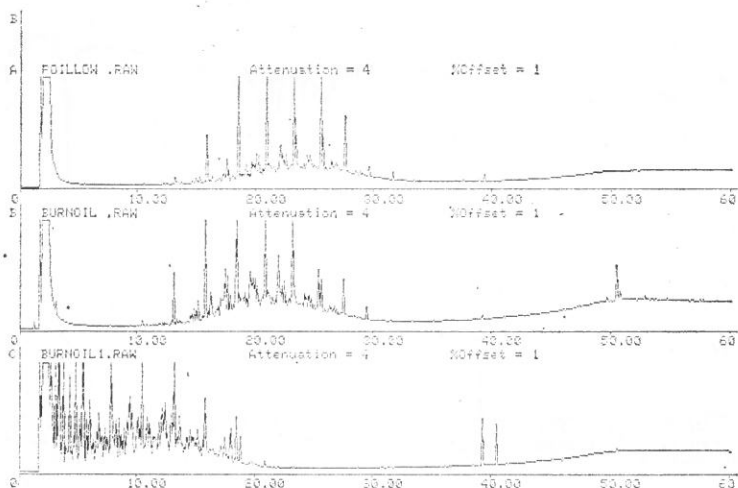


圖 6 (A) 柴油燃燒後於爐頂所收集之物質之 GC 圖譜。  
(B) 柴油燃燒後於濾片所收集之物質之 GC 圖譜。  
(C) 柴油燃燒後於集氣瓶所收集之物質之 GC 圖譜。

前後其組成物結構之改變。如：本來在  $1,380\text{ cm}^{-1}\sim 1,480\text{ cm}^{-1}$  的兩強烈吸收帶幾乎完全消失，彼等為 C-H bending vibrations，由此現象可推測柴油中之飽和烴燃燒時會裂解成較小的化合物。另一方面，圖中之 C-H out-of-plane bending mode ( $900\sim 675\text{ cm}^{-1}$ ) 則有增強之趨勢（圖 7(A) 及圖 7(B)）。

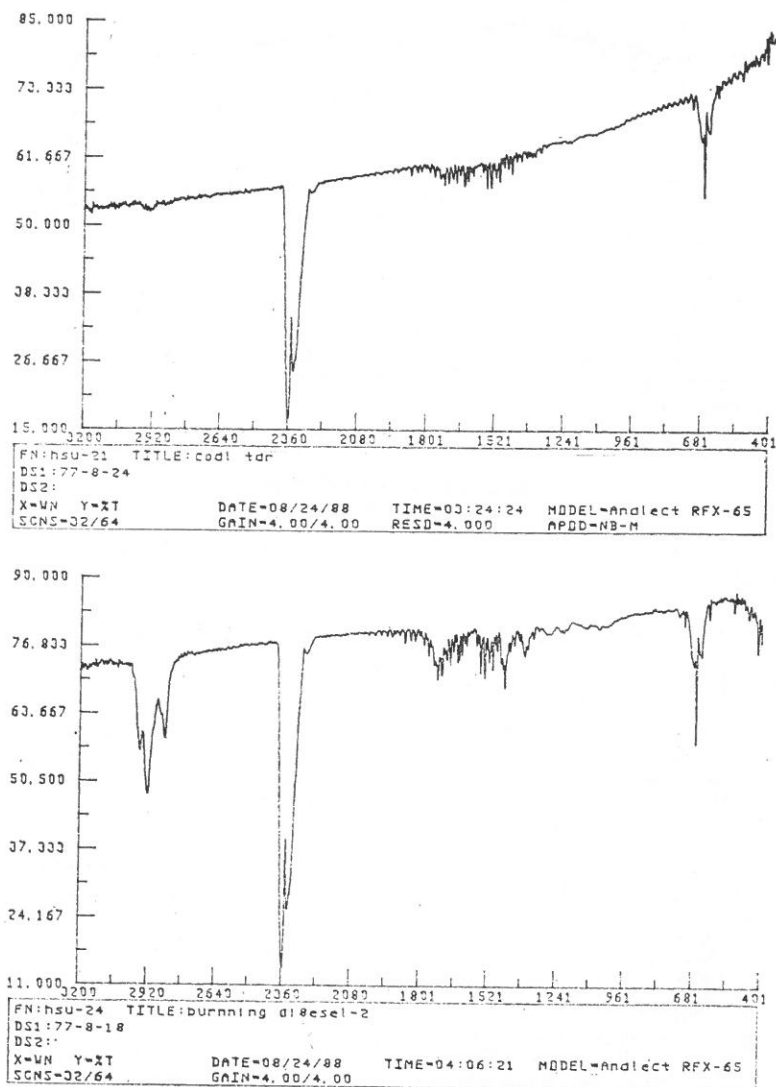


圖 7 (A) 柴油燃燒後在爐頂上所收集物質之 FTIR 圖譜。

(B) 柴油燃燒後在集氣瓶上所收集物質之 FTIR 圖譜。

(b) 汽油：圖 8(A) 及圖 8(B) 為二行程機車所使用之汽油的 GC 及 FTIR 圖譜，若比較汽油與柴油在結成物分佈上之不同（圖 8(A) 與圖 5(A)），可以看出汽油所含之成份較柴油的少，且多為分子量較低之物質，由汽油之 FTIR 圖（圖 8(B)）中亦可看出其中不乏芳香族的化合物（ $620\text{ cm}^{-1} \sim 820\text{ cm}^{-1}$ ），圖 9(A)，圖 9(B) 及圖 9(C) 為汽油在模擬燃燒爐中燃燒後在不同的三個位置上（爐頂，濾片及集氣瓶中）所得到的萃取物的 GC 圖，物質分佈的情形大致與柴油燃燒後的三部分 GC 圖相同，即在爐頂所得到的為分子量最大及沸點最高的物質；濾片上所得到的為其次；而在集氣瓶中所得到的則為分子量小且沸點低之物質，在爐頂及濾片上所收集到的物質（圖 9(A) 及圖 9(B)）為分子量及沸點高的物質，此類物質在汽

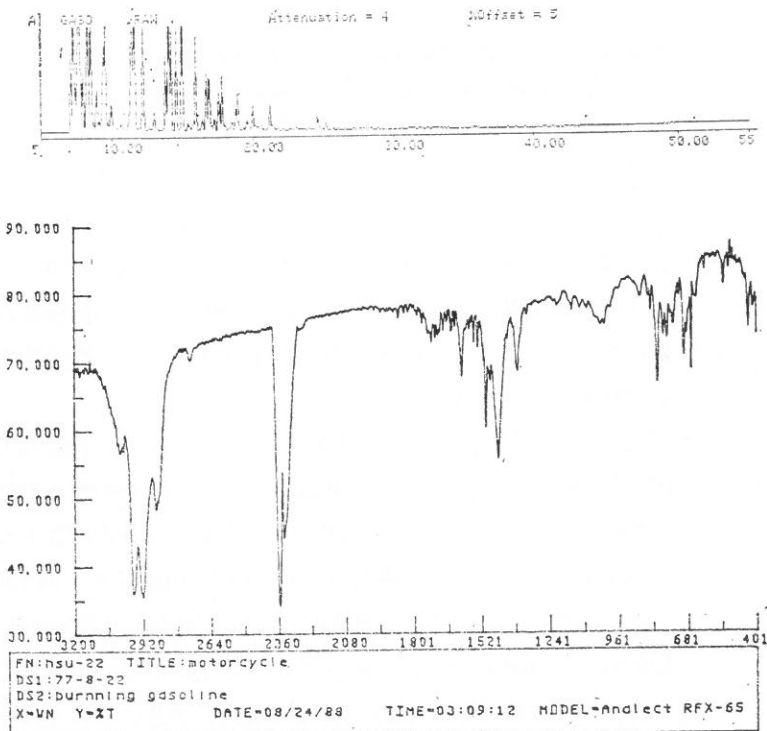


圖 8 (A) 二行程機車所使用之汽油的 GC 圖譜。

(B) 二行程機車所使用之汽油的 FTIR 圖譜。

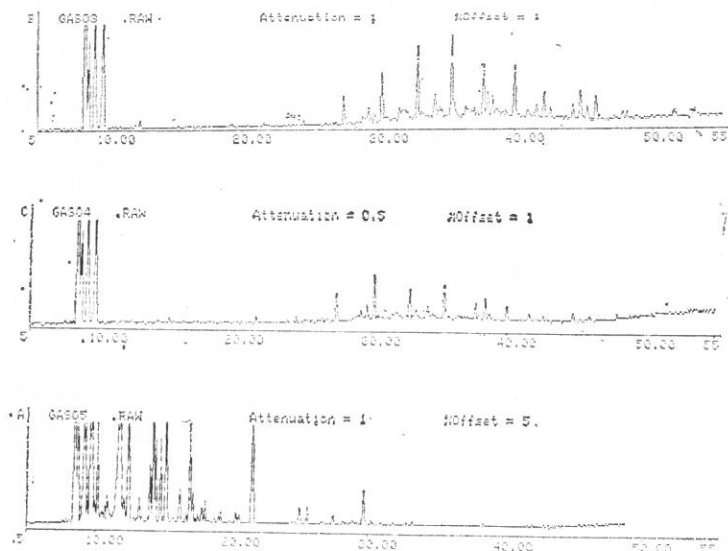
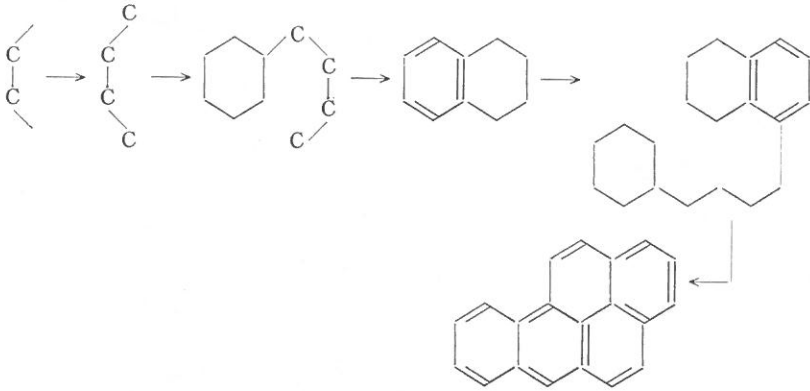


圖 9 (A) 汽油燃燒後於爐頂收集到的物質的 GC 圖譜。  
 (B) 汽油燃燒後於濾片收集到的物質的 GC 圖譜。  
 (C) 汽油燃燒後於集氣瓶收集到的物質的 GC 圖譜。

油本身並不存在 (圖 8(A))，此外，圖 11(A)，圖 11(B) 及圖 11(C) 的 FTIR 圖譜中亦可看出位於  $1,480\text{ cm}^{-1}$  附近的吸收帶明顯的增強 (此為  $\pi$  之 Ring stretching mode)，所以汽油在燃燒後亦會產生頗豐之芳香族化合物。

- (c) 正己烷：把正己烷作如上述的燃燒，取其三部份分析，發現其 GC 圖 (圖 10(A)，圖 10(B) 及圖 10(C)) 上的分佈情形與汽油較類似，燃燒後在集氣瓶中的物質種類較少，但分佈之範圍則較廣，再由 *n*-hexane 燃燒前後的 FTIR 圖譜中 (圖 12(A)，圖 12(B)，圖 12(C) 及圖 12(D))，可以看出在燃燒後的三部份物質中， $620\text{ cm}^{-1} \sim 820\text{ cm}^{-1}$  及  $1,460\text{ cm}^{-1}$  附近均有非常明顯的強烈吸收帶，可見單純的直碳鍊化合物在燃燒後會產生相當豐富的芳香族化合物，其中更不乏許多高沸點及分子量大的物質，這個結果也可以證實 Badger 等人<sup>(1)</sup>所提示有關 Benzo (a) pyrene 的生成機構：



Benzo (a) pyrene 在臨床上已被確認為致癌物，Badger 所提出之上述機構是對所有含有 C-C 的化合物而言，亦即只要含有 C-C 的化合物在燃燒時都有可能形成多環的芳香族化合物，此種情形在燃燒不完全的情況下更甚。

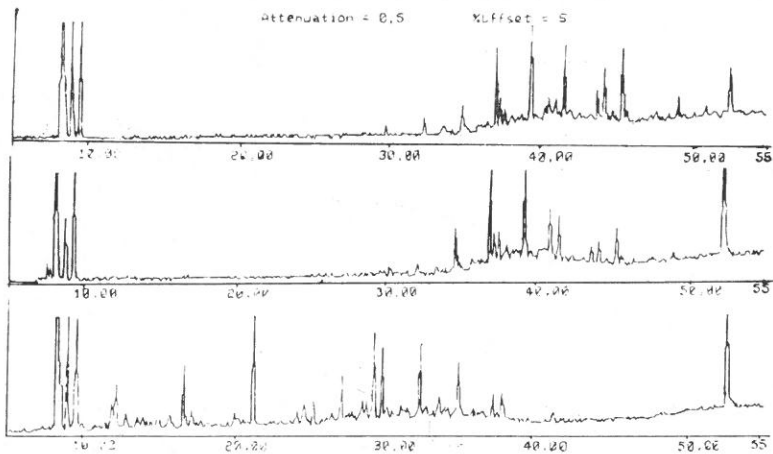


圖10 (A) 正己烷燃燒後於爐頂所收集物質之 GC 圖譜。  
 (B) 正己烷燃燒後於濾片所收集物質之 GC 圖譜。  
 (C) 正己烷燃燒後於集氣瓶所收集物質之 GC 圖譜。

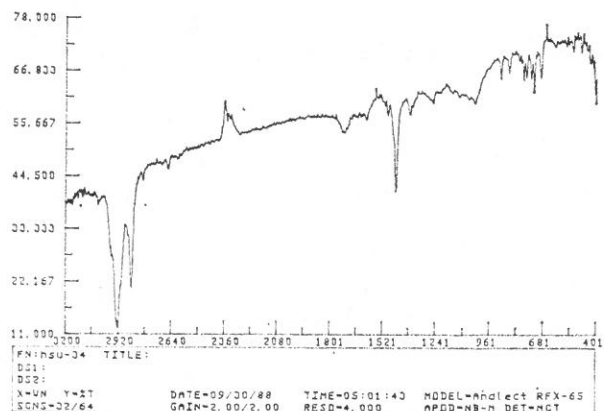
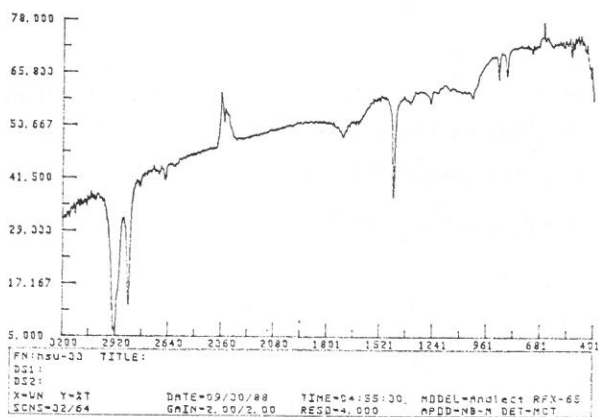
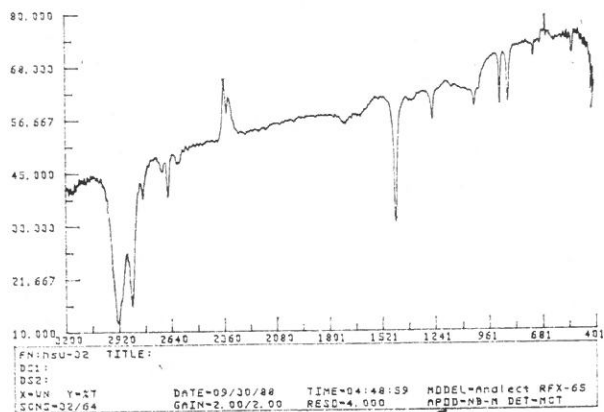


圖11 (A) 汽油燃燒後於爐頂所收集物質之 FTIR 圖譜。  
 (B) 汽油燃燒後於濾片所收集物質之 FTIR 圖譜。  
 (C) 汽油燃燒後於集氣瓶所收集物質之 FTIR 圖譜。



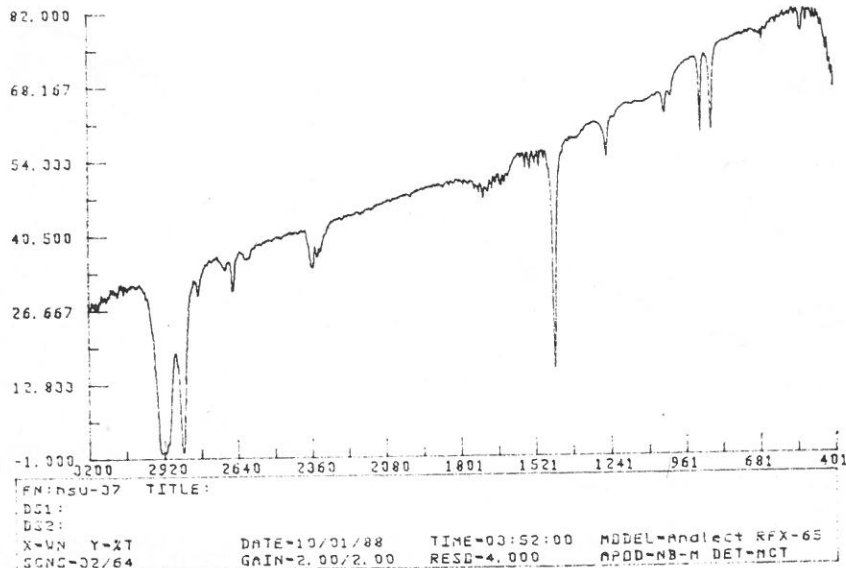
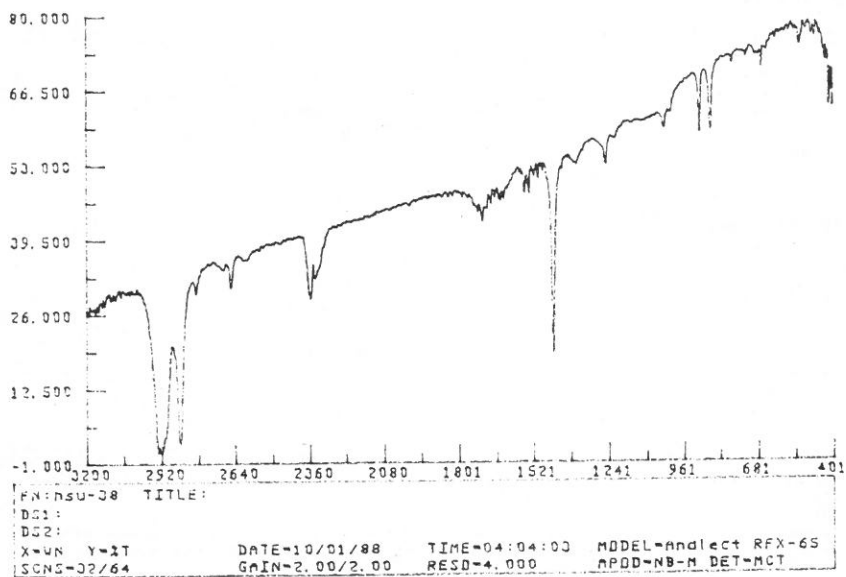


圖12 (A) 正己烷燃燒後在爐頂所收集物質之 FTIR 圖譜。

(B) 正己烷燃燒後在濾片所收集物質之 FTIR 圖譜。

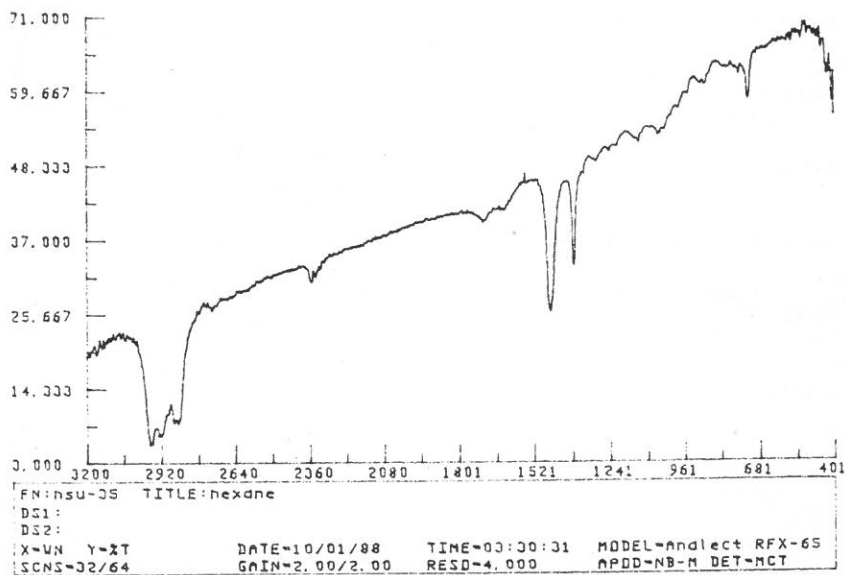
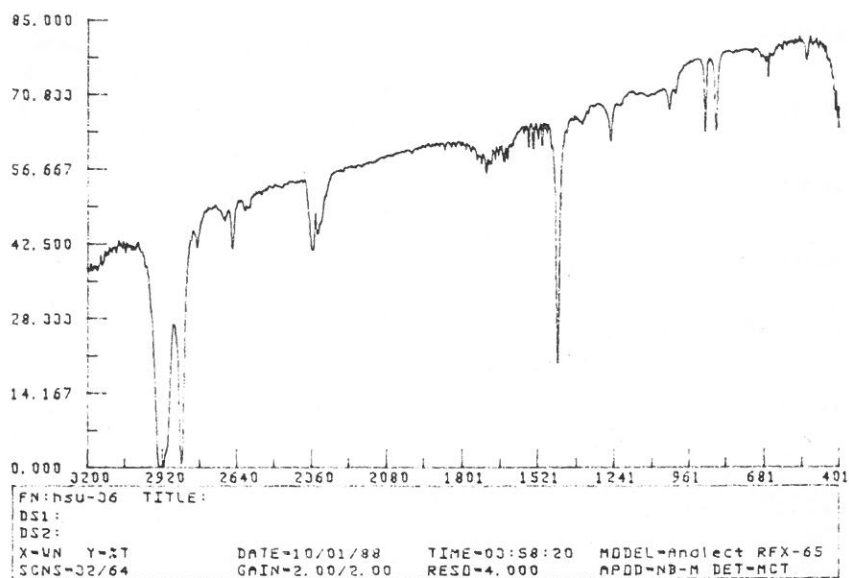


圖12 (C) 正己烷燃燒後在集氣瓶所收集物質之 FTIR 圖譜。

(D) 正己烷之 FTIR 圖譜。

若將柴油，汽油及正己烷燃前後的 GC 圖譜作一比較，會發現汽油與正己烷在燃燒過程中會合成分子量較大的物質（其中又以正己烷較明顯）；而柴油本身由於已含有相當多分子量較大及高沸點的物質，所以在燃燒過程中由小分子碳氫化合物組成較大分子量的現象較不顯著，相反的，裂解現象會較明顯。

再者，當我們在燃燒上述三個不同物質時（柴油，汽油及正己烷），發現柴油在燃燒時的溫度最低，汽油次高而正己烷的最高，這可能是造成柴油在燃燒過程中裂解成較多分子量小且沸點低的物質的主要原因。而汽油及正己烷由於在燃燒時的溫度較高，因此較易產生自由基，可隨意組合成較穩定的化合物。於是我們推測，在實驗室內的模擬燃燒過程中若碳氫化合物的燃燒熱愈大，則有利於形成高分子量及高沸點的物質易裂解為低分子量及低沸點的物質。

- (2) 採集二行程機車在開動時所排放的廢氣：汽油或柴油在交通工具內燃燒的情形與在實驗室內的模擬燃燒不盡相同，我們預測石油產物在內燃機燃燒後所產生的物質會包含我們在實驗室內所收集的三段不同的物質，我們用 Handy sampler 收集兩部不同機車（註）在開動後所排放出的廢氣，其 FTIR 圖分別為圖 13(A) 及圖 13(B)。若把它們與未燃燒前的汽油（圖 8(B)）相比較，可以很清楚的看出在排出的廢氣中含有較多的芳香族化合物，圖 14 為機車所排出廢氣的 GC 圖，若把它與圖 8(A) 相比較，我們更可以肯定地說：汽油在燃燒後會產生分子量較大的物質。

我們對上述各項樣品只作一整體性的分析討論，由於樣品中組成物質繁雜，未能一一鑑定，有關空氣中懸浮粒子有機污染物之鑑定則在本文下半段敘述之。

- (3) 由於收集柴油在真正內燃機燃燒後所排放的廢氣的技術尚未突破，因此我們沒有做有關這方面的分析。

## 2. 大型空氣採樣器

經過多次採集空氣樣品之結果顯示：GFF 的 TSP 在 NFA 及 WPFA 兩個不同的編號系列中，其重量分佈分別為 0.2798~0.8053 克及 0.2203~0.4078 克，我們是隨意方式採樣，採樣時間為 24 小時，採樣地點主要是在臺北新莊輔仁大學校門口及臺北民權西路與重慶北路交界之加油站附近。輔仁大學正門與後門均面對省道，交通繁頻，加上附近大小工廠林立，實為空氣採樣佳區，而加

註：機車 A 為民國七十年出廠，排氣量 90 cc 之二行程機車。

機車 B 為民國七十三年出廠，排氣量 125 cc 之二行程機車。

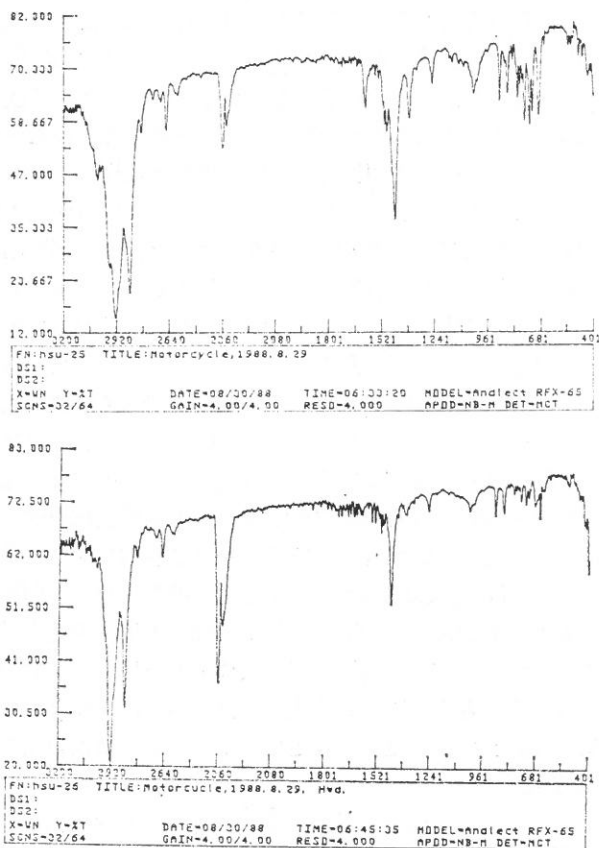


圖13 (A) 機車A排放廢氣之 FTIR 圖譜。

(B) 機車B排放廢氣之 FTIR 圖譜。

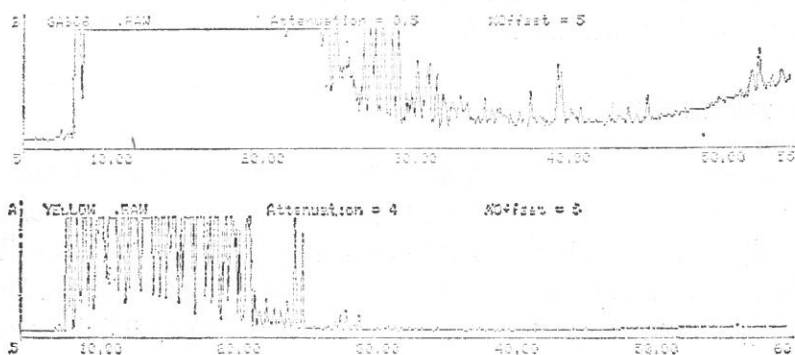


圖14 (A) 機車A所排放廢氣之 GC 圖譜。

(B) 機車B所排放廢氣之 GC 圖譜。

油站附近所採之樣品一定會含有由交通工具所排放之廢氣，預測會有為數不少之 PAHs。故此二採樣主要地區之選擇實具有相當的代表性。

試驗過五種不同密度之 PUF 後，我們最後選定密度為  $37.8 \text{ kg/m}^3$  之白色 PUF，因經過相同之清潔步驟之後，它在 GC 圖譜上所呈現的波峯數目最少，在一切的實驗過程中，完全不使用任何的潤滑劑或塑膠產品，以減少不必要之污染。

由於我們所要分析的對象是以 PAHs 為主，它們是無極性或微極性之化合物，故在管柱上的選擇亦以無極性系列為主，我們所採用的為 SE-54，SPB-5 或 DB-5 三種不同的管柱，610-M PAHs 混合標準物在 Inject temperature 為  $230^\circ\text{C}$  時之 GC 圖如圖 14 所示，其所含不同之 PAHs 成份皆逐一出現於圖譜中，故於日後分析時，該項溫度即設定為  $230^\circ\text{C}$ ，就管柱階進提高之速度曾試過每分鐘  $3^\circ$ ， $4^\circ$ ， $5^\circ$  及  $6^\circ\text{C}$  等四種速度，最後以不影響解析度，且節省時間為原則，選定  $4^\circ\text{C/min}$  為階進提高溫度之速度。

經萃取，濃縮及過濾後的樣品溶液，可以 GC/FID 作初步之分析，圖 15 為採樣前後 PUF 之 GC 圖譜，圖 15(A) 為經過清潔步驟後之 PUF，可以看出在最後的環己烷溶劑內仍含有少量的雜質，但這些雜質對於 PUF 所吸附的空氣中的有機污染物並沒有造成很嚴重的干涉（圖 15(B)）。圖 16(A) 為沉積在 GFF 上的空氣中懸浮粒子之萃取液的 GC 圖，而圖 16(B) 則為在 PUF 上所吸附到的空氣樣品，比較後，可以知道 PUF 能吸附一些揮發性比較大的物質，由 GFF 所收到的則為分子量較大的物質，故把 PUF 與 GFF 一起採樣會收相輔相乘之效，會比單獨使用 GFF 的效果好。

圖 17 為編號為 P3A0401 空氣樣品之 RIC (Reconstructed Ion Current) 圖，為避免訊號之損失，不能忽略圖中之微小波峯，所以，我們採用下列條件：

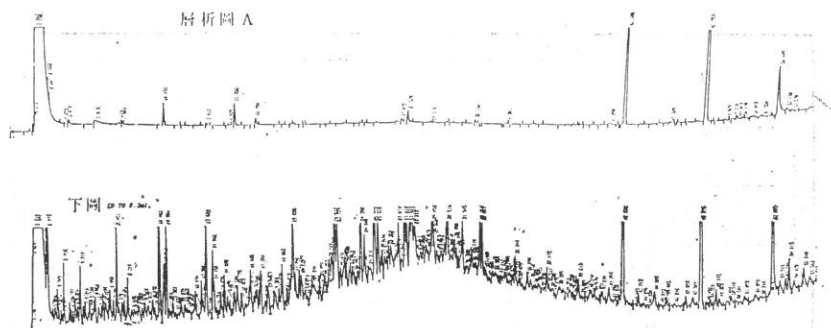


圖15 (A) PUF 空白試驗之 GC 圖。

(B) 在 PUF 中所萃取出來的空氣中有機污染物之 GC 圖。

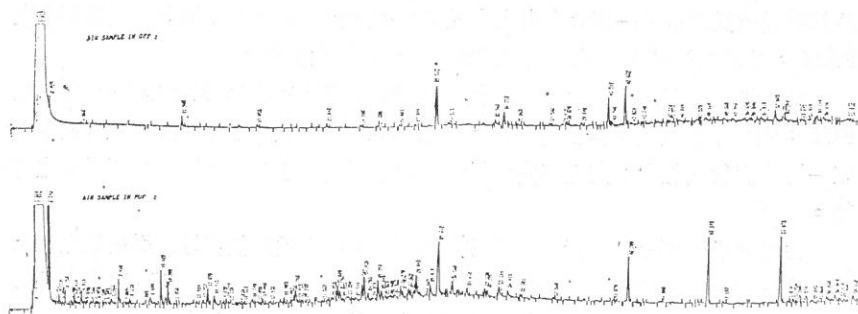


圖16 (A) 在 GFF 上懸浮粒子萃取液之 GC 圖。

(B) 在 PUF 內有機污染物萃取液之 GC 圖。

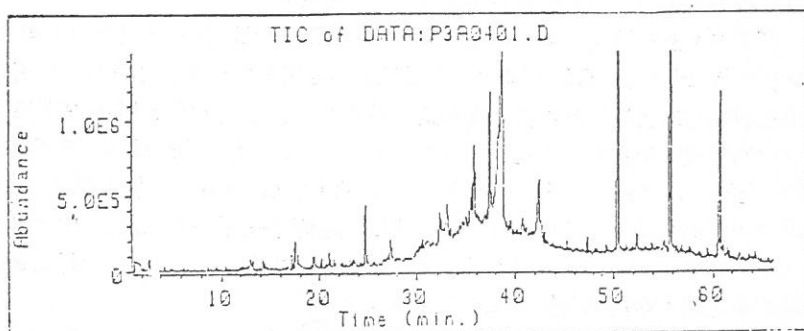


圖17 在 PU 泡綿中的空氣中有機樣品，編號為 P3A0401 之 GC/MS 的 IC 圖。

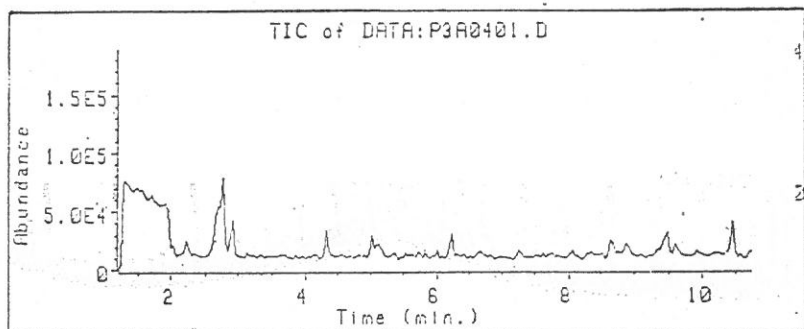


圖17(A) 為圖 11 中 0~10 min 放大圖。

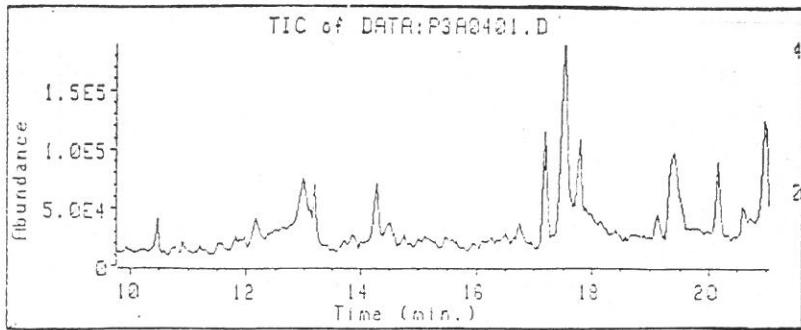


圖17(B) 爲圖 11 中 10~20 min 放大圖。

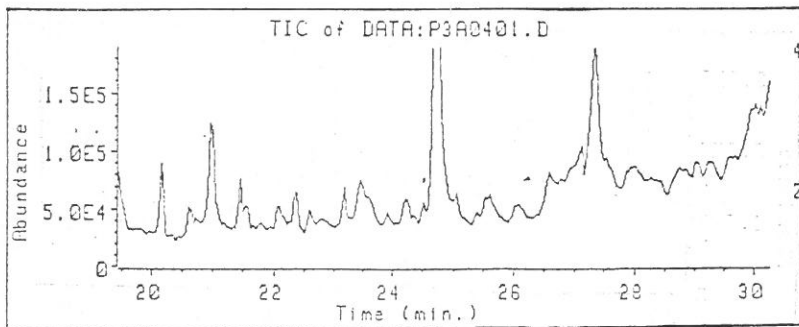


圖17(C) 爲圖 11 中 20~30 min 放大圖。

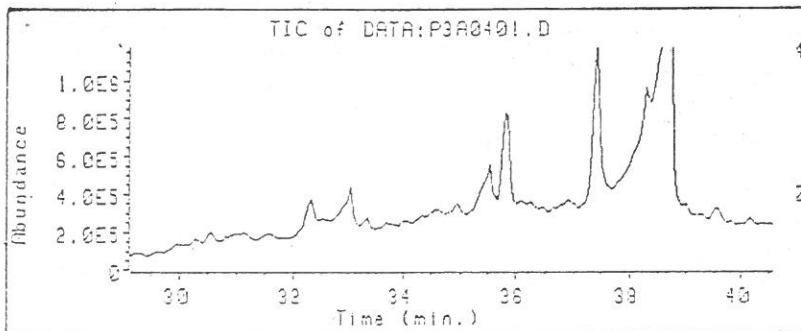


圖17(D) 爲圖 11 中 30~40 min 放大圖。

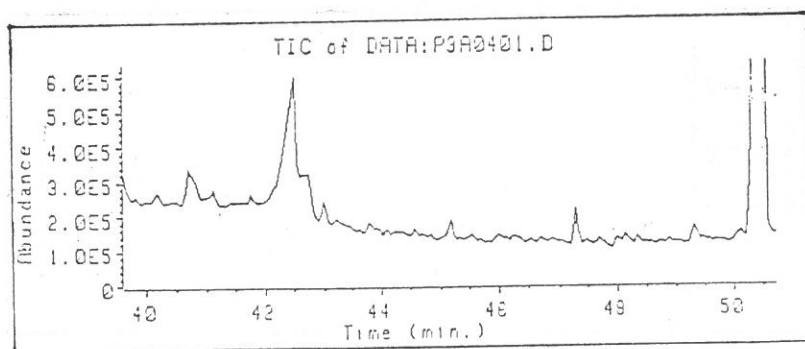


圖17(E) 為圖 11 中 40~50 min 放大圖。

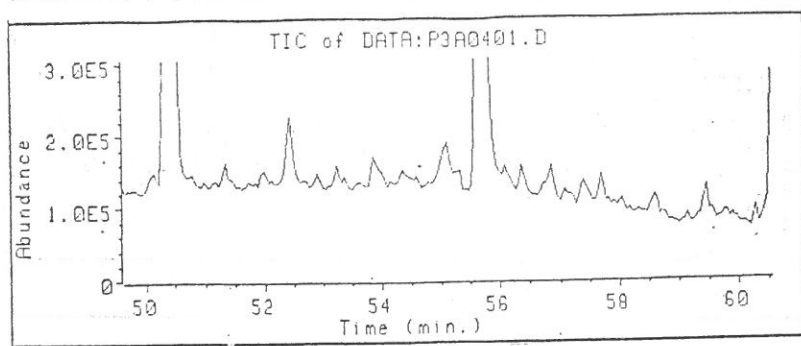


圖17(F) 為圖 11 中 50~60 min 放大圖。

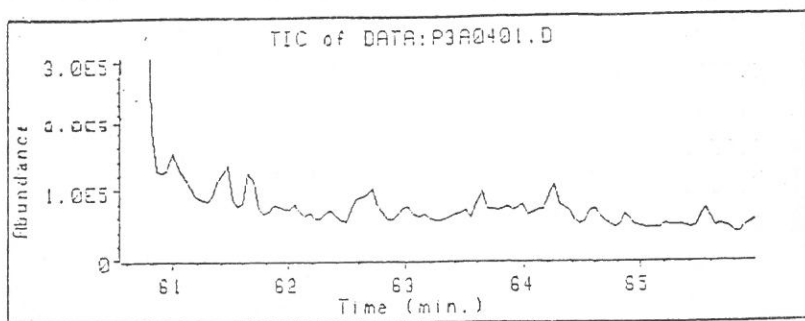


圖17(G) 為圖 11 中 60~65 min 放大圖。



- (1) MS 之 Scan time 以 0.25 sec 為宜，此乃比較 6，5，0.5 及 0.25 sec 之結果。
- (2) 區部放大圖形之設施（如圖 17(A) 至圖 17(G) 為在不同時段內的放大圖）；再有耐心的一一去做 Library search 的工作，便不致於今失去許多訊號，而使 Library search 的結果能更有效的反應樣品中所含各成份之化合物的名稱。

我們鑑定樣品的其中一個方法為滯留指數法 (Retention Indices Method)，這是一種線性回歸法，根據 M. L. Lee<sup>(3)</sup> 等人在文獻上的報導，可以利用下式計算出兩百多種不同 PAHs 之 R. I.：

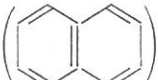

$$I = \frac{T_{R(S)} - T_{R(CZ)}}{T_{R(CZ+1)} - T_{R(CZ)}} + 100Z$$

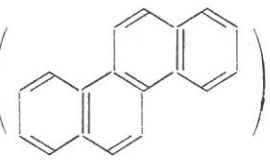
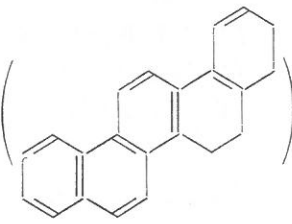
$T_{R(S)}$ ：樣品中某一成份之滯留時間

$T_{R(CZ)}, T_{R(CZ+1)}$ ：特定  $T_{R(S)}$  前、後標準樣品之滯留時間

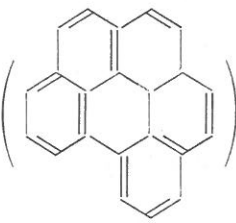
$C_Z, C_{Z+1}$ ：特定  $T_{R(S)}$  前、後標準樣品之環數

如欲以上述程序算出空氣樣品中各成份的滯留指數，尚須四種標準物質作為

參考物質，計為 Naphthalene ()，Phenanthrene ()

，Chrysene () 及 Picene ()

，它們的 PAHs 滯留指數分別訂為 200，300，400 及 500，由於 Picene 昂貴且不易獲得，故 Rostad<sup>(4)</sup> 提議用 R. I. 與 Picene 相近且便宜易得之

Benzo (ghi) perylene () 來代替，PAHs 之 R. I. 為一固定

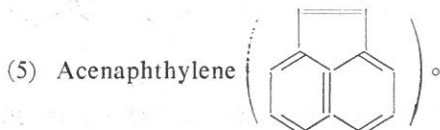
之常數，在同一類型的管柱中，不受 GC 之溫度及流速之影響，在 PAHs 標準樣品無法一一得到的情形之下，R. I. 實為一良好之鑑定準繩，可藉它來區別 GC/MS 所不能區分之同分異構物（如 Fluoranthene 及 Pyrene 有相同之 MS

圖，彼等之  $m/e=202$ ，但它們的 R. I. 則分別為 344.01 及 351.22)。

圖 18 為  $P_3A_{0.461}$  樣品中某一成份之質譜圖（最上層者），中間有四個質譜圖：第一個為上圖之縮小圖，而第二至第四的質譜圖則為 Library search 的結果，取其相似比率（Purity）最高的三個化合物名稱，底部為報表，列出與該樣品某成份最為相似的十個化合物的名稱及它們的相似比率，而該圖名稱所示的化合物名稱乃依據兩種以上之鑑定方法所得出之結論，即除了 GC/MS 之外，再加上 Internal standard method 或 Retention indices method 加以鑑定之綜合結果，如在圖 18 中，為同分異構物之 Azulene 及 Naphthalene 兩化合物在 Library search 的結果，與該樣品在特定時間內（Scan time=13.183 min）的特定成份，兩者在相似比率上分居首位與次位，但由於 GC/MS 中的 MS 無法區別同分異構物，故我們再以單一 Naphthalene 之標準樣品，經 Internal standard method 加以鑑定，即知該成份應為 Naphthalene 而非 Azulene。甚至於再以 M. L. Lee<sup>(3)</sup> 等人所提之 R. I. 法，對 Azulene 及 Naphthalene 再加以探討；知 Naphthalene 在 R. I. 比 Azulene 少 19.95；所以 Naphthalene 在層析圖上會先出現，由以上三種不同方法鑑定之結果，我們可以肯定該成份為相似比率居次位之 Naphthalene 而非居首位之 Azulene，故 Naphthalene 便成為圖 18 之名稱。

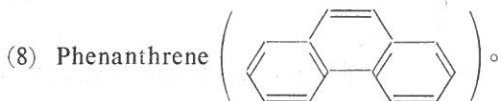
在我們所分析過的空氣樣品中，以上述方法（GC/MS 與 R. I. 或 GC/MS 與 Internal standard method）所鑑定出的常見物質如下：

- (1) Naphthalene。
- (2) 1, 1'-Biphenyl。
- (3) Naphthalene, 1-Ethyl or Naphthalene, 2-Ethyl。
- (4) Naphthalene, 1, 3-Dimethyl。

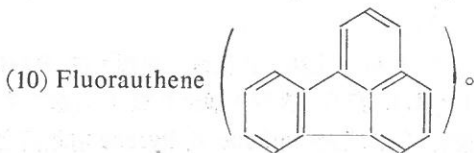


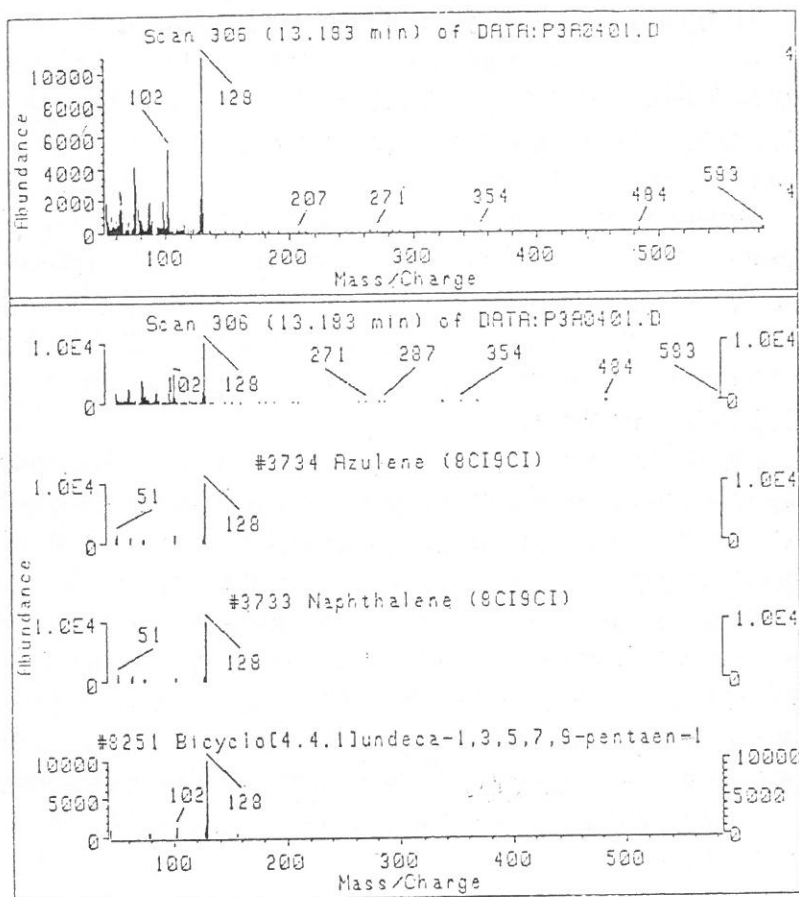
- (6) Naphthalene, 2, 3, 6-trimethyl。

- (7) 9H-Fluorene。



- (9) 1, 2-Benzenedicarboxylic acid, Butyl 2-methyl (di-butyl phthalate)。





## LIBRARY SEARCH RESULTS

Scan 306 (13.193 min) of DATA:P3A0401.D

Library File: NBS\_REVE.L

Library name: NBS MASS SPECTRAL DATABASE

|  | CAS #    | Library Index # | Match Quality |
|--|----------|-----------------|---------------|
| 1: Azulene (8CI9CI)                              | 275514   | 3734            | 8592          |
| 2: Naphthalene (8CI9CI)                          | 91203    | 3733            | 8358          |
| 3: Bicyclo[4.4.1]undeca-1,3,5,7,9-pentaen-1      | 36828005 | 8251            | 8051          |
| 4: 1H-Indene, 1-methylene- (9CI)                 | 2471843  | 3735            | 6235          |
| 5: 1,2-Benzenedicarbonitrile (9CI)               | 91156    | 3752            | 7707          |
| 6: 1,4-Benzenedicarbonitrile (9CI)               | 623257   | 3753            | 7375          |
| 7: 1,3-Benzenedicarbonitrile (9CI)               | 626175   | 3754            | 7636          |
| 8: Cyclohexanecarboxylic acid, 1-(1,1-dimethyl-) | 27334436 | 12715           | 7568          |
| 9: Fyridine, 3,3'-(1a,2,7,7a-tetrahydro-1,2      | 50557665 | 27788           | 7552          |
| 10: Benzene, 1-chloro-3-ethoxy- (9CI)            | 2555836  | 8360            | 7311          |

圖18 Naphthalene 之質圖譜。

(11) 1, 2-Benzene dicarboxylic acid, Di-isooctyl (di-isooctyl phthalate)。

由上列化合物中，我們確知 PAHs 存在於我們生活的空間內，但大部份是兩環的 Naphthalene 及其衍生物，亦有環數小於四的 PAHs，此與 K. E. Thrane 及 A. Mikalsen<sup>(5)</sup> 等人在挪威南部所採收之空氣樣品內含高環之 PAHs，如 Benzo (ghi) perylene 大不相同。

我們曾經把市面上所購得之柴油以 Benzene : *n*-hexane = 1 : 1 (v/v) 之混合溶劑，經 TLC 分離中柴油中的芳香族化合物，發現其中亦以 Naphthalene 及其衍生物為主要成份，與我們所採收的空氣成份吻合，輔仁大學旁邊為一客運車站，我們在校門口所採集的空氣中沒有較高環的 PAHs，可能是因為在廣大的空間中，PAHs 的濃度太稀薄，而且，大氣中實被其它濃度較高的物質所污染，故沒有偵測到微量之高環 PAHs。

我們發現在輔大校門口所採收的空氣樣品中，均含有相當多之鄰苯二甲酸酯類的化合物，而在臺北加油站附近所採收到的空氣樣品中並沒有此類化合物，在分析空氣樣品之前，曾注射純的環己烷溶劑入 GC 內做空白試驗，結果顯示在溶劑及 GC 內並沒有被此類化合物所污染，它確是存在於空氣樣品中，可知新莊輔大附近的空氣確實是被鄰苯二甲酸酯類的化合物所污染。疑為附近燃燒垃圾或工廠廢氣未回收完全所致，此類物質為塑膠工業上所用的可塑劑(Plasticizers)，由於與塑膠本身沒有真正的化學鍵結，易脫離塑膠而逃逸到大氣中，在此處要提醒的是：Di-isooctyl phthalate 對動物有致癌性，我們應該力求使用該成份之工業界人士，必需加強防止該類物質外洩於大氣中而污染空氣，影響國民的健康。

在本研究中所收集到的空氣中有機污染物，雖種類繁多，但大致上仍可歸納成三大類：

- (1) 一般碳氫化合物及其衍生物：如 Octadecane, 1-Chloro, 1-Heptanol, 2-Propyl。
- (2) 鄰苯二甲酸酯類：如 Di-butyl phthalate 及 Di-isooctyl phthalate。
- (3) 芳香族化合物類：
  - (a) 苯及苯的衍生物：如 Benzene, 1, 5-Cyclohexadien-1-yl。
  - (b) 雜環類：如 1-H-pyrrole-2, 4-diphenyl。
  - (c) 多環芳香族化合物類：如 Naphthalene 及其衍生物 Fluoranthene 等。

由於汽油在模擬燃燒爐中燃燒後所得出的物質分佈之情形與我們採集機車所排放出來的廢氣結果大致相似，所以，若柴油在真正的引擎內燃燒後的結果亦與我們在模擬燃燒爐的結果相似的話，則我們在校門口（客運站旁）所收集的空氣污染物內不含高環之 PAHs 是不容置疑的。

## 參 考 文 獻

- (1) G.M. Badger, R.G. Buttery, R.W.L. Kimler, G.E. Lewis, A.G. Moritz and I.M. Napier, *J. Chem. Soc.*, 2449 (1958).
- (2) W.P. Lee, C.S. Chu, F.H. Wen and J.S. Lai, *Fu Jen Studies*, **19**, 69 (1985).
- (3) M.L. Lee, D.L. Vassilaros, C.M. White and M. Novatny, *Anal. Chem.*, **51**, 786 (1979).
- (4) C.E. Rostad and W.E. Pereira, *HRC&CC*, **9**, 328 (1986).
- (5) K.E. Thrane and A. Mikalsen, *Atmos. Environ.*, **15**, 909 (1981).

## Analysis of Polynuclear Aromatic Hydrocarbons (PAHs) in Petroleum Products and Air Particulates

YUE-JAU YEH, KWO-FENG HSIAO

AND WAI-PING LEE

Department of Chemistry  
Fu Jen Catholic University

### ABSTRACT

Pollution in the natural environment caused by polycyclic aromatic hydrocarbons (PAHs) is becoming a serious problem. Diesel fuel and gasoline are studied before and after combustion in a simple simulated combustor. A modified hi-volume sampler is used for sampling: glass fiber filter (GFF) and polyurethane foam (PUF) are placed in the sampler at the same time. GFF is for the measurement of the total suspended particles (TSP) and PUF is for the more volatile compounds. The main analytical instruments used in this research are the Fourier transform infrared spectrometer (FTIR), gas chromatograph (GC) and gas chromatograph/mass spectrometer (GC/MS).



# 自動化多功能實驗卡

汪彥緯 陳壽椿

化 學 系

## 摘 要

本文將一般的資料量測介面卡，重新設計並擴充功能，成為一套適用於化學實驗室的資料收集與控制系統。16 channels、16 bits 的類比至數位轉換系統，2 channels、16 bits 的數位至類比轉換系統，並配合儀器放大器做 0.25 至 1,000 倍放大，以及在  $\pm 10$  伏特之間的信號位準 (Signal conditioning) 亦可調整。系統電路中也加入 potentiostat，以利電化學的分析。另外亦納入 FIA 的驅動及偵測電路。

## 一、前 言

隨着電子及資訊的蓬勃發展和個人電腦的快速普及化，自動化的需求已快速地走進實驗室。Faulkner<sup>(1)</sup> 等人就在文獻中明白地指出，本世紀已進入化學儀器的電子時代，而在量測方式中，電子化已被視為主要的媒介在另一方面 Kowalski<sup>(2)</sup> 等人所著的計量化學 (Chemometrics) 中，指出如今的分析化學已進入資訊化學 (Information science) 的領域，分析化學家更須具備數學、統計及電腦科學的知識。例如利用電腦的高速度及資料收集和控制系統，來收取大量且多種類的化學資訊；再應用計量化學中的訊號處理方式，使資料的品質達到最佳化 (Optimization)；而其中的檢量法 (Calibration)<sup>(3)</sup> 更是利用 MLR (Multiple Linear Regression)，PCR (Principal Component Regression)，及 PLS (Partial Least Square Regression) 等基本工具來解析電化學中波峰重疊的問題；最後，配合人工智慧 (Artificial intelligence) 中的圖形辨識 (Pattern recognition) 和專家系統 (Expert systems)，則可初步達到以專家的眼光來辨別大量化學資訊的自動化系統。

## 二、方塊圖描述

圖 1 為本文將介紹的自動化系統方塊圖，亦是自行設計組合之硬體設備。

### 1. 電源部份

電腦電源是切換式的 (Switching)，因此產生的雜訊和漣波 (Ripple) 會影

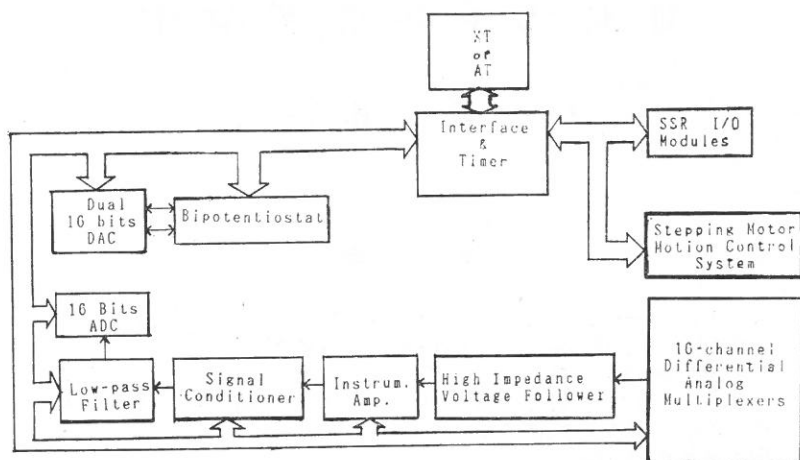


Fig. 1. Laboratory card block diagram.

響資料收集系統的品質，而採用獨立電源就可避免其干擾。在交流電源線上加裝電源濾波器，消除外界雜訊，同時使用高精密、低雜訊的 AC/DC 轉換器<sup>(4)</sup>，以獲得良好品質的電源，而達到高精確度的量測。另外，步進馬達的電源亦是獨立的，以免互相干擾，見圖 2。

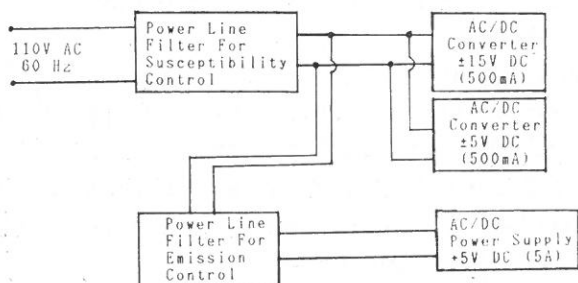


Fig. 2. Power supply block diagram.

## 2. 數位介面部份

此單元為電腦介面電路，解碼的邏輯元件採用高速、省電的 HCMOS<sup>(5)</sup> 積體電路，另外亦配合 PPI (Programmable Peripheral Interface) 82C55A 和



PIT (Programmable Interval Timer) 82C54<sup>(6)</sup>。PPI 可做為 8 bits/16 bits 資料的傳送或暫存，其 port C 可做為個別的控制信號，如 valves 和 pump 的 on/off 信號。PIT 可做為計時器或計數器，在本系統中則為插斷信號和時脈信號。

### 3. 信號處理部份

取樣的電壓信號，必須經過放大、位移、濾波之後才會被類比／數位轉換器 (ADC) 所轉換。利用兩顆 dual 8 channels 的類比多工器，組成一個差動輸入，16 channels 的類比多工器。而一些電化學槽的內阻甚高，因此在後級接上高輸入阻抗的電壓隨耦器，才能取樣出所要的電壓信號。

為提高抗雜訊能力和增益範圍，採用差動輸入儀表用直流放大器<sup>(7)</sup>。CMRR (Common Mode Rejection Ratio) 可達 120 dB，增益範圍 0.25 至 1,000 倍，是一個高精度、低雜訊的儀器放大器。

使信號水平位準在  $\pm 10$  伏特之間調整的信號準位電路，可使用一顆運算放大器和兩顆數位／類比轉換器 (DAC) 組成，一組為粗調 ( $\pm 10$  V,  $V=0.078$  V)，而另一組為微調 ( $\pm 0.64$  V,  $V=0.005$  V)。

化學信號的頻率大多低於 10 Hz，為提高 S/N (Signal/Noise) 比值，而裝入低通濾 (Low pass) 波器。本系統為單位增益狀態變數濾波器<sup>(8)</sup>，其形式是二階貝索 (Bessel)，而截止頻率可有四種選擇，分別為 100, 10, 1 及 0.1 Hz，可隨外界信號的頻率，做最佳的配合。

另外，16 bits ADC 的輸入電壓範圍有  $\pm 10$  伏特和  $\pm 5$  伏特兩種，可配合輸入電壓範圍而切換，以提高解析度。

### 4. Potentiostat 部份

有鑑於市售的 potentiostat 價格昂貴且未必適用於本系統，故自行製作以供實驗之用。Jayaweera 和 Ramaley<sup>(9)</sup> 提出四種常見的 potentiostat 電路。不同之處在於控制放大器 (Control amplifier) 的電路設計和取樣電流信號的方式，同時對 cell 的雜訊、響應速度、穩定度皆不同。

Bard 和 Faulkner<sup>(10)</sup> 則詳細說明 potentiostat 電路的基本原理及正迴授補償 (Positive feedback compensation) 的原理和其必要性。而其中的 bipotentiostat 電路為本系統所採用。為獲取準確的控制電號及降低誤差，消除 IR drop 是必須的。目前最新的方式是 He 和 Faulkner<sup>(11)</sup> 在 1986 年的文獻中所詳述的電路及處理方法，而將一個 12 bits 的數位／類比轉換器，當成一個數位控制的分壓器來使用。本系統前採用 14 bits 的數位／類比轉換器，以提高精確度。

由圖 3，cell 的兩種等效電路，可以預知因運算放大器等元件的時間延遲 (Time delay)，加上 cell 的時間常數 (Time constant) 所造成的延誤；因此，隨着溶液中未補償電阻 (Uncompensated Resistance,  $R_u$ ) 因正迴授補償而漸減少時，系統將愈來愈不穩定，若  $R_u$  因補償為零時，很有可能產生持續性的振盪現象，甚至系統失控而破壞了電極。

所以穩定電路的加入亦是非常重要的。文獻<sup>(11)</sup>中是在參考電極和輔助電極之間加上一個穩定電容 (Stabilizing capacitor)，但其電容值必須隨 cell 的不同而改變。另外，Kissinger 和 Heineman<sup>(12)</sup> 等人的著述中，更利用圖解法來說明產生振盪的原因及消除之法。所謂圖解法也就是繪出控制放大器開迴路的增益／頻率波德圖 (Bode plot)，藉以利用作圖的方式來改變控制放大器的增益／頻率特性，犧牲一些增益來換取系統的穩定，同時也可減少控制放大器的相位時間延遲 (Phase-time lag)。實際上就是在控制放大器的輸出端和反相輸入端之間，接上一組串聯的電阻、電容元件，其值因 cell 的不同而改變。

Potentiostat 的工作電極影響着取樣電流的大小，若採用微電極，電流很可能只有 pico 安培的範圍，故電流／電壓轉換器所使用的運算放大器，必須是 ultra low bias current 的運算放大器<sup>(13)</sup>。

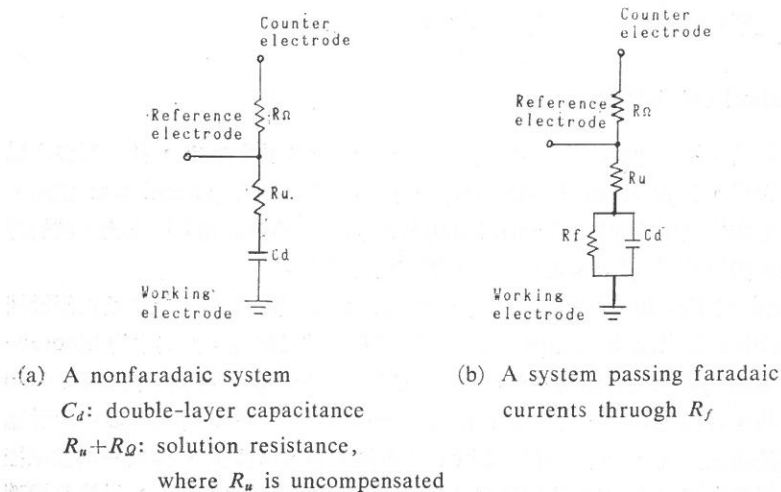


Fig. 3. Cell equivalent circuits.

## 5. FIA 的步進馬達和 SSR 控制部份

此處 FIA (Flow Injection Analysis) 是採用二組步進馬達，作流體推動及取樣的動作，而二者之動靜是由微電腦來協調。基本上步進馬達可分為 VR 型 (Variable Reluctance Type) 和 PM 型 (Permanent Magnet Type)。不同的步進馬達，激磁的方式也相異，故應採用不同的分配電路<sup>(14)</sup>。本系統使用兩個 SANYO 製的四相步進馬達，分配電路可選擇三種激磁方式：1 相，2 相，1-2 相激磁。圖 4，為控制步進馬達的方塊圖，利用光學編碼器和解碼／計數介面電路<sup>(15)</sup>，可測知其運轉量。

固態繼電器 (SSR) 的控制方式，是以邏輯信號位準的 high/low 來定其 on/off。總共 11 組的 SSR，除 1 組為 pump 的開關外，其餘 10 組為 valves 的控制開關；藉以 valves 的開關變化，來選擇不同的管路。

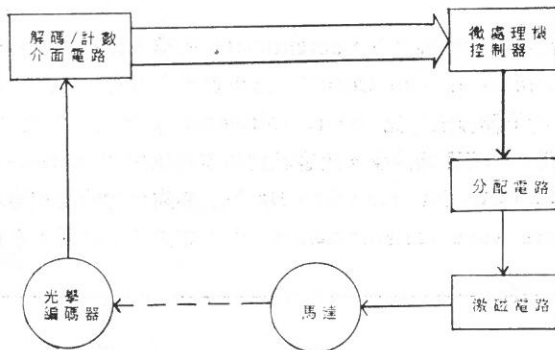


Fig. 4. Stepping motor block diagram.

## 三、結果與討論

實驗室自動化，必須有電子的硬體設備和資訊的軟體系統，配合具有高偵測速度、高靈敏度、低偵測極限特性的化學感測器 (Sensor)。故將本篇的多功能實驗卡應用在分析儀上，即可成為圖 5 的智慧型分析系統。此系統可自由選擇使用 HPLC 或 FIA；利用機械手臂取樣，可減少人為因素的誤差，而最近的文獻亦提及，配合專家系統 (Expert systems) 和知識庫系統 (Knowledge-based system) 所指揮的智慧型機械手臂<sup>(16)</sup>。

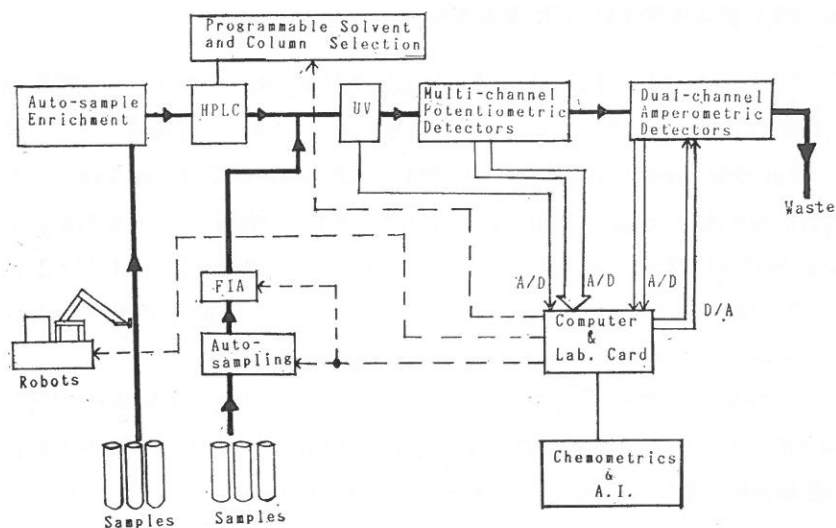


Fig. 5. Block diagram for the intelligent analytical system.

由於一切在電腦的控制之下，potentiostat 的輸入波形，依需要而做任何的變化。Ploegmakers 和 Van Oort<sup>(17)</sup> 已用實驗的方式，證實 square-wave voltammetry 的偵測極限可比 cyclic voltammetry 低約 10 倍，而花費在資料處理上的時間，亦明顯地減少。故嘗試使用本系統中的 square-wave 功能，如圖 6，分析 Fe、Co、Ni、Cu、Cr、Hg 等金屬鉗合物的混和溶液，並繪出三度空間的 square wave voltammogram<sup>(3,18)</sup>，如圖 7；結果本系統效果良好。

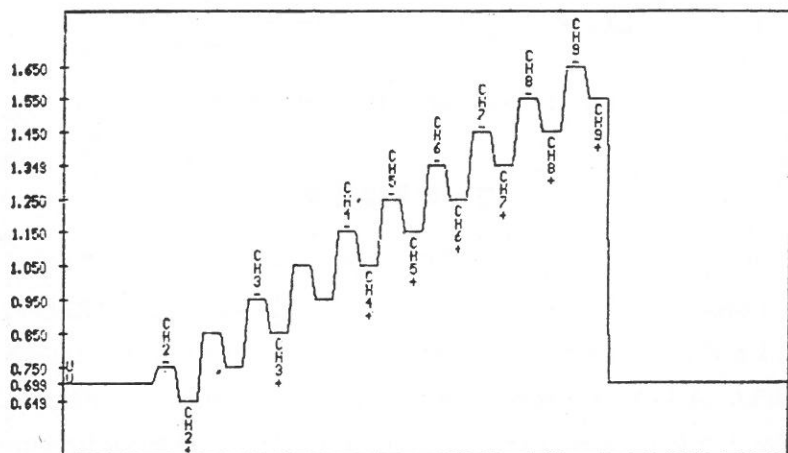


Fig. 6. Square-wave.

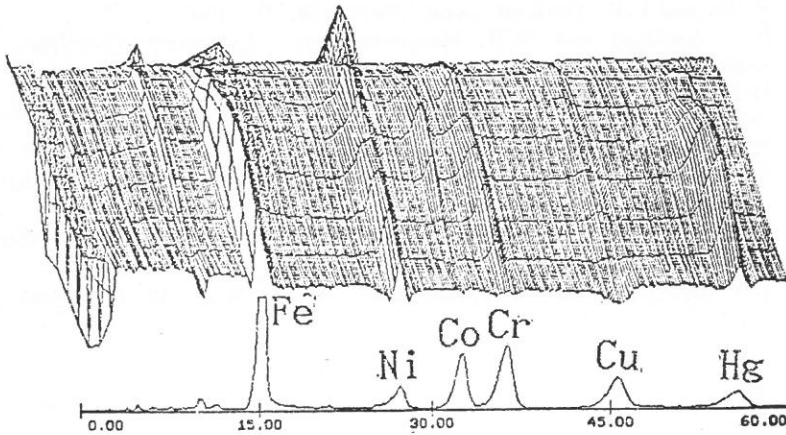


Fig. 7. Square-wave voltammogram.

為配合往後的需要，程式方面採用模組化，以方便新功能的加入，而硬體方面也預留擴充用的電路。然而，本系統尚在實驗階段，部份功能不及測試，以待後續改進。

#### 四、結 論

展望未來，自動化的需求將日益迫切，隨著新一代「神經電腦」的發展和新一代數學「悟性控制理論 (Fuzzy math)」的廣泛運用，實驗室動化又將邁入另一個新紀元。

#### 參 考 文 獻

- (1) P. He, J.P. Avery and L.R. Faulkner, *Anal. Chem.*, **54**, 1313A (1982).
- (2) M.A. Sharaf, D.L. Illman and B.R. Kowalski, *Chemometric*, Wiley, New York (1986).
- (3) 陳天鐸, 「智慧型分析儀」, (輔仁大學碩士論文, 78年 6 月)。
- (4) Linear Products Databook, Analog Devices, Inc. (1988).
- (5) Philips Data Handbook (1988).
- (6) UMC Databook (1986-1987).
- (7) W.G. June, "IC-OP amp. cookbook".
- (8) Burr-Brown Databook (1989).
- (9) P. Jayaweera and L. Ramaley, *Anal. Instrum.*, **15**(3), 259 (1986).
- (10) A.J. Bard and L.R. Faulkner, *Electrochemical Methods*, Wiley, New York (1980).

- (11) P. He and L.R. Faulkner, *Anal. Chem.*, **58**, 517 (1986).
- (12) P.T. Kissinger and W.R. Heineman, Eds., *Laboratory Techniques in Electroanalytical Chemistry*, Marcel Dekker, New York (1984).
- (13) H.J. Huang, P. He and L.R. Faulkner, *Anal. Chem.*, **58**, 2889 (1986).
- (14) 許溢适編譯, 「步進馬達原理與應用」, 全華科技, 72 年 12 月。
- (15) "Optoelectronics", Hewlett Packard (1988-1989).
- (16) T.L. Isenhour, S.E. Eckert and J.C. Marshall, *Anal. Chem.*, **61**, 805A (1989).
- (17) H.H. , J.L. Ploegmakers and W.J. Van Oort, *Anal. Chem.*, **16**(4), 467 (1987).
- (18) J.G. Osteryoung and R.A. Osteryoung, *Analy. Chem.*, **57**, 101A (1985).

## A Multifunction Laboratory Card for Automation

YEN-WEI WANG AND SHOW-CHUEN CHEN

Department of Chemistry

### ABSTRACT

The integration of chemometrics into modern chemical laboratories to implement intelligent instrumentation often involves data acquisition, signal processing, microcomputer-based instrument design and a control system for peripherals. The present intelligent interface system, in the form of a Laboratory Card, includes a 16-channel/16-bit ADC, a 2-channel/16-bit DAC, a 0.25-1,000 current booster and a signal conditioner. The hardware for electrochemical analysis, flow injection analysis and peripheral devices are also included.

# 聚吡咯及其衍生物之電化學合成及 金屬離子吸附現象之研究

饒忠儒 劉保華 陳壽椿

輔仁大學化學系

## 摘 要

本文對 Ppy 一族，作一系列有關其導電性、反應機構、及金屬吸附機構之研究。以 SEM 來測量金屬吸附的情形，並推測其可能的反應機構。在電化學方面，着重於金屬吸附的電化學特徵。由的結果發現，Ppy 的聚合度及金屬的吸附程度，受到 CV 掃描速率的影響頗大；掃描速率越慢，單位顆粒的半徑越大，且金屬的吸附是以一氧化，吸附再還原的順序進行，而和 Ppy 薄膜的成長相互獨立。SEM 和電化學的結果，不但對 Pletcher 提出的「多步驟反應」機構提供直接的證據，更提供了在大電極上所無法觀測到，有關於反應機構的，更詳細，更深入的證據。

## 一、引 言

聚吡咯 (Polypyrrole ; Ppy) 因為具有高穩定性 ( $\sim 250^\circ\text{C}$ )、P 型半導體 ( $100\ \Omega^{-1}\text{cm}^{-1}$ )、及在氧化態導電性的特性，故可做氧化還原反應中之電極；電量貯存<sup>(1)</sup>，亦可作為控制藥物釋出的物質<sup>(2~4)</sup>。在本實驗中，則電着塗裝於金屬膜極列上的電極，同時將溶液中的改質添加劑帶入載體中，以作改質電極。

關於 Ppy film 的生成，其反應機構，及電化學特性的研究，雖早在 1980 年初就已開始<sup>(5~11)</sup>，但僅知基本單位為一四環相連的聚合物  $-(\text{py-py-py-py})^+n-$ ，外帶一正電荷。

Diaz<sup>(12)</sup> 推測有關自由基偶合的反應機構，分為 Py 的氧化 (Oxidation) 及雙聚合 (Dimerization) 二步驟<sup>(12~16)</sup>。而且一 Py 的 CV 圖具有的特性為：(1) 非可逆的電化學反應。(2) 波形較寬廣。

Film 的生長與時間成正比，此結果符合假設的一「自由基偶合」步驟 (Radical coupling step)。一般溶液的親核性要低，且電極正電位要够大，才能氧化 Pyroole ( $E_{pa}=1.2\text{ V vs. SSCE}$ )。如果電位小於氧化 Py 的單體 (Pyrrole monomer)，則 Ppy film ( $E^\circ=-0.2\text{ V vs. SSCE}$ ) 不會繼續成長，故最基本的條件是 Py 單體要先被氧化<sup>(13)</sup>。

在 Py 衍生物的導電性研究中<sup>(17~19)</sup>，在 Py 族中，以單純的 Py 所形成之 Ppy 在氧化態之導電性最好<sup>(3)</sup>。

近年來 SEM (Scanning Electron Microscopy) 和電化學的結合，是一新的趨勢。以往 SEM 常用來觀察物質的表面結構<sup>(20)</sup>，近年來和電化學結合後，則常用來觀察電極的表面現象，和離子吸附的情形<sup>(21~23)</sup>，而提供更直接的訊息。最近又將此技術用於觀察導電塑膠之表面上，尤其是用於 Ppy<sup>(6,12,21)</sup>，及 Polyaniline<sup>(24)</sup> 上更為普遍。本實驗即是利用此一技術，觀察 Ppy 及其衍生物在不同的電化學條件下，其生長的表面現象，以及金屬離子的吸附情形，期能得到直接的證據。

## 二、實 驗

### 1. 藥品及儀器

本實驗所採用的藥品：Pyrrole, 1-Methylpyrrole, 1-Phenylpyrrole 以及 1-(Dimethylamino)pyrrole，均為 Aldrich, GR 級的藥品，除了 1-Phenylpyrrole 為固體外，其餘的均為液體。Pyrrole, 1-Methylpyrrole 及 1-(Dimethylamino)pyrrole 在實驗前，必須在完全乾燥的玻璃儀器中，做真空蒸餾純化。1-Phenylpyrrole 不需再經純化過程，可直接用於本實驗。以  $\text{Ag}(\text{NO}_3)$ ,  $\text{Cu}(\text{NO}_3)_2$  以及  $\text{Pb}(\text{NO}_3)_2$  配製金屬離子， $\text{KNO}_3$  為輔助電解質。以上金屬化合物，除  $\text{Ag}(\text{NO}_3)$  為 Merck ultra pure 級的藥品外，其餘均為 Merck, GR 級的藥品。使用的電化學儀器為 BAS-100A 電化學分析儀，參考電極為標準  $\text{Ag}/\text{AgCl}$  參考電極，輔助電極為 0.3 mm 的 Pt 金屬線電極，工作電極為  $5\text{ }\mu\text{m}$  厚度， $5\text{ mm}\times 2\text{ cm}$  的不銹鋼薄片電極 (HASBERG, 西德)，浸入溶液中之深度 1 公分。所有的工作電極在實驗前，均先用溶劑洗過。SEM: JEOL JSM-T330A。

### 2. Ppy 的電化學合成

Ppy 的電化學合成法，大約可分為二大類：一是在有機溶液中做電化學合成，其溶劑多採用 Acetonitrile<sup>(13,14,21,26)</sup>，另一則是在水溶液中做電化學合成<sup>(12,18,27)</sup>。在有機溶液系統中，所採用的輔助電解質有  $\text{LiClO}_4$ <sup>(13,14)</sup>， $\text{Et}_4\text{NBF}_4$ <sup>(25)</sup>，及 Heteropolyanion<sup>(33)</sup> 等；而水溶液系統中則多採用  $\text{KNO}_3$ <sup>(12,18)</sup>，及  $\text{K}_3\text{Fe}(\text{CN})_6$ <sup>(27)</sup>。為了實驗上的方便起見，本實驗採取較為平常的水溶液，而以 0.1 M 的  $\text{KNO}_3$  為輔助電解質<sup>(12,18)</sup>，加入 50 mM 的 Py 單體，在  $-900\sim 1,300\text{ mV}$  間，以  $100\text{ mV/sec}$  的掃描速率，掃描 CV 30 週。實驗先後以銀絲、銀片、及  $5\text{ }\mu\text{m}$  的不銹鋼膜片為工作電極。

本實驗起先以一連串實驗測試 CV 波峰的位置，最後以最大 Scan 範圍為主 ( $-800\sim 1,700\text{ mV}$ )，Scan 速率定為  $100\text{ mVs}^{-1}$ 。



### 3. SEM 之校正及測試

在目前可用的儀器中，能提供訊息最多的分析技術為 SEM。在實驗初期，曾以普通顯微鏡觀察銀棒的 Ppy，能看出突起物如纖維般交錯。在含硝酸銀中所形成之 Ppy 亦能明顯看出銀的白色針狀結晶之存在，SEM 所得之資料頗有可觀之處；而實際在文獻方面，研究金屬離子的影響亦借助 SEM 甚多<sup>(6,12,20~24)</sup>。對 Ppy 而言，其導電性已足夠測 SEM，不需以碳或金蒸鍍其表面。

### 4. Ppy 及其衍生物的金屬吸附

本實驗所用的藥品為 1-(Dimethylamino)pyrrole，1-Methylpyrrole，1-Phenylpyrrole，以及 Pyrrole 等 (Aldrich Chemical Company, Inc.) 四種，樣品濃度為 50 mM，並加入 5~100 mM 不同濃度的金屬離子，0.1 M 的硝酸鉀為輔助電解質，以 100 mV/sec 的掃描速率，-900~1,300 mV 的掃描區間，在 BAS-100A 上作 CV 掃描，完成後再照 SEM。以 CV 圖譜上的吸收配合 SEM 的圖形，探討不同金屬離子，在不同的濃度下，在聚合薄膜上成長的情形及對於薄膜的影響。每一樣品均配成三種溶液，金屬離子的種類及含量分別為： $\text{Cu}^{++}$  10 mM， $\text{Ag}^+$  10 mM，及不含金屬離子等三種。

## 三、結果和討論

### 1. SEM 上的特徵

#### (1) CV 掃描速率對合成之 Ppy 表面的影響及其在 SEM 上的特徵

實驗針對 CV 的掃描速率對 Ppy 的表面影響，做一連串的測試，其溶液的條件如前，而改變速率為 100, 80, 及 50 mV/s 三種，待 Ppy 合成後即以 SEM 觀察其表面，圖 1 及圖 2 為 100 mV/s 合成之 Ppy 的 SEM 圖。由圖 1 可以明顯看出，不銹鋼表面的 Ppy 有纖維狀突起的皺褶，成「人」字形交叉如山谷般交錯排列，掃描速率越快則皺褶越密，坡度越陡；掃描速率越低則表面越平滑，坡度越平緩。在高倍下觀察 Ppy 之表面，如圖 2 所示，則可以明顯的看到，Ppy 的結構乃是先聚合成一個個球狀的顆粒，再相互堆砌結合而成。圖 2 的放大倍率為 2,000 倍，由圖中的比例尺換算，可以得出在 100 mV/s 的掃描速率下，每一單位顆粒的直徑約為 0.714~0.952  $\mu\text{m}$ ，在 80 mV/s 下為 1.43~1.91  $\mu\text{m}$ ，在 50 mV/s 的合成速率下則約為 2.14~2.18  $\mu\text{m}$ 。此一結果顯示掃描速率越高，則單位顆粒的直徑越小，亦即聚合的程度越差。而如要找出最適當的實驗條件，在生成 Ppy film 前就需控制 CV 之掃描範圍，然後再求出掃描速率對其之影響。

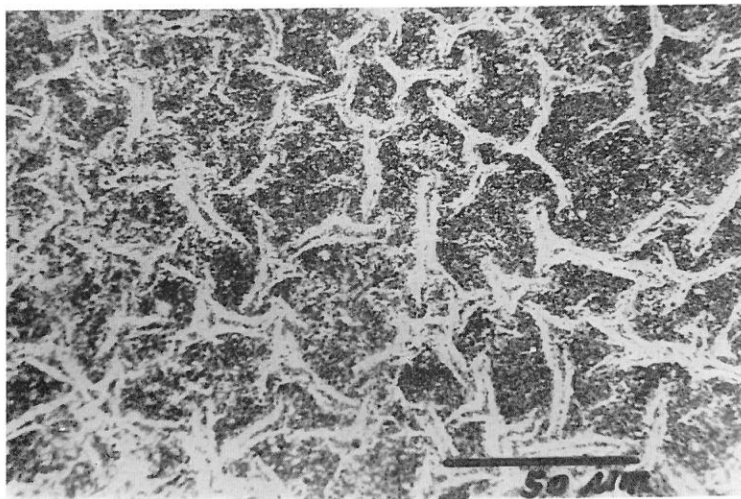


圖 1 以 100 mV/s 掃描速率所合成的 Ppy 之 SEM 圖，SEM 條件：加速電壓 15 KV，電流 5 mA，放大倍率 500 倍。

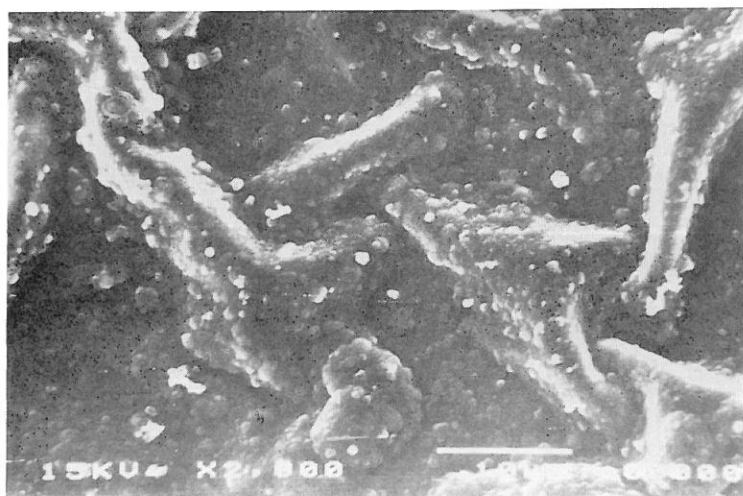


圖 2 以 100 mV/s 掃描速率所合成的 Ppy 之 SEM 圖，SEM 條件：加速電壓 15 KV，電流 5 mA，放大倍率 2,000 倍。

## (2) Ppy 及其衍生物的金屬吸附在 SEM 上的特徵

在實驗中，以銀和銅二種離子，來探討 Ppy 及其衍生物的金屬吸附行為。純 Ppy 的 SEM 圖形可見圖 1 及圖 2，其銅吸附的 SEM 圖在圖 3 中，在圖的左下角突起處，可以見到不規則狀的銅結晶；銀的吸附圖形列於圖 4 中，銀的針狀結晶在圖中清晰可見。

1-Methylpyrrole (MPpy) 及其金屬的吸附圖形列於圖 5 及圖 6 中，圖 5 為純 MPpy 放大 750 倍的 SEM 圖形，由圖中可以見到有許多平行的凹槽，這似乎顯示着，在聚合反應的過程中，聚合物的成長是依一定的方向進行成長的，亦即是說，其聚合反應的反應機構為一維 (One dimension) 的反應機構。而其金屬離子的吸附行為並不明顯，圖 6 為吸附銀時的 SEM 圖形。銅的吸附幾乎看不見，而銀的吸附量也很少，只在皺褶間看到稀稀落落銀的針狀結晶。此顯示當有金屬離子共存於水溶液中時，聚合會使聚合物的表面皺褶加多加深，使表面較為粗糙。另外由圖 6 亦可以發現，MPpy 的結構亦和 Ppy 差不多，均是先聚合成單位顆粒，再由單位顆粒再行聚合而成。唯一不同者為其單位顆粒均似圖 5 一般的呈線狀平行排列，而不似 Ppy 般的呈二度空間的散狀堆砌。據此推斷聚合反應的反應機構，應是先以一維的方式進行，而形成線狀的結構，當線狀結構的長度達一定長度後，再於線和線之間作交聯 (Crosslink) 聚合反應，而非一開始就以二維或三維的方式進行聚合，亦非 Diaz 所提之簡單一維反應機構。

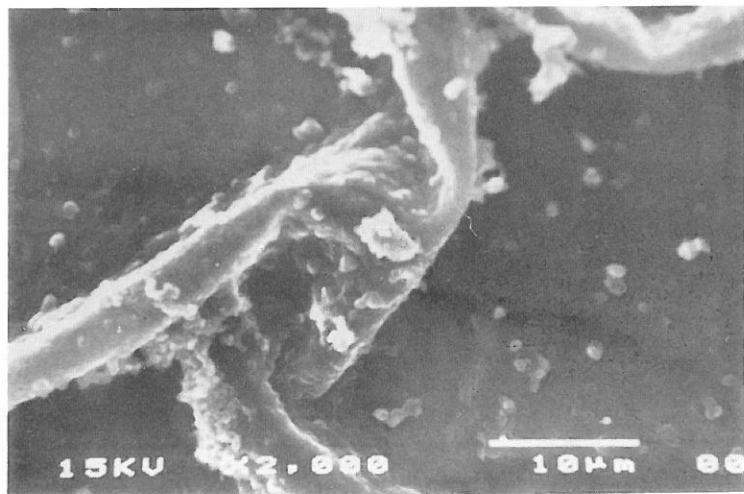


圖 3 銅吸附之 Ppy 的 SEM 圖，SEM 條件：加速電壓 5 KV，電流 6 mA，放大倍率 2,000 倍。

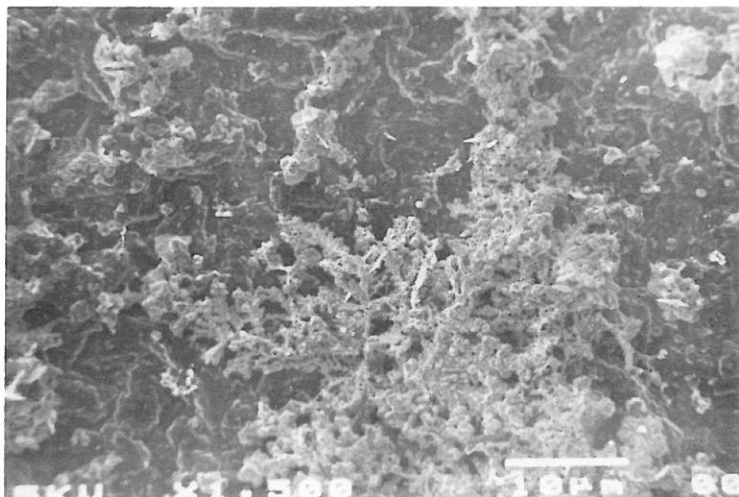


圖 4 銀吸附之 Ppy 的 SEM 圖，SEM 條件：加速電壓 5 KV，電流 6 mA，放大倍率 2,000 倍。

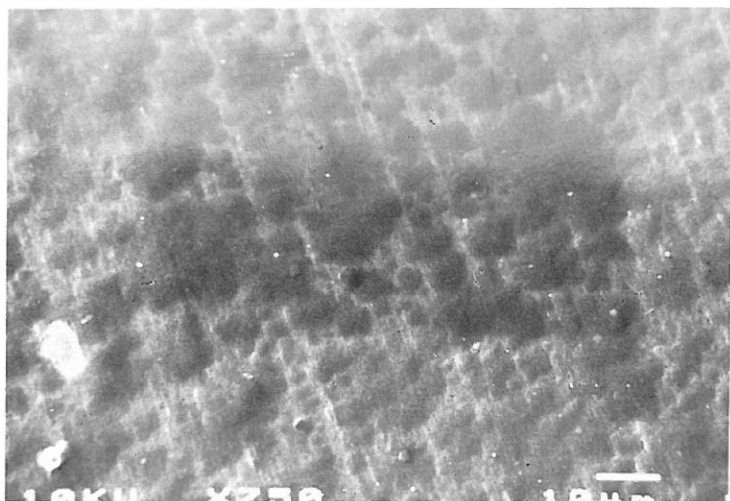


圖 5 純 MPpy 的 SEM 圖，SEM 條件：加速電壓 10 KV，電流 6 mA，放大倍率 750 倍。

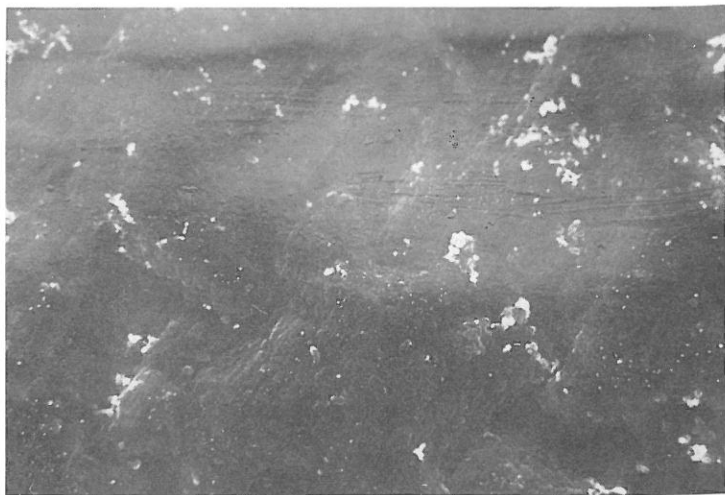


圖 6 銀吸附之 MPPy 的 SEM 圖，SEM 條件：加速電壓 15 KV，電流 5.5 mA，放大倍率 2,000 倍。

1-Phenylpyrrole (PhPpy) SEM 圖中的雜訊極大，此乃因 PhPpy 之導電性較差，而造成 SEM 雜訊增大的緣故。雖然其金屬結晶清晰可見，但二者相較仍可發現，銅的結晶較為疏鬆，且體積較小，而不似銀的結晶那般的大而濃密，銀花的排列亦呈現規則線狀的平行排列結構。

1-(Dimethylamino)pyrrole (DMAPpy) 的 SEM 圖形，有許多纖維狀的突起皺褶，且和 Ppy 及其他 Ppy 衍生物的皺褶結構不大相同。銅吸附圖形，雖然和其他 Ppy 衍生物的結構相似，仍是呈直線平行排列的結構，但銅花的結構較大，較密，這和其他 Ppy 衍生物之情形大異其趣，可能是因為多了一個胺基取代，而使得金屬離子更易於附着成長之故。銀吸附的 SEM 圖形在圖 7 中，放大倍率同樣為 2,000 倍，但可以看出，此時銀花的體積為其他 Ppy 衍生物的數倍。且當 SEM 聚焦於背景時，銀花的結構就極不清楚，而聚焦於銀花結構時，則背景幾乎看不見，此亦顯示此時銀花突出表面的程度較其他 Ppy 衍生物者為高。

由四種樣品的 SEM 圖來看，其大致均有纖維狀突起物，但與 Ppy 不同的是突起物的形狀。不含  $\text{Cu}^{++}$ 、 $\text{Ag}^+$  離子的情況下，如聚焦於 Film 之表面，可清楚看出突起物，如 MPpy 的聚合物較肥大，DMA-Ppy 的聚合物形狀較不均勻，而 PhPpy 的突起物較不明顯。三種聚合物的導電度並不好，亦影響了 SEM 的觀察，尤其當表面有  $\text{Cu}^{++}$ 、 $\text{Ag}^+$  結晶的話，常使背景模糊黯淡，而結

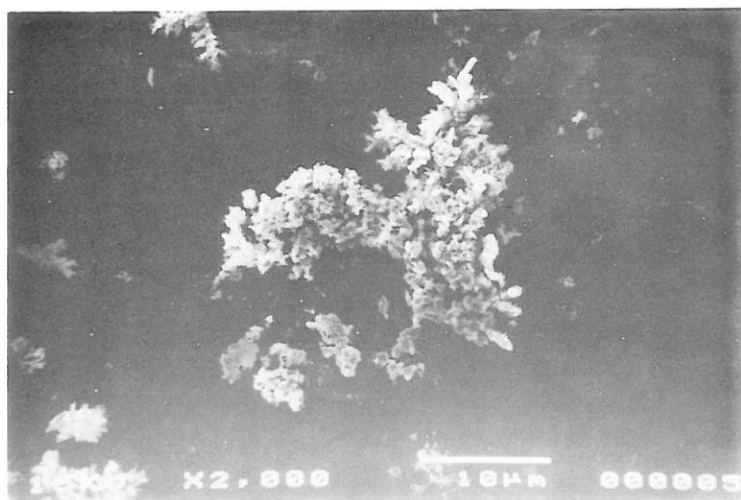


圖 7 銀吸附之 DMA-Ppy 的 SEM 圖，SEM 條件：加速電壓 10 KV，電流 6 mA，放大倍率 2,000 倍。

晶則清楚可見：此亦為何此處常分二次拍攝，一次着重結晶，一次着重背景。另一特殊現象是 Film 表面有明顯平行線條排列的情形，可由圖 5，圖 6，及圖 7 看出，初步推斷此一結果是和聚合物生成的反應機構有關。此外 DMAPpy 之聚合物上銅結晶十分明顯，這是以前做有關  $\text{Cu}^{++}$  實驗所未見的。

表一為 IBM 所列有關各種 Py 衍生物的 CV 資料。在其文獻上<sup>(7)</sup>曾提到 Py 的衍生物在電極表面的反應常生成可溶的產物。以不銹鋼膜片做實驗亦能觀察到此一情形，雖然事前以硝酸清洗，但膜片表面所附着之聚合物極薄（與 Py 比較，同樣為掃描 60 次），而溶液顏色卻慢慢加深。至於 CV 數據方面，氧化電位（Oxidation potential）會隨 Py 上的取代物種類而變，此由  $E_{pa}$  值可看出，此乃因分子的  $\pi$ -dipole moment 的改變所致<sup>(6)</sup>。

## 2. 電化學的特徵

### (1) Ppy 的合成及金屬離子的吸附

在單純的 Py 水溶液中作 CV 時，在 690 及 1,050 mV 處可看到兩個氧化波峰（圖 8）。雖然大多數的文獻認為 Ppy 的聚合機構目前仍不清楚<sup>(6,7,12,13)</sup>，但 Pletcher 認為可能在 0.65~1.2 V 間經過一多步驟的氧化聚合反應<sup>(12)</sup>，但是他亦沒有明顯的證據以支持他的理論。此外由圖 8，可以明顯的看到兩個氧

表一 Py 及其衍生物在 CV 圖譜中之特徵波峰\*

| Compound                                      | $E_{pa}/V$  | Rel. $i_{pa}$ | $\mu/D$ |
|---|-------------|---------------|---------|
| Pyrrole                                       | 1.20 (1.2 ) | Shoulder      | 1.80    |
|   | 1.54        |               |         |
| 1-Methylpyrrole                               | 1.14 (1.19) |               | 1.92    |
| 1-Ethylpyrrole                                | 1.22        |               | 1.96    |
| 1-( <i>n</i> -Propyl)pyrrole                  | 1.24        |               |         |
| 1-Phenylpyrrole                               | 1.80        |               | 1.32    |
| 2,5-Dimethylpyrrole                           | 0.84        |               | 2.08    |
| 1,2,5-Trimethylpyrrole                        | 0.82        | 1.0           | 2.07    |
|   | 1.15        | 0.3           |         |
| 2-Methyl-5-phenylpyrrole                      | 0.85        | 1.0           |         |
|   | 1.23        | 0.1           |         |
|   | 1.33        | 0.1           |         |
| 1,2-Dimethyl-5-(3',4'-dimethoxyphenyl)pyrrole | 0.72        | 1.0           |         |
|   | 1.22        | 0.4           |         |
| I   | 1.32        | 1.0           |         |
|   | 1.71        | 0.3           |         |
| II  | 1.30        | 1.0           |         |
|   | 1.69        | 0.2           |         |
| III   | 1.01        | 1.0           |         |
|   | 1.34        | 0.2           |         |
|   | 1.50        | 0.4           |         |
| IV  | 0.98        | 1.0           |         |
|   | 1.30        | 0.2           |         |
|   | 1.53        | 0.3           |         |

\* Measured in  $\text{CH}_3\text{CN}$  containing 0.1 M  $\text{Et}_4\text{NBF}_4$  using Pt vs. NaCE electrodes, and using 0.7-2.0 mM pyrrole concentration.

化波峰，可見在形成聚合物時，反應的步驟應在兩步以上，可以說對 Pletcher 的理論，提出了較為實際的證據。但是，由於目前使用的電極仍嫌太大，掃描速率 100 mV/s 又太快了一點，造成圖譜的解析度不夠，因此計劃將電極換為微電極，「掃描速率放慢」，再運用其它電化學的技術，期能找出更進一步的證據。

至於金屬離子在 Ppy 的吸附研究方面，採用 Cu, Pb 及 Ag 之硝酸鹽水溶液做為產生金屬離子的來源。選用金屬硝酸鹽，使其與輔助電解質的系統一致，以簡化電化學系統。對銅離子之研究，由圖 9 中，可以發現，除了在 650 及 1,000 mV 附近的兩個 Ppy 氧化液峰外，在 390~510 mV 間多出了一個很強的



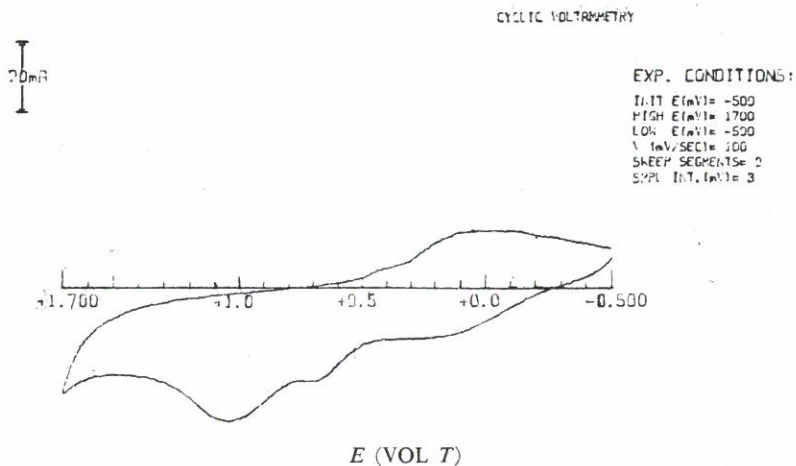


圖 8 50 mM Pyrrole 在 0.1 M 硝酸鉀溶液中，合成 Ppy 的 CV 圖譜。

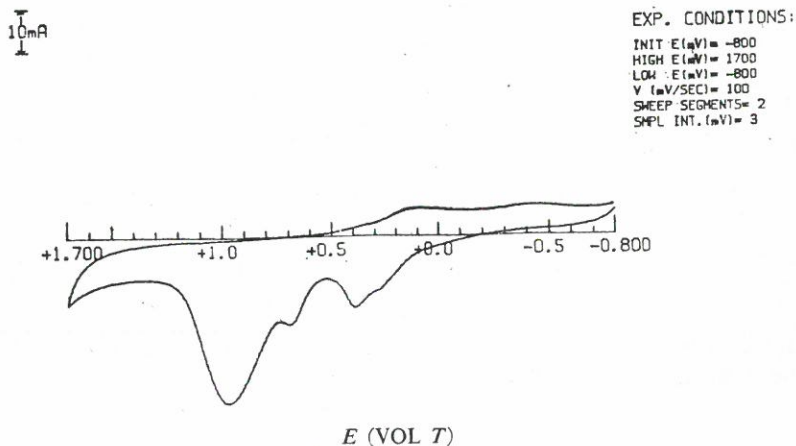


圖 9 50 mM Pyrrole, 0.1 M 硝酸鉀在 5 mM 硝酸銅存在下，合成 Ppy 的 CV 圖譜。

波峰，而且原在 1,050 mV 附近的波峰，漂移至 980 mV 附近。初步判斷此三現象，是由於銅離子和 Ppy 的同時吸附所造成。爲了鑑定 390~510 mV 間的這一多出的波峰，我們將此一波峰的電流和 650 mV Ppy 的波峰電流相除，



以電流比對銅離子濃度作圖，發現具有線性關係的存在，經線性迴歸分析後，發現其  $r$  值（相關係數）可達 0.9991，因此我們判定此一波峰為銅離子吸附所造成，且和銅離子有很好的定量關係；此一結果列於圖 10。另外，我們也在 SEM 圖中，清楚的看到銅的吸附結晶，亦可證明金屬吸附的現象，這一部份在本文 SEM 一節中，已有詳述不贅言。

銀離子和鉛離子的吸附圖譜就和銅離子大不相同，銀離子的 CV 圖譜列於圖 11 中，如圖中可以看到 Ppy 在 1,050 mV 附近的波峰，已漂移至 1,000 mV 附近，而 650 mV 的波峰消失，並在 -100 mV 附近出現一很強的還原波峰，是在其它 Ppy 系統中所未見過的，輔以 SEM 的結果，初步推斷應為銀離子還原所形成的，但是詳細的結果，仍有待進一步的實驗。而鉛離子的吸附則較難判定，其 CV 圖譜列於圖 12 中，由圖形可以發現 Ppy 在 1,050 mV 的波峰漂移至 950 mV 附近，且在 550~650 mV 間有一小的波峰伴隨出現。由上述的討論，我們已可以推斷，950 mV 附近的波峰，是由於金屬離子的介入時的通性。而 550~650 mV 間的波峰，較難界定，雖然一般 Ppy 形成的氧化電位，不會

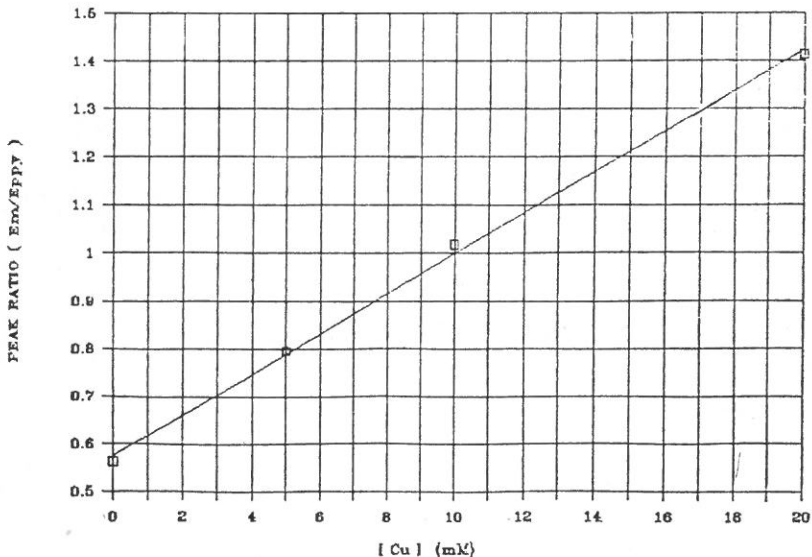


圖10 Pyrrole 和銅離子共存以 CV 合成 Ppy 時，銅離子之液峰電流和 Ppy 之形成波峰電流之比，對銅離子濃度之校正曲線。

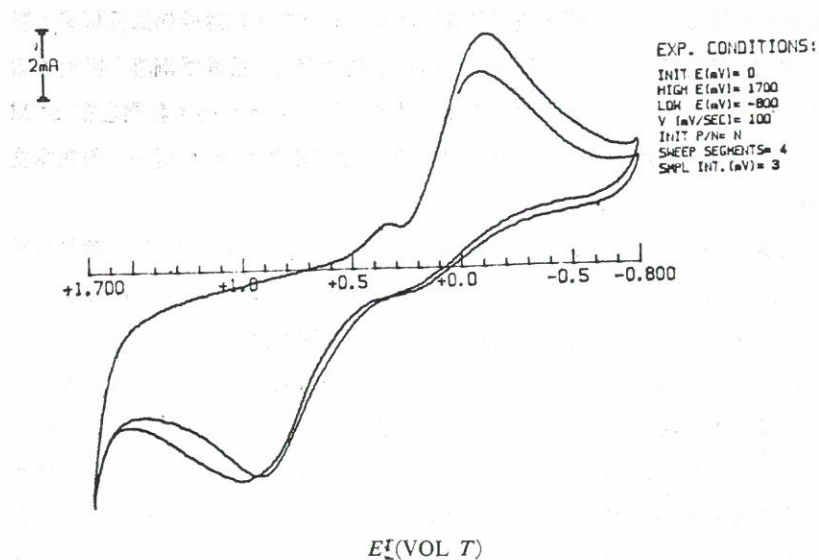


圖11 銀吸附之 Ppy 的 CV 圖譜。

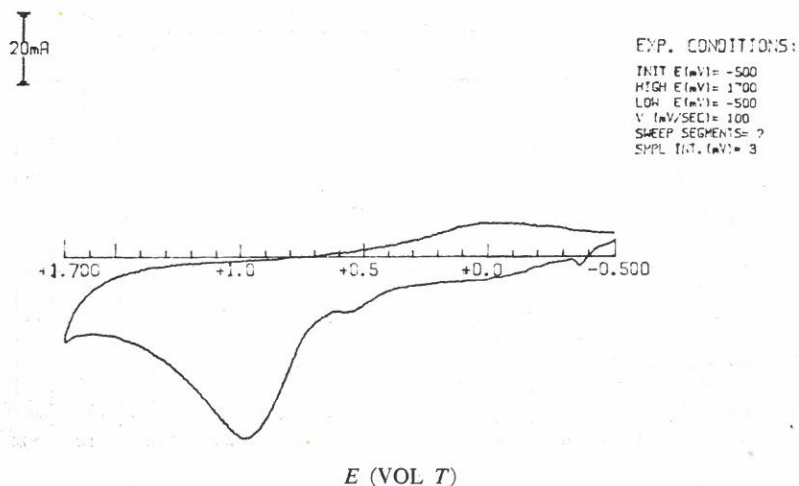


圖12 50 mM Pyrrole, 0.1 M 硝酸鉀在 100 mM 硝酸鉛存在下, 合成的 Ppy 之 CV 圖譜。

低於 600 mV，但是由於此一波峰和 Ppy 形成的氧化電位非常的接近，因而造成推斷上的困難。它極有可能是鉛離子的陽極波峰，但也有可能是 Ppy 的形成電位波峰，抑或是二者均有，仍不得而知。但是由於鉛離子在 Ppy 薄膜上，在 -800 mV 附近應有一還原波峰<sup>(18)</sup>，因此似乎可以將還原電位的範圍延至 -800 mV，以此一還原波峰的存在與否，來鑑定鉛離子的存在與否，這也是有待進一步實驗而予以證實部份。

## (2) 金屬吸附的機構

由上述的結果，我們已可確定金屬會隨聚合物一併吸附的事實，但是其吸附的方式和機構，亦是我們極感興趣的部份。圖 13 是銅離子在和 Py 共存下，CV 掃描連續 20 週的結果。由圖中可以發現，由銅離子吸附所產生在 390~510 mV 間的波峰，只在第一及第二週出現，而且第一週的波峰，比第二週的波峰要大得多，而在 -100 及 -500 mV 左右的波峰卻持續到第二十週仍可以明顯的看出。由此，我們以為金屬離子的吸附行為是在聚合物形成之前，就以氧化態的形式吸附於電極上，再經還原而以零價金屬的情況存在於電極之上。據此推斷為一氧化吸附——還原的過程，是在實驗中不斷的持續而至實驗結束的，且其生成的速率也大於聚合物 Film 的形成速率。因為在 SEM 的圖片中可以很明顯的看出，不同的金屬晶形。如果 Film 的生成速率大於金屬的吸附速率，則金

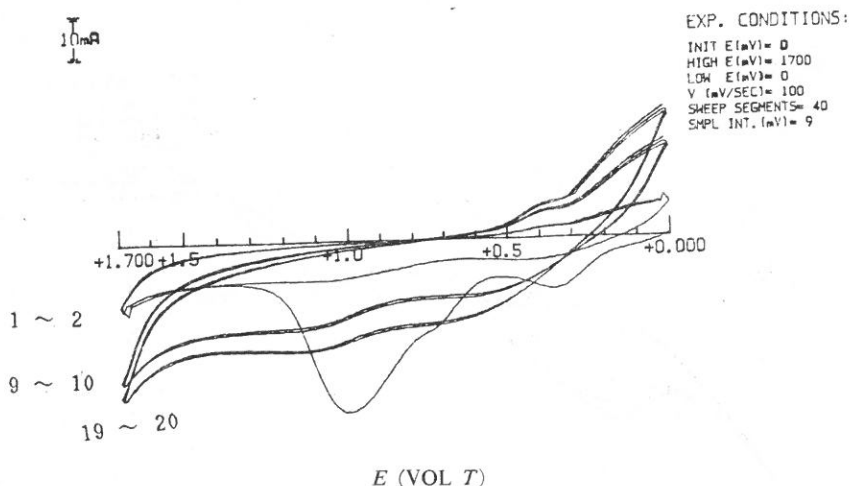


圖13 50 mM Pyrrole, 0.1 M 硝酸鉀在 5 mM 硝酸銅存在下，合成 Ppy 的 CV 連續圖譜。

屬勢必被 Film 包住，而看不出任何的晶形，而我們卻沒有看到如此的現象，而且在 CV 圖中，我們亦可很明顯的看到 Ppy 在 1,050 及 650 mV 附近的波峰，在第二週起就很不明顯了，而金屬還原的波峰，卻可持續到最後一週。

### (3) Ppy 衍生物的金屬吸附現象

DMA-Ppy 在單純的電解質水溶液時，由圖 14 中可以看出其氧化電位在 950 mV 附近，而加入銅離子後，此一電位就漂至 1,100 mV 附近，且在 670 及 750 mV 附近出現了連續的兩個氧化波峰，且在第一周的氧化過程中，在 -600 mV 附近亦有一氧化波峰，相較於 Cu-Ppy film -600 mV 附近的吸收。DMA-Ppy 的銅吸附波峰在 670 及 750 mV 附近為兩個連續的波峰，而非 Cu-Ppy film 的單一波峰。銀離子吸附於 DMA-Ppy 和 Ag-Ppy film 類似，它具有一強的還原波峰，只是電位已漂移至 -200~-350 mV 附近。MPpy 及 PhPpy 亦有相類似的特性，其在 700~500 mV 間的強氧化波峰，是為銅離子吸附的特徵；而銀離子的特徵，則是在 0~-500 mV 間的強還原吸收。雖然其電位會隨著聚合物的種類不同而有所漂移，但是這些特徵仍是明顯可見的，所有 Ppy 及衍生物的 CV 特徵均列於表二之中。

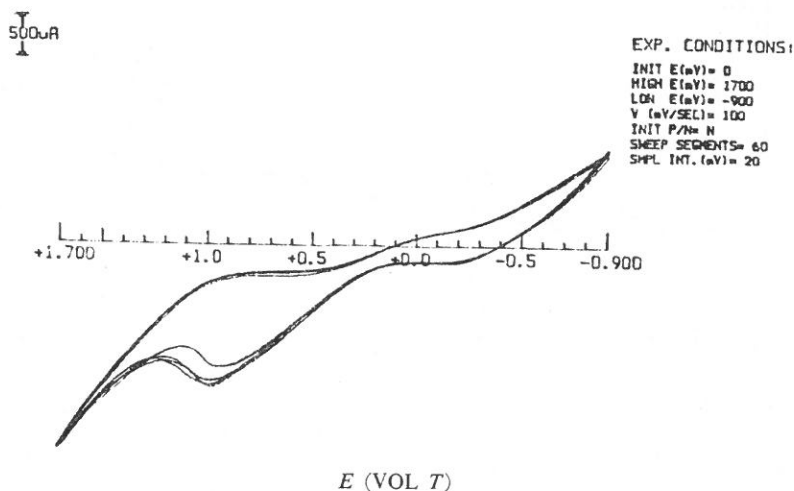


圖14 DMA-Ppy 的 CV 圖譜。

表二 Ppy 及其衍生物在不同金屬存在下，CV 圖譜之波峰特徵

|                           |              |   | Anodic   |          | Cathodic          |          |            |
|---------------------------|--------------|---|----------|----------|-------------------|----------|------------|
|                           |              |   | Peaks    |          | Cross<br>$E$ (mV) | Peaks    |            |
|                           |              |   | $E$ (mV) | $A$ (mA) |                   | $E$ (mV) | $A$ (mA)   |
| Pyrrole                   | PURE         | { | 1,050    | 72.857   |                   |          |            |
|                           |              |   | 690      | 51.492   |                   |          |            |
|                           | Pb           | { | 950      | 38.571   |                   |          |            |
|                           |              |   | 670      | 14.286   |                   |          |            |
|                           | Cu           | { | 990      | 31.429   |                   |          |            |
|                           |              |   | 380      | 18.570   |                   |          |            |
|                           |              |   | 750      | 18.214   |                   |          |            |
|                           | Ag           | { | 1,024    | 4.929    |                   | 320      | 1.443      |
|                           |              |   |          |          |                   | -139     | 5.411      |
|                           |              |   | 943      | 4.740    |                   | -90      | 4.385      |
| 1-(Dimethyl-amine)pyrrole | PURE         |   | 950      | 1.929    |                   |          |            |
|                           | Cu           | { | 1,100    | 10.714   |                   |          |            |
|                           |              |   | 750      | 21.784   |                   |          |            |
|                           |              |   | 680      | 20.357   |                   |          |            |
|                           |              |   | -600     |          |                   |          |            |
|                           | Ag           |   | 500      | 8.570    |                   | -350     | 28.929 200 |
| 1-Methyl pyrrole          | PURE         |   | No       |          | 750               | 200      | 1.143      |
|                           | Cu           |   | 200      | 4.286    | 850               |          | -450       |
|                           | Ag (Cycle 1) | { | 720      | 19.286   | 1,000             | -50      | 17.857 200 |
|                           |              |   |          |          |                   |          | 330        |
|                           | Ag (Cycle 2) | { | 650      | 15.714   | 1,000             | -270     | 12.587 200 |
|                           |              |   |          |          |                   |          | 300        |
| 1-Phenyl pyrrole          | PURE         |   | No       |          |                   |          |            |
|                           | Cu (Cycle 1) | { | 550      | 11.421   |                   |          | 0          |
|                           |              |   | -450     |          |                   |          |            |
|                           | Cu (Cycle 2) | { | 500      | 10.571   |                   |          | 0          |
|                           |              |   | 950      | 5.429    |                   |          |            |
|                           | Ag (Cycle 1) |   | 670      | 8.571    |                   | -300     | 19.286 70  |
|                           | Ag (Cycle 2) |   | 620      | 6.786    |                   | -350     | 17.825 70  |

#### 四、結 論

在此一系列 Ppy 族的研究中，以 SEM 來測量金屬離子的吸附情形，並同時發現了一些聚合物形成及金屬吸附反應機構的初步證據。在電化學方面，特別着重於金屬離子吸附的電化學特徵，1,050 mV 在金屬存在時，附近的氧化電位會隨離子種類的不同以及單體的不同，而有着不同程度的漂移。而 650 mV 附近的聚合物的生成電位之波峰，卻不一定會出現。如果離子為銅離子時，在 Ppy 形成電位前的強氧化波峰為其 CV 圖的特徵。如果為銀離子，則強的還原波峰為其特徵波峰。而只要 Ppy 的形成電位 ( $\sim 650$  mV) 的波峰有出現，我們均可以金屬離子特徵波峰的電流，和 Ppy 形成電位的電流比，而直接求出溶液中金屬離子的含量。至於 Ppy 的反應機構和金屬吸附的機構，本文亦稍有提及，但仍有待於更進一步的證實。今後的研究方向，當是再運用更進步的電化學技術及微電極的技術，以求能找出反應機構的直接訊息，並嘗試各種其它的金屬離子，求出定量的關係，再嘗試以此類聚合物製做微電極，以直接用於程序分析之上，運用此一類物質的特性，來鑑定水溶液中各金屬的含量。

#### 五、謝 誌

非常感謝臺北工專錢憲行教授在電化學方面之指導，以及惠予借用 SEM。

#### 參 考 文 獻

- (1) B.J. Feldman, P. Burgmayer and R.W. Murray, *J. Am. Chem. Soc.*, **107**, 872 (1985).
- (2) B. Zinger and L.L. Miller, *J. Am. Chem. Soc.*, **106**, 6861 (1984).
- (3) A.F. Diaz, K.K. Kanawa and G.P. Garidini, *J. Chem. Soc. Comm.*, **635** (1979).
- (4) A.F. Diaz and J.I. Castillo, *J. Chem. Soc. Comm.*, **397** (1980).
- (5) R.A. Bull, F.R.F. Fan and A.J. Bard, *J. Electrochem. Soc.*, **129**, 1009 (1982).
- (6) D. Yaniv and M. Ariel, *J. Electroanal. Chem.*, **129**, 301 (1981).
- (7) G. Zotti, S. Cattarin and N. Comisso, *J. Electroanal. Chem.*, **235**, 259 (1987).
- (8) T. Shimidzu, A. Ohtani and K. Honda, *J. Electroanal. Chem.*, **251**, 323 (1988).
- (9) M. Maeda, H.S. White and D.J. McClure, *J. Electroanal. Chem.*, **200**, 383 (1986).
- (10) C.K. Baker and J.R. Reynolds, *J. Electroanal. Chem.*, **251**, 307 (1988).
- (11) K. Tanaka, T. Shichiri and T. Ymabe, *Synthetic Metals*, **14**, 271 (1986).
- (12) S. Asavapiriyant, G.K. Chandler, G.A. Gunawardena and D. Pletcher, *J. Electroanal. Chem.*, **177**, 229 (1984).

- (13) E.M. Genies, G. Gidan and A.F. Diaz, *J. Electroanal. Chem.*, **149**, 101 (1983).
- (14) A.F. Diaz, J.I. Castillo, J.A. Logan and W.Y. Lee, *J. Electroanal. Chem.*, **129**, 115 (1981).
- (15) A. Diaz, *Chem. Scr.*, **17**, 145 (1981).
- (16) A. Diaz, M. Salmon, A. Logan, M. Krounbi and J. Bargon, *Mol. Cryst. Liq. Cryst.*, **83**, 1297 (1982).
- (17) A.F. Diaz, A. Martinez and K.K. Kanazawa, *J. Electroanal. Chem.*, **130**, 181 (1981).
- (18) S. Asvapiriyant, G.K. Gunawardena and D. Pletcher, *J. Electroanal. Chem.*, **177**, 245 (1984).
- (19) C.P. Andrieux and P. Audebert, *J. Electroanal. Chem.*, **261**, 443 (1989).
- (20) G.L. Wilkes, *Chemtech.*, 174 (1983).
- (21) P. Burgmayer and R.W. Murray, *J. Electroanal. Chem.*, **147**, 339 (1983).
- (22) C.J. Pickett and K.S. Ryder, *J. Chem. Soc. Comm.*, 1362 (1988).
- (23) G.D. Adzic, D.M. Drazic and A.R. Despic, *J. Electroanal. Chem.*, **239**, 107 (1988).
- (24) P. Nunziante and G. Pistoia, *Electrochimica Acta.*, **34**, 223 (1989).
- (25) K.K. Kanazawa, A.F. Diaz, W.D. Gill, P.M. Grant, G.B. Street, G.P. Grandini and J.F. Kwak, *Synthetic Metals.*, **1**, 329 (1979/80).
- (26) G. Bidan, E.M. Genies and M. Lapkowski, *J. Electroanal. Chem.*, **251**, 297 (1988).
- (27) G. Lian and S. Dong, *J. Electroanal. Chem.*, **260**, 127 (1989).

## Study of the Electrosynthesis and Metal Ion Adsorption of Polypyrroles

JONG-RU RAU, BAO-HWA LIOU

AND SHOW-CHUEN CHEN

Department of Chemistry

### ABSTRACT

This study investigates the conductivity, reaction mechanisms and surface adsorption mechanisms of the heavy metal ions of polypyrroles. Results from the SEM study reveal (1) that the growth of Ppy films and metallic crystals are two separate events—each growing via cyclical oxidation, adsorption and reduction sequences and (2) that the crystal grain size increases as the CV scan rate decreases. The marriage of SEM with electrochemistry conducted on microelectrodes not only provides more positive evidence for Pletcher's proposed mechanism, but also gives more insight into the mechanistic details, which were not previously available.



# NMR INVESTIGATION OF THE INTERACTION BETWEEN ATP AND MACROCYCLIC POLYAMINES

ELIZABETH H. MEI\*

Department of Pharmaceutical Chemistry  
University of California, San Francisco

## ABSTRACT

An NMR investigation of the interaction between  $[18]\text{N}_2\text{O}_4$  and ATP in aqueous solution is reported. A comparison of this result with other work on the polyamines,  $[24]\text{N}_6\text{O}_2$  and  $[18]\text{N}_6$  is also made.

## 1. INTRODUCTION

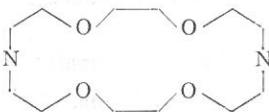
For a living cell to behave normally demands transport of nutriment and ions across the cell membrane. So far several transport models have been proposed and are well accepted. (1) The carrier-mediated transport model holds that ions such as  $\text{Na}^+$  and  $\text{K}^+$  complex with the ionophore embedded in the membrane and therefore this complexed ionic species can diffuse through the hydrophobic medium of the membrane and release the  $\text{Na}^+$  at the intracellular side. (2) Channel type transport is due to the gramicidine dimer. This dimer forms a channel to help the ions tunnel through the membrane. Hydrolysis of ATP occurs via a highly efficient enzymatic reaction catalyzed by ATPase and plays a key role in the active transport. Therefore there has been considerable interest in analyzing the controlling factors and mechanism of these reactions, especially, metal-ion-promoted non-enzymatic hydrolysis<sup>(1)</sup>. However, very little is known about the catalysis of ATP-hydrolysis by organic molecules. Biological polyamines, e.g., spermine, complex nucleotides ATP, ADP, AMP have virtually no effect on the rate of ATP hydrolysis. Protonated macrocyclic polyamines have

\* E. Mei, Ph.D. is an alumnus of Fu Jen Catholic University.  
Contact Address: P.O. Box 1231 Millbrae, Ca 94030.

recently been shown to bind AMP, ADP, ATP with affinities similar to those found in enzyme-substrate complexes<sup>(2)</sup>. Among all the macrocyclic polyamines [24]-N<sub>6</sub>O<sub>2</sub> forms a supermolecular complex by binding with ATP and providing significant rate enhancement in ATP cleavage<sup>(3)</sup>. From the facts collected in Lehn's group at Strasbourg, France, the derivative of [24]-N<sub>6</sub>O<sub>2</sub> will slow down the hydrolysis of ATP, but the reaction is still 40-70 times faster than with water. Based on chemical shifts of ATP by <sup>31</sup>P NMR study, they suggested that the alternation of O-P<sub>β</sub>-O angle contributes the most significant structure effect of the triphosphate.

After the installation of the newly arrived QE-300 NMR spectrometer, there was free instrument time and compound [1] was available. I did following experiment to illustrate the factors influencing the interaction of macrocyclic polyamine with polyanion ATP.

[1]



1,7,10,16-tetraoxa-4,13-diazacyclootadecane C<sub>12</sub>H<sub>26</sub>N<sub>2</sub>O<sub>4</sub> (C22 or [18]N<sub>2</sub>O<sub>4</sub>)

## 2. EXPERIMENT

Na<sub>2</sub>ATP was purchased from Aldrich chemical company, Inc. and converted to tetrabutylammonia salt by passage through a Dowex 50 W-X hydrogen form cation exchange resin (Bio-Rad Lab) column and then titrated with (TBA)OH, tetrabutylammonium hydroxide, (Aldrich analyze chemical 40% aqueous solution). The concentration of ATP was determined by UV/VIS spectrometry (HP 89,500) at pH=7.0<sup>(4)</sup>.

Kryptofix 22[C<sub>12</sub>H<sub>26</sub>N<sub>2</sub>O<sub>4</sub>] was purchased from MCB manufacturing chemist, Inc. (Ohio) and purified<sup>(5)</sup>. All NMR measurements were done in a 5 mm precision thin wall tube on GE-300 multinuclear NMR spectrometer. Both the TMS and 85% H<sub>3</sub>PO<sub>4</sub> references were measured externally. The concentration of compound [1] was 0.01 M and later ATP solution was added to it. The ratio of [ATP]/[C22] was kept close to a value of 1/4.

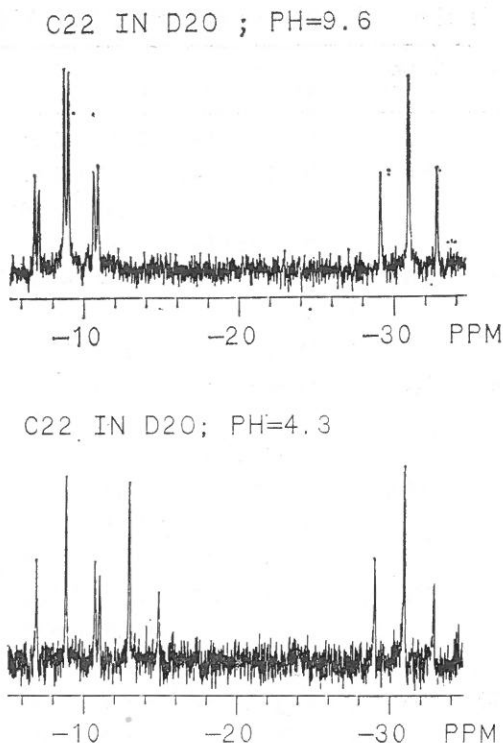


Fig. 1. CMR spectra for C22=0.01M at various pH values in aqueous solution.

### 3. RESULTS AND DISCUSSION

The chemical shift measurements in acidic and basic aqueous solutions of  $\text{Na}^+$  and  $\text{TBA}^+$  counterion of ATP are listed in Table 1. The small amount of chemical shift variation and linewidth change indicates that interaction between ATP and C22 does exist. Also it shows that the counter ion effect still plays a role in this weak interaction. The mixture of C22 and ATP samples were followed for 2 weeks at room temperature and there still was no indication of observable decomposition of ATP. But there was an observable trace with occasional heating. This illustrates that the nucleophilic nature is greatly reduced when the N atoms are replaced by O atoms in comparison with  $[\text{24}]\text{-N}_2\text{O}_2$ .

Table 1. P-31 chemical shifts (vs 85%  $H_3PO_4$ ) of ATP at 23.5°C

| Macrocyclic compound | pH   | Counter ions | ppm ( $\alpha$ $d\nu_{1/2}$ Hz)    | ppm ( $\beta$ $d\nu_{1/2}$ Hz)                       | ppm ( $\gamma$ $d\nu_{1/2}$ Hz)  |
|----------------------|------|--------------|------------------------------------|--|----------------------------------|
| [1]*                 | 5.5  | Na           | { -10.63 (13.54)<br>-10.48 (13.54) | { -21.95 (18.61)<br>-21.77 (18.61)<br>-21.63 (23.26) | { -7.92 (11.63)<br>-7.76 ( 9.30) |
| [1]*                 | 5.4  | TBA          | { -10.67 (29.54)<br>-10.52         | { —<br>-21.44 (45.81)<br>—                           | { -7.80 (36.51)<br>-7.69         |
| [1]                  | 9.6  | Na           | { -10.33 (12.95)<br>-10.48 (10.63) | { -20.31 (12.95)<br>-20.46 (12.95)<br>-20.62 (19.93) | { -4.86 ( 3.65)<br>-5.02 ( 3.65) |
| [1]                  | 9.0  | TBA          | { -10.88 (18.26)<br>-10.71         | { -21.51 ( 6.95)<br>-21.35<br>-21.17 (27.56)         | { -5.77 (13.61)<br>-5.60         |
| None                 | 5.02 | Na           | { -10.70 (13.04)<br>-10.55 (11.28) | { -22.06 ( 3.39)<br>-22.22 ( 4.26)<br>-22.38 ( 6.9 ) | { -9.87 ( 7.77)<br>-9.71 ( 6.02) |
| None                 | 9.83 | Na           | { -10.58 (10.88)<br>-10.42 (13.85) | { -21.21 ( 3.95)<br>-21.05 ( 3.85)<br>-21.89 ( 4.94) | { -5.44 ( 2.47)<br>-5.28 ( 2.47) |

\* Same sample measured at 73°C linewidth of  $P(\alpha)$  25.67 Hz,  $P(\beta)$  49.0 Hz,  $P(\gamma)$  25.67 Hz for (TBA) ATP and  $P(\alpha)$  13.64 Hz  $P(\beta)$  11.20, 23.39 and 23.39 Hz,  $P(\gamma)$  11.20, 8.76 Hz for (Na)ATP Fig. 3. showed the evidence of ATP-hydrolysis.

The model of hydrolysis of ATP by [24]- $N_6O_2$  (8 atoms with lone pair electrons on the framework) was proposed by Lehn's group and from the Fig. 2 it is seen that this macrocyclic polyamine is big enough to cover all the triphosphate bonds and flexible enough to have one N atom attack  $P(\gamma)$  to initiate the dissociation of the triphosphate bond. In compound [1] (6 atoms with lone pair electrons on the molecular framework) in the acidic environment, one of the protonated N atom may be more localized at  $P(\gamma)$  with the other protonated N atom on C22 shifting between  $P(\beta)$  and  $P(\gamma)$ . The linewidth indicates that  $P(\gamma)$  fluctuates most among the three phosphates which also implies that C22's

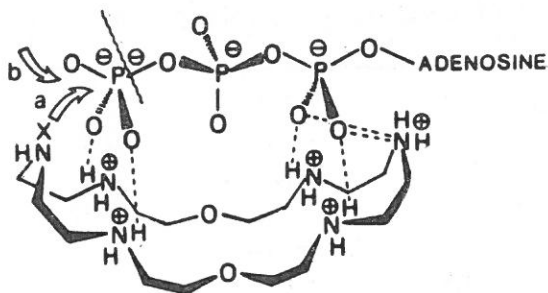


Fig. 2.  $[24]\text{-N}_6\text{O}_2$  and ATP complex.

protonated N can have two possibilities, (1) both  $>\text{N-H}^+$  groups surround the  $\text{P}(\gamma)$  phosphate, (2) one  $>\text{NH}^+$  group is on  $\text{P}(\gamma)$  phosphate and the other on the  $\text{P}(\beta)$  phosphate. The ratio of these two conformations depends on the O-P-O bond angles and the conformational flexibility of C22 to match ATP's best geometry. Since NOE is hardly observable in this system to measure the distance of interaction, a theoretical estimation of the angles may be the best alternative.

Consider the reactivity of the 3 polyamines  $[18]\text{N}_6\text{O}_4$ ,  $[24]\text{N}_6\text{O}_2$  and  $[18]\text{N}_6$ , the reaction rate reported<sup>(6)</sup> by Lehn's group and the current results are listed in Table 3. Note that  $[18]\text{N}_6$  has the same number of atoms as C22 but all oxygen atoms were replaced by nitrogen atoms. The protonation number can go up to 6 protons, therefore it has a stronger nucleophilic nature.

The results shown in Table 3 are very illustrative of the factors which influence the hydrolysis of ATP aqueous solution. We especially note two factors (1) the comparable size of the ligand and ATP; and (2) an accessible nucleophilic site on the macrocyclic framework to catalyze the hydrolysis. The work reported here was done under very limited supplies but illustrates the controlling factors of ATP-hydrolysis. With a better supply of equipment and chemicals, this study could be a very educational project for BS/MS students.

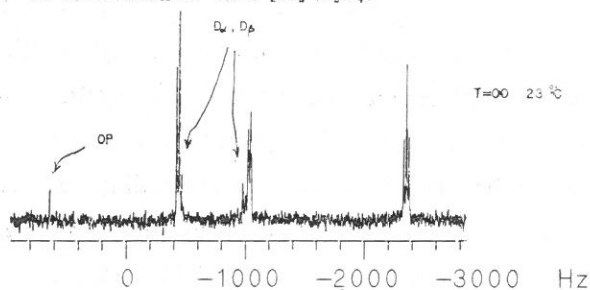
Table 2. C-13 Chemical shifts (vs. TMS) ppm of C22 in ATP solution at 23.5°C

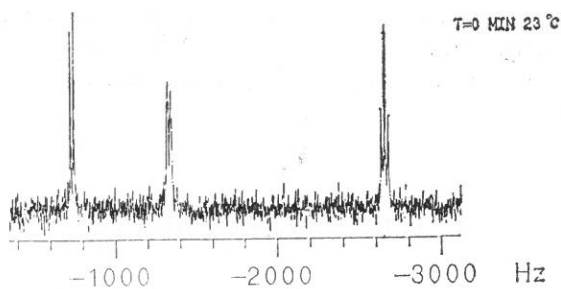
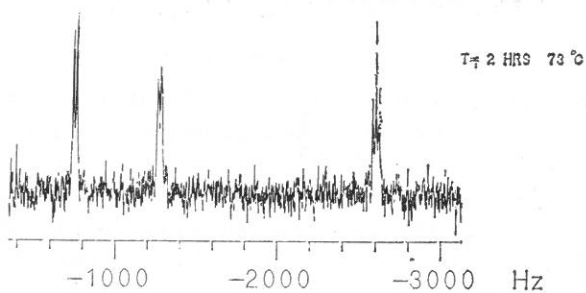
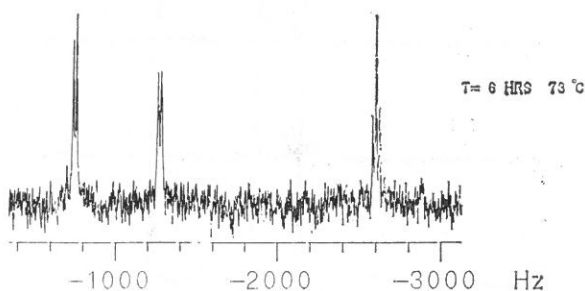
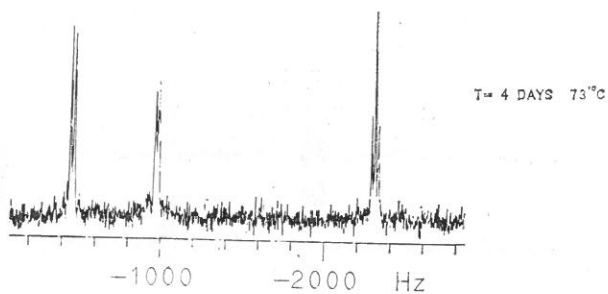
| pH  | Counter ion | C(1)   | C(2)    | C(3)   |
|-----|-------------|--------|---------|--------|
| 5.5 | Na          | - 8.20 | -12.29  | -30.31 |
|     |             | -10.10 | -14.20  | -32.22 |
|     |             | -11.99 | -16.11  | -34.13 |
| 5.4 | TBA         | - 8.22 | -12.27  | -30.27 |
|     |             | -10.11 | -14.21  | -32.18 |
|     |             | -12.03 | -16.12  | -34.09 |
| 9.4 | TBA         | - 8.54 | - 8.734 | -30.79 |
|     |             | -10.43 | -10.63  | -32.58 |
|     |             | -12.31 | -12.52  | -34.38 |
| 9.6 | Na          | - 8.91 | - 9.35  | -31.17 |
|     |             | -10.79 | -11.24  | -32.94 |
|     |             | -12.68 | -13.12  | -34.72 |

Table 3. First-order rate constant ( $k_{obs} \times 10^3 \text{ min}^{-1}$ ) for hydrolysis of Na-ATP

| Macrocyclic compounds              | pH  | ATP                              | Temperature (°C) |
|------------------------------------|-----|----------------------------------|------------------|
| None                               | 3.5 | ~1.1, 1.7*                       | 70               |
|                                    | 5.4 |                                  |                  |
| [24]-N <sub>6</sub> O <sub>2</sub> | 5.5 | 85                               | 70               |
| [18]-N <sub>6</sub>                | 7.5 | 18                               | 70               |
|                                    | 3.5 | 22                               |                  |
| [18]-N <sub>2</sub> O <sub>4</sub> | 5.5 | * not observable on NMR in 1 day | 23 and 73        |

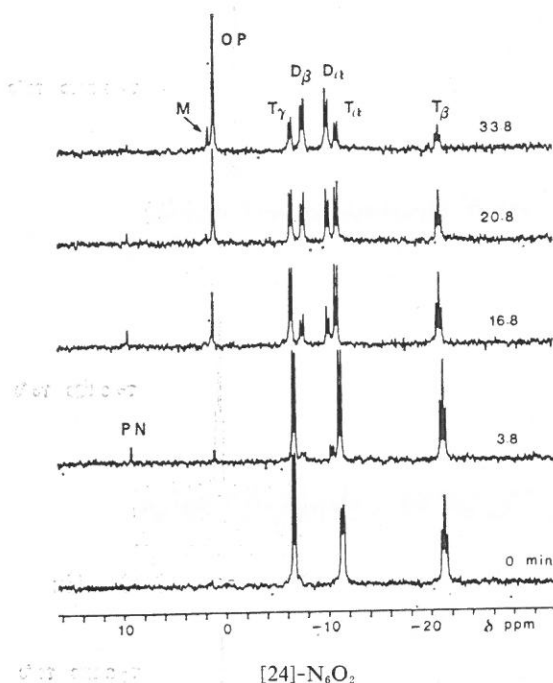
\* (TBA)ATP

Fig. 3. Observation of ATP-hydrolysis by P(31)-NMR spectroscopy as a function of time [18]-N<sub>2</sub>O<sub>4</sub>.



[18]- $\text{N}_2\text{O}_4$

- (A)  $^{31}\text{P}$  NMR spectra (300 MHz) of 0.01 M ATP and 0.01 M of at a apparent pH of 7.31 in  $\text{D}_2\text{O}/\text{H}_2\text{O}$  mixture at  $73^\circ\text{C}$ .  $T=0 \text{ min}$  corresponds to a spectrum taken without heating,  $T=\infty \text{ min}$  corresponds to a spectrum taken at room temperature after days of heating\*.



(B) Proton-decoupled P(31) NMR spectra (81 MHz) of 0.03 M ATP and 0.03 M of [24]-N<sub>6</sub>O<sub>2</sub> at an apparent pH of 7.0 in D<sub>2</sub>O/H<sub>2</sub>O mixture at 65±3°C

$T=0$  min corresponds to a spectrum taken without heating. The chemical shifts are in ppm relative to external 85% H<sub>3</sub>PO<sub>4</sub>; The signals are identified by the following symbols;  $T_\alpha$ ,  $T_\beta$ ,  $T_\gamma$ , for  $\alpha$ -,  $\beta$ -,  $\gamma$ - phosphate groups of ATP;  $D_\alpha$ ,  $D_\beta$  for ADP, M for AMP; OP for inorganic phosphate and PN for the intermediate species assumed to be a phosphoramidate derivative of the [24]-N<sub>6</sub>O<sub>2</sub>. (Reprinted from J-M Lehn et al., 1983)

#### 4. ACKNOWLEDGEMENTS

I would like to thank the University of California, San Francisco, Pharmaceutical Chemistry Department for the use of NMR and UV/VIS spectrometers. Thanks also to the group of Prof. T.L. James for their helpful support.



## REFERENCES

- (1) (a) B.S. Cooperman, in "Metal ions in Biological Systems", Vol. 5, ed., H. Sigel, Marcel Dekker Inc., New York, p. 79 (1976).  
(b) H. Sigel in "Coordination Chemistry of Metalloenzymes", eds., I. Bertini, R.S. Drago and C. Luchinat, D. Reidel Publ Co, Dordrecht, p. 65 (1983).
- (2) B. Dietrich, M.W. Hosseini, J-M Lehn and R.B. Sessions, *J. Am. Chem. Soc.*, **103**, 1282 (1981).
- (3) J-M. Lehn, *Angew. Chem., Int. Ed. Engl.*, **27**, 89-112 (1988).
- (4) Fu Jen Studies, No. 20, p. 31 (1986).
- (5) P.B. Dietrich, J-M. Lehn and J.P. Sauvage, *Tetrahedron Letters*, **34**, 2885 (1969).
- (6) M.W. Hosseini, J-M, Lehn, K.C. Jones, K.E. Pluter, K.B. Mertes and M.P. Mertes, *J. Am. Chem. Soc.*, **111**, 6330 (1989).

## 核磁共振光譜研究腺苷三磷酸 與大環多胺化合物之作用力

梅 宏 綺

藥物化學系

### 摘 要

此篇報告影響 ATP 水解的速率，在  $[^{18}\text{N}_2\text{O}_4]$  存在的情形下用核磁共振方法來觀察，結果與其他作者報導比較以做結論。



# ABSTRACTS OF PAPERS BY FACULTY OF THE COLLEGE OF SCIENCE AND ENGINEERING THAT APPEARED IN OTHER REFEREED JOURNALS DURING THE 1988 ACADEMIC YEAR

## On the Effectiveness of Adaptive Chebyshev Acceleration for Solving Systems of Linear Equations

KANG C. JEA AND DAVID M. YOUNG\*

Journal of Computational and Applied Mathematics,  
24, 33-54 (1988), North-Holland

A symmetrizable basic iterative method  $u^{(n+1)} = Gu^{(n)} + k$  can be greatly accelerated by Chebyshev acceleration. This method requires estimates of the extreme eigenvalues  $m(G)$  and  $M(G)$  of the iteration matrix  $G$ . An adaptive procedure for finding the eigenvalues was introduced by Hageman and Young (1981). We describe a scheme of using contours to test the effectiveness of this adaptive Chebyshev acceleration procedure. We conclude that the adaptive process is not sensitive to the starting estimate unless it is very close to  $M(G)$ . Moreover, the adaptive procedure takes at most 35% more work than the optimal nonadaptive procedure.

\* Center for Numerical Analysis, The University of Texas at Austin, Austin, TX 78712, U.S.A.

## Anomalous X-ray Atomic Scattering Factor for Some Light Elements

M. S. WANG\* AND SHEAU-HUEY CHIA

Physical Review A, 38(3), 1286-1288 (1988)

We calculate, using the Dirac-Slater potential, the anomalous X-ray atomic scattering factor  $f'$  for the elements F, Na, Si, Cl, K, and Ca and compare the calculated values with Creagh's experimental values

[D. Creagh, Phys. Lett. 103A, 52 (1984)]. For certain cases the theoretical values agree with the experimental values, but for most cases the theory disagrees with the experiment, even when experimental errors are taken into account. The experimental values tend to be lower than the theoretical values, in contrast to the cases of Si for Ag  $K\bar{\alpha}$  and Mo  $K\bar{\alpha}$  energies.

\* Department of Physics, National Central University, Chung-Li, Taiwan 32054, Republic of China.

### **Model Dependence of the Anomalous X-ray Atomic Scattering Factor**

M. S. WANG\* AND SHEAU-HUEY CHIA

Physical Review A, 38(11), 5639-5641 (1988)

We investigate the model dependence of the real part of the anomalous X-ray atomic scattering factor  $f'$ . Both the Dirac-Slater and the Dirac-Kohn-Sham potentials with theoretical and experimental binding energies are considered. The values of  $f'$  are found to be sensitive to the models in the neighborhood where  $f'$  changes sign. Deviations of the values of  $f'$  between different models can be as large as 20% (or more) in this region. Comparisons between the theoretical and experimental results in this region will tell us which model is better for the calculations of  $f'$ .

\* Department of Physics, National Central University, Chung-Li, Taiwan 32054, Republic of China.

### **Correlation Analysis of VHF Radar Echoes and Layer's Vertical Motion**

CHIA HSIU-YUNG LUE AND FU-SHONG KUO\*

Proc. Natl. Sci. Counc. ROC (A), 12(5), 314-321 (1988)

The echo parameter of MST radar signals, which is defined as the ratio between the layer reflection contribution and the volume scattering contribution to the echo signals, is calculated for SOUSY data between

the height of 1.8 km and 7.2 km over two different time periods under different dynamical conditions. The correlation among the time variations of the echo parameter, echo power and layer's vertical motion in each height range are analyzed. Statistics show that the echo power as well as the amplitudes of layer's vertical motion are predominantly controlled by the strength of the turbulence.

\* Department of Physics, National Central University, Chung-Li, Taiwan, Republic of China.

### **The Expansion of Product Probability Distributions from Trajectory Calculations in Two-dimensional Fourier Series**

F. E. BUDENHOLZER, S. C. HU, D. C. JENG  
AND E. A. GISLASON\*

J. Chem. Phys., 89(4), 1958 (1988)

The procedure for expanding product probability density functions determined from a classical trajectory study in a two-dimensional Fourier series is developed. This method has the advantage that essentially all of the information obtained from the trajectories is retained in the expansion; consequently, the resolution of the density functions is high. A smoothing technique using a Gaussian filter is also presented. The results are applied to a quasiclassical study of the  $F+H_2$  reaction, and new insights are obtained for this reaction.

\* Department of Chemistry, University of Illinois at Chicago, Chicago, Illinois 60680.

### **Comment on "A Modified Leps Potential Energy Surface for the $F+H_2$ Reaction" by T. Takayanagi and S. Sato**

F. E. BUDENHOLZER AND D. C. JENG

Chemical Physics Letters, 156(4), 411 (1989)

Center-of-mass velocity flux contour maps are calculated from quasiclassical trajectory results for the  $F+H_2$  reaction at a relative

translation energy of 3.0 kcal/mol. Results using a modified LEPS surface (T. Takayanagi and S. Sato, Chem. Phys. Letters 144 (1988) 191) and the number five surface of Muckerman (Theoretical chemistry: advances and perspectives, Vol. 6A (1981) p. 1) are presented. Neither surface gives results in qualitative agreement with experiment.

### **Comparison of the Effects of Sulphenyl, Sulphinyl, and Sulphonyl Substituents on Diene Reactivity and Regioselectivity in the Diels-Alder Reaction**

SHANG-SHING P. CHOU AND DER-JEN SUN

J. Chem. Soc., Chem. Commun., 1176 (1988)

The Diels-Alder reactions of 2-phenylthiobuta-1,3-dienes with PhS, PhSO, and PhSO<sub>2</sub> groups in position 3 indicate that both reactivity and regioselectivity follow the order PhS > PhSO > PhSO<sub>2</sub>.

### **2-Acetyl-3-(phenylthio)-1,3-butadiene: A Novel Diels-Alder Diene and Dienophile**

SHANG-SHING P. CHOU AND CHUNG-YING TSAI

J. Org. Chem., 53, 5305-5308 (1988)

The title compound **3** was readily obtained by the thermolysis of 3-acetyl-4-(phenylthio)-3-sulfolene (**2**), which was prepared from 3-(phenylthio)-3-sulfolene (**1**) by Friedel-Crafts acylation. Compound **3**, bearing an electron-donating phenylthio group and an electron-withdrawing acetyl group, reacted as both a diene and a dienophile in the Diels-Alder reaction. In many cases it was more convenient to use the sulfolene precursor **2** directly in these reactions. In the reaction with electron-deficient dienophiles, the regiochemistry was dominated by the phenylthio group. On the other hand, a hetero Diels-Alder reaction was observed when an electron-rich dienophile, ethyl vinyl ether, was used. In the presence of an electron-rich diene such

as 2-(trimethylsiloxy)-1,3-butadiene or cyclopentadiene, the diene **3** reacted as a dienophile with complete chemoselectivity and high stereoselectivity.

### **Regiospecific and Stereospecific Synthesis of *E*- and *Z*-Trisubstituted Alkenes via 2,2-Disubstituted Vinylsilanes**

SHANG-SHING P. CHOU, HWEI-LON KUO,  
CHUNG-JEN WANG, CHUNG-YING TSAI  
AND CHUNG-MING SUN

J. Org. Chem., **54**, 868-872 (1989)

Treatment of terminal alkynes **1** with the organocopper reagents derived from Grignard reagents, cuprous iodide, and lithium bromide (molar ratio 2:1:2) at low temperature followed by the addition of chlorotrimethylsilane gave the 2,2-disubstituted vinylsilanes **2** with complete regio- and stereospecificity (syn addition). Electrophilic substitution of **2** with ICl, Br<sub>2</sub>, and acetyl chloride gave the corresponding vinyl iodides, bromides, and  $\alpha,\beta$ -unsaturated ketones **5** with retention of configuration. Epoxidation of **2** with MCPBA gave the epoxy silanes **6**, which upon treatment with concentrated HX and BF<sub>3</sub>·Et<sub>2</sub>O gave the vinyl halides **7** with net inversion of configuration. If the epoxy silanes **6** were first converted to the  $\beta$ -hydroxy silanes **8** by Gilman's reagents, either *E*- or *Z*-trisubstituted alkenes **9** and **10** could be obtained by treatment with acid or base. Vinyl halides **7** could also be stereoselectively converted to other functionalities via the vinylolithium intermediates.

### **The Diels-Alder Reaction of Dienes Derived from Substituted 3-(Phenylthio)-3-Sulfolenes**

SHANG-SHING P. CHOU, SHY-YEON LIOU  
AND CHUNG-YING TSAI

Journal of the Chinese Chemical Society, **35**, 379-386 (1988)

Substituted 3-(phenylthio)-3-sulfolenes (**3**) and (**4**) are good precursors for 2-(phenylthio)-1,3-butadienes (**5**) and (**6**). The Diels-Alder

reaction of the dienes derived from (3) and (4) with various dienophiles was studied. It was found that heating of sulfolenes (3) with methyl propiolate and *N*-phenylmaleimide afforded the Diels-Alder adducts of (5) directly and with complete regio- and stereospecificity. The same reaction with methyl vinyl ketone gave a mixture of endo and exo addition products. If sulfolenes (3) were first converted to the dienes (5) using lithium aluminum hydride and then reacted with methyl vinyl ketone in the presence of anhydrous zinc chloride, the stereoselectivity could be improved. Sulfolenes (4) also underwent cycloreversion/cycloaddition with methyl acrylate, methyl vinyl ketone, and *N*-phenylmaleimide, but gave mostly the double bond-isomerized cycloaddition products. The regiochemistry of cycloaddition was delicately dependent on the dienophiles used.

### **The Diels-Alder Reaction of 2, 3-Disulfur-Substituted 1, 3-Butadienes**

SHANG-SHING P. CHOU AND DER-JEN SUN

Journal of the Chinese Chemical Society, **35**, 437-442 (1988)

The 2, 3-disulfur-substituted 1, 3-dienes (1) can be readily prepared from their stable 3-sulfolene precursors (2) by thermal extrusion of SO<sub>2</sub>. The Diels-Alder reaction of diene (1) with several dienophiles has been studied. The substituent effect on the reactivity and regioselectivity follows the order of PhS > PhSO > PhSO<sub>2</sub>. Lewis acid can greatly increase the regioselectivity of this reaction. The diene (1c), bearing a strong electron-withdrawing sulfonyl group, also reacted as a dienophile.

### **Selective Synthesis of 1-Alkyl-2-(Phenylsulfonyl)-1, 3-Butadienes**

SHANG-SHING P. CHOU, CHUNG-YING TSAI  
AND CHUNG-MING SUN

Journal of the Chinese Chemical Society, **36**, 149-152 (1989)

Selective synthesis of the title compounds from the corresponding sulfonyldienes is described.



## Synthesis and Reactions of a Stable Precursor to Dienes Containing Both Silicon and Sulfur Substituents

SHANG-SHING P. CHOU, CHUNG-YING TSAI  
AND CHUNG-MING SUN

Journal of the Chinese Chemical Society, **36**, 227-234 (1989)

3-(Phenylthio)-4-(trimethylsilyl)-3-sulfolene (**2**) was readily prepared by chlorosulphenylation-dehydrochlorination of 3-(trimethylsilyl)-3-sulfolene (**4b**). Treatment of **2** with *n*-butyllithium at  $-105^{\circ}\text{C}$  followed by an alkylating agent gave only C5 alkylation products **6** demonstrating the stronger carbanion stabilizing ability of phenylthio group than that of trimethylsilyl group. 2-(Phenylthio)-3-(trimethylsilyl)-1,3-butadiene (**3a**) was readily prepared by thermal extrusion of sulfur dioxide from **2**. Selective oxidation of **3a** with MCPBA gave the sulfinyl (**3b**) and sulfonyl (**3c**) derivatives. The Diels-Alder reactions of **3a-c** were studied, and the regiocontrolling power of the substituents follows the order  $\text{PhS} > \text{PhSO} \sim \text{PhSO}_2 > \text{Me}_3\text{Si}$ .

## Regiochemical Control in Palladium(0) and Palladium(II) Catalysed Alkene-Formate Ester Carbonylation Reactions

VAN J. B. LIN AND HOWARD ALPER\*

J. Chem. Soc., Chem. Commun., 248 (1989)

Palladium(0) complexes  $[\text{Pd}(\text{PPh}_3)_4]$  or  $[\text{Pd}(\text{dba})_2]$ , (dba=dibenzylidene-acetone) in the presence of 1,4-bis(diphenylphosphino)butane, can catalyse the reaction of alkenes and formate esters to give linear carboxylic esters as the major product, while the branched chain isomer was the principal ester obtained by use of a palladium(II) complex  $[\text{bis}(\text{triphenylphosphine})\text{palladium dichloride}]$  as the catalyst.

\* Ottawa-Carleton Chemistry Institute, Department of Chemistry, University of Ottawa, Ontario, Canada K1N 9B4.

**Structural Analysis and the Continued Occurrence of  
Spermatogenesis in the Adult Testes of *Heliothis Armigera*  
(Hübner) (Lepidoptera: Noctuidae)**

G. AMALDOSS

Phytophaga, 2, 73-90 (1988)

The histology and ultrastructure of the adult testes of *Heliothis armigera* are described and illustrated. Using the techniques of LM, TEM, the continued occurrence of spermatogenesis in the adult testes is traced, maturing conditions of spermatocytes and the spermatids within the follicles are described. The sertoli or apical cells and their relation to growing spermatocytes and spermatids are discussed. Occurrence of sperm dimorphism seen through the TEM is reported.

**Spermatophore Formation in *Spodoptera litura*  
Fabricius (Lepidoptera: Noctuidae).  
Phylogeny, Structure and Reproductive Functions  
of the Spermatophore**

G. AMALDOSS

Symposium on Insect Biochemistry and Physiology,  
pp. 113-129 (1988)

**Effect of Feeding, Ageing and Diapausing on Longevity  
and Oviposition in the Adult Females of the Army Worm,  
*Spodopters litura* (Fabricius) (Lepidoptera: Noctuidae)**

G. AMALDOSS AND KAI-DWEN YANG

Proc. Indian Acad. Sci. (Anim. Sci.), 97(1), 29-34 (1988)

Adult females are fed at regular intervals after emerging from the puparium, then forced to diapause at temperatures ranging from 5-10°C. Longevity, oviposition and the diapausing period are recorded. Ageing is indirectly proportional to the diapausing ability and directly proportional to the maturation of the gonads and oviposition.

**Fine Structure with Regard to Sperm Functions of the  
Ductus Ejaculatoris Duplex of the Male Reproductive Tract  
of *Heliothis armigera* (Hübner) (Lepidoptera: Noctuidae)**

G. AMALDOSS

Proc. Indian Acad. Sci. (Anim. Sci.), 98(1), 1-13 (1989)

The 'S' shaped duplex gland, the shortest among the male reproductive glands, ultrastructurally exhibits only a single cell type, characterized by the presence of multishaped rough endoplasmic reticulum, polymorphic Golgi bodies and vesicles. The frequent mode of secretion appears apocrine, with occasional merocrine and holocrine. Continuous with the height of secretory activity, the epithelia degenerates leaving only basement membrane and muscle layers.

**Concurrent Occurrence of Holocrine Type-Degeneration  
Along with High Reproductive Function in the Secretory  
Epithelia of the Duplex of Two Noctuid Species,  
*Spodoptera litura* (F) and *Heliothis armigera* (H)  
(Lepidoptera: Noctuidae)**

G. AMALDOSS

Proc. Indian Acad. Sci. (Anim. Sci.), 98(1), 15-25 (1989)

Ductus ejaculatorius duplex is the major sperm storage organ in male reproductive tract of Noctuid species. Although seminal vesicles and duplex are functionally sperm storage organs, duplex plays an important role in sperm functions on its transport from male to female. At the zenith of the reproductive function, duplex exhibits holocrine type-degeneration (secretion) concurrent with the height of secretory activity wherein the duplex secretion facilitates the transport of the spermatozoa into the female via spermatophore and contributes rich materials for spermatozoa maturity and physiological activity.

## Suppression of Snake-Venom Cardiotoxin-Induced Cardiomyocyte Degeneration by Blockage of $\text{Ca}^{2+}$ Influx or Inhibition of Non-Lysosomal Proteinases

WOAN-FANG TZENG AND YEE-HSIUNG CHEN\*

Biochem. J., **256**, 89-95 (1988)

The incubation of  $10^5$  single neonatal rat cardiomyocytes with  $1\ \mu\text{M}$ -cardiotoxin in a bath medium, Tyrode solution in the presence of  $1\ \text{mM}$ - $\text{Ca}^{2+}$ , at  $37^\circ\text{C}$  evoked the following chain of events. Firstly, there appeared a latent period of about 10 min during which the cells behaved normally. Neither lactate dehydrogenase nor ATP leaked from the cells. Cytosolic free  $\text{Ca}^{2+}$  increased considerably, as measured by the fluorescence intensity of fura-2- $\text{Ca}^{2+}$  complex. At the same time a large portion of endogenous ATP was depleted. Secondly, after the latent period, the cell beating became irregular and eventually stopped. Thirdly, blebs appeared on the cell surface, leading to cell degeneration. If, before the appearance of blebs, the cells were washed with the bath medium exhaustively or incubated in the presence of the toxin antibody, cytosolic free  $\text{Ca}^{2+}$  and endogenous ATP returned to normal levels and cells resumed regular beating. Preincubation of the cells with  $3.75\ \mu\text{M}$ -flunarizine or  $3.75\ \mu\text{M}$ -diltiazem (both are  $\text{Ca}^{2+}$  antagonists), or  $1.5\ \mu\text{M}$ -fura-2 acetoxymethyl ester (a chelate for  $\text{Ca}^{2+}$ ), or  $200\ \mu\text{M}$ -leupeptin or  $50\ \mu\text{M}$ -antipain (both are proteinase inhibitors) considerably suppressed the toxin's ability to degenerate the cells. On the other hand, lysosomal proteinase inhibitor, autophagy inhibitor, serine proteinase inhibitor, phospholipase inhibitor and calmodulin antagonist did not inhibit the toxin's activity. The results suggest that the toxin may act on the extracellular surface of intact cardiomyocytes to increase cytosolic free  $\text{Ca}^{2+}$ . The subsequent cell degeneration may result from the activation of a  $\text{Ca}^{2+}$ -dependent non-lysosomal proteolytic system.

\* Institute of Biochemical Sciences, College of Sciences, National Taiwan University, and Institute of Biological Chemistry, Academia Sinica, Taipei, Taiwan 10764, Republic of China.

## **The Characteristics of the Virus Isolated from the Gill of Clam, *Meretrix lusoria***

C. F. LO, Y. W. HONG, S. Y. HUANG  
AND C. H. WANG

Fish Pathology, 23(3), 147-154 (1988-1989)

The electron microscopic examination of the abnormally dark regions of the gill from hard clam, *Meretrix lusoria*, revealed that there were virus-like particles present in the cytoplasm of necrotic cells. With TO-2 cell line, the virus was isolated. Electron microscopic examinations showed that there were no detectable differences in morphology and location of virions in the gill cells of clam and TO-2 cells except that virus crystals were infrequently observed in clam gills. The subsequent serological and biochemical studies indicated that all the virus isolates from clam were similar to AB IPNV (infectious pancreatic necrosis virus). These studies represent the first complete characterizations of virus isolated from clam in Taiwan.

## **Functional Morphology of Sex-Pheromone Glands in Female Moths**

CHUNG-HSIUNG WANG

Symposium on Insect Biochemistry and Physiology,  
pp. 95-101 (1988)

It has been known for nearly four decades that sex pheromone plays an essential role in sexual behavior of insect, especially in that of noctuid moths. Sex pheromones are released by female moths that effect the physiology and behavior of male moths of the same species. A great deal of interest in insect sex pheromones is not only because of their role in insect physiology or behavior but also because of their potential for use in pest control. Recently many successful instances have shown that the synthetic sex pheromones or relative compounds are applied in the field with an excitable result by so-called sex-pheromone traps or disruption methods.

Using bioassay with male moths to determine the present relative amount and optimal releasing condition of sex pheromone have shown that (1) sex pheromones are practically existing in female moth; (2) pupae contain no detectable pheromone, and (3) the pheromone content of the gland increases considerably from eclosion to 2 days after eclosion, reaches a maximum after 2 to 4 days, and declines in older insect (Jacobson, 1972). Furthermore the morphological studies have revealed that the relative concentration of sex pheromones in the moths of different age correlates with structural and ultrastructural changes (Smithwick and Brady, 1971; Wang, 1987).

The sex-pheromone glands of only a very few species among many thousands of Lepidoptera species have been examined. The reviewed works on the anatomy and physiology of the glands that produce sex pheromones in both male and female Lepidoptera have been published in many books and journals (Jacobson, 1972; Percy and Weatherston, 1971; Tamaki, 1985).

On the basic concept of functional morphology, we want to discuss the relationship between morphological aspects and some physiological phenomenons. We hope that this report will facilitate future studies on the physiology, biochemistry, histochemistry and ultrastructure of sex-pheromone gland.

**On the *Plistophora* Infection in Eel**  
**II. The Development of *Plistophora anguillarum***  
**in Experimentally Infected Elvers,**  
***Anguilla japonica***

WEN-HUEI T'SUI, CHUNG-HSIUNG WANG  
AND CHU-FANG LO

Bull. Inst. Zool., Academia Sinica, 27(4), 249-258 (1988)

In order to investigate the development of *Plistophora anguillarum*, elvers were artificially infected with this Microporea by immersing them in spore-containing water. Following the histological preparations of



infected elvers sacrificed at one day intervals, the developmental stages of *P. anguillarum* were observed. The time of first appearance of schizonts, sporonts, cysts and the free spores was also recorded. The results showed that at 25°C, it was at least 13 days for *P. anguillarum* to complete the life cycle. The sporogony phase began at the 6th day after infection. No inflammatory response was observed until the cysts ruptured (late sporogony phase). According to the present data, it was suggested that the routes of infection of *P. anguillarum* in the elvers were through both skin and digestive tract. Furthermore, the schizonts might reach the infection sites via circulatory system rather than via direct migration through the coelom.

### Characterization and Cloning of Enterotoxin Genes of *Salmonella typhimurium*

MEI-KWEI YANG AND MIAN-SHIN TAN

Proc. Natl. Sci. Council. B. R.O.C., 13(2), 109-118 (1989)

Five of fifty five strains of *Salmonella typhimurium* of human origin were hybridized with both the LT-A and LT-B gene of *Escherichia coli*. The remarkably erythromatous and indurated response on rabbit skin and significant elongation of Chinese Hamster Ovary (CHO) cells indicated the production of enterotoxin of these isolates. The *Salmonella* enterotoxin is heat-labile and is not a secretory product.

The LT gene of *E. coli* was used to analyze the chromosome and plasmid DNA from *Salmonella typhimurium* strains for toxin gene sequences. Southern blot analysis demonstrated that the toxin gene was located on the plasmid but not on the chromosome. Restriction enzymes *Bam*HI, *Eco*RI, *Hind*III and *Pst*I were used to analyze the DNA isolated from salmonella strains Nos. 22, 52, 55 and 59. Three DNA fragments with size of 5.2 Kb of strain 22, 5.0 Kb of strain 52 and 8.6 Kb of strain 59 were identified as containing the enterotoxin gene. Plasmid pUC19 was used as the vector to clone these DNA

fragments in *E. coli*. The rabbit skin permeability test indicated that Salmonella enterotoxin could be synthesized at readily detectable levels in these transformed *E. coli*.

### **Implementation of the Chebyshev Structure with Minimum Storage**

BRIAN K. LIEN AND GREGORY Y. TANG\*

IEEE Transactions on Acoustics, Speech, and Signal Processing,  
37(3), 422 (1989)

It is known that the McClellan transform can be used to design high precision multidimensional FIR filters with optimal property. The Chebyshev structure is one of the implementation techniques of the McClellan transform. The Chebyshev structure presents a good efficiency and a good roundoff noise. Its drawback is the increase of the required storage space. In this paper, we shall present a method to reduce the storage needed for the Chebyshev structure and an efficient systolic cell with minimum storage. The hardware complexity of each cell is  $1/N$  that of the filters.

\* The Department of Computer Science and Information Engineering, National Taiwan University, Taipei, Taiwan.

### **Effect of Turf Bermudagrass Meal on Egg Production, Feed Utilization, Yolk Color, and Egg Weight**

B. H. CHEN AND C. A. BAILEY\*

Poultry Science, 67, 1154-1156 (1988)

The effect of diets containing various levels of dehydrated turf bermudagrass (*Cynodon spp.*) on egg production, feed utilization, yolk color, and egg weight was studied. Milo-soybean meal diets were formulated into four treatments containing 0, 3, 6, and 9% dried turf bermudagrass. Each treatment was fed to laying hens with 4 replications for a total of 240 birds. Yolk color was measured weekly with a 1984 Roche color fan. After 4 wk, average Roche color scores were



1.3, 4.9, 7.0, and 8.7 for Treatments 1 to 4, respectively. The maximum egg production and minimum feed consumption were observed in diets containing 3% turf bermudagrass meal. There was no significant difference between egg weights of birds in control and grass-fed treatments.

\* Department of Poultry Science, Texas Agricultural Experiment Station, Texas A&M University System, College Station, Texas 77843.

### **Research Note: Carotene and Xanthophyll Changes During Growth and Processing of Turf Bermudagrass**

C. A. BAILEY\* AND B. H. CHEN

Poultry Science, 67, 1644-1646 (1988)

Experiments were conducted to determine the effect of drying method and grass-clipping length on the concentrations of carotene and xanthophyll in turf type bermudagrass (*Cynodon dactylon*). This lawn grass has potential for use as a xanthophyll source for poultry in the southern US.

Oven-drying at 150 C for 40 min, oven-drying at 70 C for 20 h, dark room-drying at approximately 25 C for 120 h, and field-drying in natural sunlight were compared with freeze-drying. The field-drying method resulted in carotene and xanthophyll concentrations of only 15 and 52 mg/kg, whereas freeze-drying yielded the best values: 499 and 886 mg/kg, respectively. Regression analysis of both carotene and xanthophyll content indicated no significant differences that could be attributed to grass-clipping length.

\* Department of Poultry Science, Texas Agricultural Experiment Station, Texas A&M University, College Station, Texas 77843.

### **Simultaneous Separation and Identification of Carotenoids and Chlorophylls in Turf Bermudagrass by High-Performance Liquid Chromatography**

C. A. BAILEY\* AND B. H. CHEN

Journal of Chromatography, 455, 396-400 (1988)

\* Department of Poultry Science, Texas Agricultural Experiment Station, The Texas A&M University System, College Station, TX 77843 (U.S.A.).

## Simultaneous Dehydration of 95% Ethanol and Extraction of Crude Oil from Dried Ground Corn

J. T. CHIEN, J. E. HOFF\* AND L. F. CHEN

Cereal Chem., 65(6), 484-486 (1988)

A column reactor operating at  $68 \pm 2^\circ\text{C}$  was used to demonstrate the feasibility of a new process that simultaneously dehydrates ethanol and extracts crude oil from dried ground corn. For each kilogram of dried ground corn, the moisture adsorption capacity was approximately 32 g using 95% (w/w) ethanol as solvent. As a result, it was possible to dehydrate 500 ml of 95% ethanol and simultaneously extract 45 g of the crude oil from each kilogram of dried ground corn. The crude-oil contained 2.1% of phospholipids on dry weight basis.

\* Department of Food Science, Purdue University, Smith Hall, West Lafayette, IN 47907.

## 環 狀 糊 精 之 研 究

### 5. 由不同澱粉生產環狀糊精產量之比較

施能仁 江晃榮\* 呂政義\*\* 丘志成

食品科學 第十五卷 第四期 第 442-451 頁 七十七年

以樹薯、馬鈴薯、甘薯、食用美人蕉、秈米、梗米、玉米、綠豆及小麥等九種澱粉為原料，分別與嗜鹼性 *Bacillus* 環狀糊精葡萄糖基轉移酶 (Alkalophilic *Bacillus* CGTase) 作用並比較環狀糊精 (CDs) 的產量。在 1% 澱粉濃度時，馬鈴薯澱粉之 74% CDs 產量為最高，而梗米澱粉之 66% 為最低，CDs 產量隨澱粉濃度增加而減少。於工業生產 CDs 所使用的 15% 澱粉濃度時，食美人蕉及綠豆澱粉的 CDs 產量為 9~10%，高於馬鈴薯及甘薯澱粉之 7~8%。

CDs 產量與澱粉成份之關係亦被探討。脫脂澱粉較未脫脂者之 CDs 產量高，而蛋白質、灰份則與 CDs 產量較無關係。於低油脂成份時，直鏈澱粉含量會影響 CDs 產量。所有澱粉樣品之破損澱粉均小於 1.34%，對 CDs 產量不具影響。因此，油脂含量低於 0.10%，直鏈澱粉含量高於 20%，且破損澱粉含量小於 1.34% 之澱粉均適合生產 CDs。

\* 生物技術開發中心

\*\* 中央研究院化學研究所

## $\beta$ -環狀糊精功能性質及應用之研究：

### 2. 增泡、粉末化、乾化及安定化

丘志威 林子清\* 呂政義\*\* 洪淑慎

界面科學會誌 第十一卷 第四期 中華民國七十七年十二月

添加 1%  $\beta$ -環狀糊精 ( $\beta$ -CD) 的蛋白泡沫排液量最少，而對照組的排液量最多，顯示  $\beta$ -CD 具穩定蛋白泡沫的效果。在沙拉醬 (salad dressing) 方面，添加葡萄糖或糊精者分別經 1 小時或 2 天儲藏後均有油水分層的現象。但是添加  $\beta$ -CD 之沙拉醬經 1 個月的儲藏仍舊沒有油水分離現象。含 10 ppm 之紅色 7 號溶液經日光照射的褪色程度隨時間而增加，添加 1.5%  $\beta$ -CD 具有保護效果。添加  $\beta$ -CD 減少者海綿蛋糕硬度及減低彈性，但是增加保水性。本研究成功地製成粉末醬油，經 1 個月儲藏試驗發現含  $\beta$ -CD 粉末醬油在風味及吸濕性方面均優於其他實驗組。初步試驗亦顯示添加 1~1.5%  $\beta$ -CD 至 methyl linoleate 溶液具有抑制氧化的效果。

\* 行政院農業委員會

\*\* 中央研究所化學研究所

## Effects of Fractionated Lard and Fish Oil on Plasma and Liver Lipids in Rats

C. M. E. TSAI, S. L. SONG, T. C. LIN\*,

H. C. TSENG AND T. S. CHEN

Nutrition Reports International, 38(6), 1289 (1988)

Five test diets including soybean oil (A), lard (B), Chingshan liquid lard (C), winterized (at 20°C) liquid lard (D), and lard+fish oil (E) were prepared. Thirty mature male Wistar rats were fed one of the experimental diets in individual cages for six weeks. The plasma total lipids (TL), triacylglycerols (TG) and cholesterol (CS) with diets B, C and D were not higher than those with diet A. The plasma TL, TG and CS were lower ( $P < 0.05$ ) with diet E than with all the other oils. The liver CS, however, varied inversely with plasma CS, which may indicate that reducing the plasma CS results in accumulation of CS in liver. Our data also suggested that the levels of polyunsaturated fatty acids in the plasma lipoproteins reflected their levels in the diet, but this was not true for saturated fatty acids.

\* Department of Food and Agriculture, Council of Agriculture Executive Yuan, R.O.C.,

## Stability of Fish Oil in a Purified Diet with Added Antioxidants: Effects of Temperature and Light

CHINGMIN E. TSAI, JOSEPH T. WOOTEN\*

AND DAVID A. OTTO

Nutrition Research, 9, 673-678 (1989)

The extent of oxidation of fish oil with added antioxidants in a purified diet was studied after storage under nitrogen at 1°C or -16°C, and after exposure to air at room temperature with direct or indirect light. The thiobarbituric acid values showed that the fish oil diet was stable for at least two weeks when stored in the dark at 1°C or -16°C. The fish oil diet was rapidly oxidized at room temperature when the diet was directly exposed to overhead fluorescent light. However, if the diet was exposed to only indirect light it was stable at room temperature for at least 8 days. These data emphasize the importance of light exposure when considering the stability of fish oil containing diets even in the presence of antioxidants. The data demonstrate that when feeding animals, daily mixing and replacement of fish oil containing diets (with added antioxidants) is not necessary if the diet is shielded from direct light.

\* Department of Research the Baptist Medical Centers Birmingham, Alabama 35211.

## 油炸油之可能毒性與其黏滯性和顏色改變之相關性

蔡敬民 張 琪 王念如 許輝吉\*

食品科學 第十五卷 第四期 第 394-406 頁 七十七年

本研究旨在探討一種較簡易的方法，來測定油炸油的可能毒性，以作為何時該停止使用此油炸油之指標。本實驗以黃豆沙拉油加熱至  $190 \pm 5^\circ\text{C}$ ，每天加熱 12 小時，各別加熱 0, 2, 4, 6, 8 天，並有一組以含水之棉花球油炸 8 天。然後以 10% 之比率拌入營養均衡，符合美國 NRC 建議量之飼料中（但不含油脂），餵飼 Long Evans 大鼠。

結果顯示，油炸油之黏滯性和顏色，隨加入時間之增加而增加，而 HPLC 分析顯示，油炸油隨油炸時間之增加，其單體逐漸減少而雙體和多體增加。大鼠

肝臟細胞壞死等病變，大致亦隨加熱程度之增加而逐漸嚴重。然而油炸含水棉花球組顯示，其黏度和顏色的改變，明顯地低於祇單純加熱同時間（8 天）之油炸油，但其導致肝臟局部壞死的程度較為嚴重，且嗜酸性變化較早出現。因此以黏滯性或顏色（包括 Fritest）作為油炸油毒性指標時可能祇適用於同一油炸條件，當油炸不同種類食物或不同含水量食物時，可能需分別測試其與毒性之相關性，而訂定不同之丟棄標準。

\* 臺灣大學醫學院病理科

## Qoheleth and Time

MARYTA LAUMANN S. SP. S.

*The Bible Today*, 27(5), 305-310 (1989)

The Old Testament book named Qoheleth or Ecclesiastes generally leaves its readers with the dis-illusioning impression that "all is vanity" anyway including all ceaseless pursuits for pleasure, achievement, success, wealth, control, security as well as such spiritual endeavors as gaining knowledge wisdom and virtue. One wonders what strength for living is to be derived from such a pessimistic, philosophy of life.

On careful reading and study, however, one cannot help but feel inclined to at least seriously admire Qoheleth's methodology of life-long observation, investigation and experimentation, which led him to put all there is under the sun to the test of time and wisdom.

The results of his untiring research are striking, going beyond the contributions made by the wisest of the O. T. wisdom teachers such as Solomon and Job:

- (1) Wisdom is not absolute but relative to time, it cannot be "frozen" into structures, doctrines and traditions. It is "liquid" i. e., "formless". Each time must "form" its own life-giving response to the needs and signs of the times, simply because "there is a time for everything".
- (2) Humans are faced with the utter inability to gain control over time by any means. It teaches us the wisdom of discovering the One beyond time, the Eternal One who is constant in all he does. It is wisdom to trust his ways rather than knowing and wanting to have all the answers and control all the details.



- (3) The beginning of wisdom is when in deep acknowledgement of our creaturehood we no longer "want to be like God" in our search for wisdom. Letting God be God we have learned to accept life as a "pure gift" and "mystery" to be revealed and lived in the now-dimension of life. We are to celebrate divine Wisdom's involvement with us at every new moment and in all its forms. Above all we are not to forget to deeply enjoy the most ordinary gifts life has to offer, such as food and drink, our work, and the "sweetness of sunlight".

### **The Biblical Version of the Origin and Significance of Clothing Based on Genesis**

MARYTA LAUMANN S. SP. S.

Journal of the International Association of Costume,  
6, 182-187 (1989)

Modesty is one of the major theories put forth to explain the origin and purpose of clothing. Moralists-supported by popular belief yet in conflict with modern psychology and anthropology-insist that humans suffer "innate" feelings of shame resulting from exposure of particular parts of the body. They base their claims mainly on Gen. 3:7. Accordingly this viewpoint came to be known as the Mosaic or Biblical theory.

This research, by means of scriptural analysis, re-interprets Gen. 3:7 in the context and in comparison with other related statements of the Book of Genesis and solves the above mentioned conflict of opinions. Moreover, taking into perspective some significant, relevant texts of the New Testament, it demonstrates how the book of Genesis explores the human experience of nakedness and clothing in its true depth by attaching to it a symbolic and prophetic significance which goes far beyond a body-centered sense of modesty with its sexual undertones. Such an integrated perspective also reveals that the clothing symbolism in Genesis carries a double meaning and is to be understood as a temporary provision only. Its significance becomes fully evident only in the light of Christ "stripped naked" on the cross and "robed in the light of glory" at his resurrection as the Firstborn of a new creation, leaving all the fragments of clothing behind in the empty tomb.